Nano-carrier Macrophage Interaction: Role of Secondary Toxicity

By

Muhammad Khan Sarfraz

A thesis submitted in partial fulfillment of the requirements for the degree of

Doctor of Philosophy

In

Pharmaceutical Sciences

Faculty of Pharmacy and Pharmaceutical Sciences
University of Alberta

Abstract

Macrophages are the primary cells of innate immunity that provide the first line of defence against any external stimuli. Their phagocytic properties enable them to engulf invading microbes or foreign particles. The phagocytic capability of macrophages plays a major role in interfering with drug targeting strategies, but can be used as a treatment advantage if the macrophage is itself the target cell. Although nano-drug delivery systems might deliver a drug contained in polymeric micelles or nanoparticles into a targeted area, the rapid accumulation of these vesicles/particles in macrophages reduces the efficiency of the targeted drug delivery. Additionally, biodegradation of polymeric nanoparticles in macrophages causes secondary toxicity, characterized by the release of different cytokines and chemokines (e.g., TNF-α, IFN-γ, IL-1β, IL-10) by macrophages.

In tuberculosis, the mycobacterium tubercle can only cause infection after invading and growing inside alveolar macrophages; where as, in cancer, macrophages are the only infiltrating immune cells into tumours and can represent up to half of its mass. They play a major role in tumour angiogenesis. Using murine alveolar macrophages (MH-S), the first study investigated secondary toxicity produced when macrophages were a target with nanocarriers and assessed the implication for disease conditions like TB. In a second study, a co-culture model for alveolar macrophages and lung cancer cells was investigated for assessing secondary toxicity effects on the viability of the cancer cells.

In the first study, two different nanocarriers—HA-TS polymeric micelles and gelatin and polyisobutyl cyanoacrylate (PIBCA) nanoparticles—were used and their induction of secondary toxicity was evaluated. HA-TS micelles were synthesized by chemical conjugation of hydrophobic α-tocopherol succinate (TS) to hydrophilic hyaluronic acid (HA) and characterized by Fourier transform infrared (FTIR) spectroscopy and nuclear magnetic resonance (NMR). The results

confirmed the structural changes incorporated during micelle synthesis. The rifampicin (RIF) entrapment efficiency of micelles, studied by HPLC, showed a drug loading of 70.7–79.1% (w/w). *In vitro* release curves revealed a sustained release of RIF from RIF-loaded HA-TS (RIF-HA-TS) micelles. Cellular uptake of RIF-HA-TS by murine alveolar macrophages (MH-S) showed that both phagocytosis (endocytosis) and active transport were responsible for cellular uptake. Cytokine profiling revealed that both E. coli lipopolysaccharide (LPS) and RIF-HA-TS micelles induced secondary toxicity. Similarly, gelatin and polyisobutyl cyanoacrylate (PIBCA) nanoparticles were evaluated for secondary toxicity using murine alveolar macrophages (MH-S). The antituberculosis drugs moxifloxacin and rifampicin were loaded into gelatin and polyisobutyl-cyanoacrylate nanoparticles synthesized by a two-step desolvation and anionic emulsion polymerization technique. IC_{50} values of polyisobutyl-cyanoacrylate nanoparticles were lower than the IC_{50} values of gelatin nanoparticles. Cytokine ELISA analysis revealed that both types of nanoparticle induced a higher release of Th1 type cytokines. The use of nanoparticles produced significantly more secondary toxicity than the use of micelles.

In the second study, secondary toxicity was further evaluated with a lung cancer model. Doxorubicin loaded nanoparticles were synthesized with the method used for gelatin and polyisobutyl-cyanoacrylate nanoparticles. The lung cancer model consists of confluent alveolar macrophage MH-S and A-549 lung cancer cells separated by a 0.4 μm porous membrane. Macrophages were treated with nanoparticles and secondary toxicity was assesed by measuring A-549 lung cancer cell viability. These effects were also investigated using anti-inflammatory dugs. The result showed that nanoparticle treatment of macrophages produced a secondary cytotoxic effect that decreased the A-549 cell viability 40–62%. However, this effect was significantly reduced to 10–48% if the macrophages were exposed to anti-inflammatory drugs. The data suggest

that anti-inflammatory treatments can decrease nanoparticle-induced macrophage cytotoxicity and thus decrease its anti-tumor effectiveness.

Macrophages exposed to nanocarriers showed secondary toxicity in murine alveolar macrophages (MH-S). This pro-inflammatory effect might strengthen the macrophage immune response to control diseases like TB. In cancer, the pro-inflammatory effect caused a significant reduction in cancer cell viability. This effect was significantly reduced with the concomitant use of anti-inflammatory drugs. The insight gained in these studies can be utilized for new treatments approaches toward macrophage oriented diseases or utilization of macrophages for other diseases like arthritis and osteoporosis as demonstrated for cancer.

Preface

This thesis is an original work by Muhammad Khan Sarfraz completed under the supervision of Prof. Dr. Raimar Löbenberg at the University of Alberta. Most of this work was performed in the Dr. Löbenberg lab facilities and Drug Development Innovation Center (DDIC). Some experiments were also carried out at different lab facilities at the University of Alberta.

Chapter 2 "Synthesis and *in vitro* characterization of Hyaluronic acid tocopherol succinate-based self-assembling micelles" and **Chapter 3** "Macrophage behavior after cellular uptake and Intracellular localization of micelles" was a collaborated project with Dr Yuan GAO under the supervision of Prof. Dr Löebenberg being the primary author. Muhammad K Sarfraz is also a co-author of this publication and contributes in different experimentation including confocal microscopy, NMR, FTIR, micro-colorimetry, X-ray diffraction and various cell viability analysis. The publication coming out of this shared project was published in **Journal of biomedical nanotechnology** with the title of "Hyaluronic Acid-Tocopherol Succinate-Based Self-Assembling Micelles for Targeted Delivery of Rifampicin to Alveolar Macrophages". Gao Y, Sarfraz MK, Clas SD, Roa W, Löbenberg R. June 2015, 11:1283-1311

Chapter 4 of this thesis has been published as Muhammad Sarfraz, Wenjun Shi, Yuan Gao, Sophie- Dorothee Clas, Wilson Roa, Nadia Bou-Chacra & Raimar Löbenberg, Immune response to anti-tuberculosis drug-loaded gelatin and polyisobutyl-cyanoacrylate nanoparticles in macrophages in **Journal of Therapeutic Delivery**. April 2016, 07:04: 213-228. Muhammad Sarfraz was responsible for data collection, analysis and write up of this manuscript, Dr. Löebenberg was the supervisory author and was involved in the formulation of the concept, analysis and composition of the manuscript.

Chapter 5 of this thesis has been published as Muhammad Sarfraz, Nadia Bou-Chacra, Wilson Roa, & Raimar Löbenberg with the title of Inflammation caused by nano-sized delivery systems: Is there a benefit? in **Journal of Molecular Pharmaceutics** *August* 2016, *13* :9: :3270–3278.

Dedication

I would like to dedicate this work to my family and parents.

Acknowledgements

I would like to express my sincere gratitude and appreciation to my enthusiastic supervisor, Dr. Raimar Löbenberg, for his continuous guidance, unlimited support and invaluable supervision throughout my work on these research projects. It was only his directions and support that made me accomplish this task. He is always approachable and willing to help. I thank him for his every moment spent with me for the sake of research and learning; it was an amazing experience working with him.

I would also like to thanks my supervisory committee members, Dr. Wilson Roa Dr. Arno Siraki and Dr. Hoon Sunwoo for their extensive guidance and advice. For being so approachable and critical in details during my research, that their efforts made me correct and refined my research.

My profound gratitude goes Dr. Yuan Gao and Wenjun Shi, who taught me several techniques and offered me valuable advice and ideas. By their training and guidance, I can accomplish my project. I would also like to thank my colleagues and lab fellows May Almukainzi, Braa Hajjar, Zhipeng Yuan and Jieyu Zuo for their help and support from time to time. I am grateful to the reviewers who had the time to review the publications which resulted from this work. Their invaluable comments and scientific critique helped me to improve the quality of the manuscripts greatly.

I am grateful to have received the financial support from the Faculty Development Programme, The Islamia University of Bahawalpur, funded by Higher Education Commission of Pakistan. Last but not least, I wish to thank all the administrative and support staff in the Faulty of Pharmacy and Pharmaceutical Sciences for their kindness. Special thanks go to Mrs. Joyce Johnson and Mr. Jeff Turchinsky.

I am thankful to Higher Education Commission Pakistan for providing the scholarship for five years for completion of this PhD under Faculty Development Program of The islamia University of Bahawalpur.

Table of Contents **Page**

List of Tables

List of Figures

List of abbreviations

A-549 Lung cancer cell lines
C Celecoxib
CMC Critical micelle concentration
Dex Dexamethasone
DLS Dynamic Light Scattering
DMF Dimethylformamide,
DMSO Dimethyl sulfoxide
DOX Doxorubicin
DS Degree of substitution
DSC Differential Scanning Calorimetry
EDA Ethylenediamine (EDA
EDC 1-ethyl-3(3-dimethylaminopropyl) carbodiimide hydrochloride
ELISA Enzyme-linked immunosorbent assay
FBS Fetal bovine serum
FDA Food and Drug Administration
FTIR Fourier transforms IR
GCs Glucocorticoids
HA Hyaluronic acid
HA-Na Sodium Hyaluronate
IB Ibuprofen
IC50 Drug concentration for 50% inhibition
IFN-γ Interferon-γ
IL-1β Interlukin-1β
IL-4 Interlukin-4
IL-10 Interlukin-10
IL-12 Interlukin-12
IMF 7 CD44 Antibody
LPS lipopolysaccharide
M1 Macrophage Subtype 1
M2 Macrophage Subtype 2
M Methotrexate

MH-S Murine alveolar macrophages

MOX Moxifloxacin

MTB Mycobacterium tuberculosis

MTT 3-(4, 5-dimethylthiazol- 2-yl)-2,5-diphenyltetrazolium bromide

NHS N-hydroxysuccinimide (NHS)

NMR Nuclear Magnetic Resonance

NPs Nanoparticles

NSAIDs Non-Steroidal Anti-Inflammatory drugs

P Prednisolone

PBS Phosphate-buffered saline

PDI Polydispersity Index

PIBCA Polyisobutyl-Cyanoacrylate

RIF Rifampicin

RIPA Radio-Immunoprecipitation Assay

RT Room Temperature

TB Tuberculosis

TEM Transmission Electron Microscope

TS α-Tocopherol-succinate

Th1 T 1helper cells

Th2 T 2 helper cells

TNF-α Tumor Necrosis Factor-α

XRD X-ray diffraction

Chapter 1

Introduction

1.1 The immune system

The immune system comprises a network of the immune system is composed of network of cell products, interacting cells and tissues that protect the body from any foreign substances, destroy the infected and malignant cells and remove the cellular debris. An immune system composed of the immune system includes thymus, lymph node and lymph tissues, stem cell, white blood cells, antibodies and lymphokines. Molecules that our immune system can recognize are considered as antigens [1]. In vertebrates, the immune cells attack the antigens in several ways that are discussed in sections 1.1.1 and 1.1.2.

1.1.1 The innate immune system

The primary host defense against pathogens or infectious agents involves monocytes, macrophages, dendritic cells (DCs), natural killer (NK) cells and plasma proteins in the immune system. Such innate immunity is natural and provides nonspecific defense against entering antigens. Pattern recognition receptor (PRR) in the innate immunity can sense an infectious agent as soon as it penetrates the epithelium—a membrane that lines all vertebrate blood vessels and organs. Invading foreign entities leave a trail of evidence, such as bacterial cell wall components (lipopolysaccharides, peptidoglycans, lipoteichoic acids), fungal molecules (β-glycans), viral proteins, and other pathogen-associated molecular patterns (PAMPs) [2]. Toll-like receptors (TLR) are PPRs that have been shown to activate pathogen uptake by phagocytic cells (macrophages, dendritic cells, neutrophils) [2].

Immune cells like macrophages are also activated by inflammation, which is a cell-ready reaction to any foreign material. The activated macrophage is responsible for the release of cytokines ((tumor necrosis factor alpha (TNF-α), granulocyte-monocyte colony stimulating factor

(GM-CSF) and interferon gamma (IFN-γ)) for initiation and maintenance of inflammation. It is resolved when activated macrophages are deactivated by cytokine antagonist or anti-inflammatory cytokines ((interleukin 10 (IL-10) and transforming growth factor beta (TGF-β)) mainly produced by macrophages. These activated macrophages also migrate to local lymph nodes to induce an adaptive immune response [3].

1.1.2 The adaptive immune system

The adaptive immune system employs T and B lymphocytes to recognize highly diverse antigens [4]. In a delayed response to extracellular microbes and microbial toxins, B lymphocytes, which originate and mature in bone marrow, activate expression of membrane-bound receptors called immunoglobulins. When B cells encounter an antigen, they differentiate into either memory or plasma secreting cells. Antibodies can neutralize an antigen or mark a pathogen for ingestion and elimination by a phagocytic cell through the complement system [5].

T lymphocytes also arise in the bone marrow but complete their maturation in the thymus. T cell receptors (TCRs) recognize antigens that are bound to the major histocompatibility complex (MHC), a group of cell surface proteins that bind peptide fragments of pathogens. CD4+ T cells bind to MHC class II, and CD8+ T cells bind to MHC class I. Antigen presenting cells (APCs) like macrophages must display additional costimulatory signals to activate T cells fully [6].

1.2 Significance of macrophages

In response to microorganisms and host mediators, macrophages are functionally polarized to establish a link between innate and adaptive immune systems. In the current study, two diseases were selected in which macrophage polarization plays a key role: lung cancer, which is characterized by the uncontrolled proliferation of cells in lung tissue, and tuberculosis, an infection

caused by the Mycobacterium tuberculosis. The mode of spread, pathogenesis, diagnosis, prognosis and management in both diseases is different. The macrophage roles in lung cancer and tuberculosis are discussed in sections 1.3 and 1.4

1.3 Tumor Immunology

Paul Ehrlich first proposed the ability of the immune system to identify and destroy tumor cells in 1909 [6]. After 50 years Ehrlich's theory was advanced by Burnet and Thomas, who introduced the concept of cancer immune surveillance by predicting that lymphocytes were responsible for the elimination of continuously arising transformed cells [7]. Their hypothesis was supported by studies of immune deficient mice and later by observations in humans. A theory that immunity not only protects a host from tumor development but also promotes tumor growth was later proposed by Schreiber and colleagues and is referred to as "cancer immune editing" [8,9]

1.3.1 Hallmarks of cancer

Genetic and epigenetic alterations lead to changes in cell growth, proliferation, and differentiation, and thus cause the development of tumors. Hanahan and Weinberg suggested six essential alterations in cell physiology that could contribute to the transformation of normal cells into malignant cells as a hallmark of cancer [10]. This includes (a) self-sufficiency in growth signals, (b) insensitivity to antigrowth signals, (c) limitless replicative potential, (d) evasion of apoptosis, (e) sustained angiogenesis and (f) tissue invasion and metastasis. These transformative cellular activities are shown in Figure 1.1 and detailed in the following subsections.

(a) Self-sufficiency in growth signals. Cells normally do not divide unless they receive a growth signal. Cells that acquire an ability to grow in the absence of programmed growth signal initiate a positive feedback loop creating uncontrolled proliferation.

(b)Insensitivity to antigrowth signals. Growth inhibiting signals are established within the normal tissue to maintain tissue homeostasis. For example, transforming growth factor-β (TGF-β) prevents activation of transcriptions factors responsible for the cell cycle machinery. Tumor cells can disable components of the TGF-β-mediated signalling pathway achieving insensitivity to growth inhibitory signals.

(c) Limitless replicative potential. Normal cells face limits to cell replication. Malignant cells escape this limitation by upregulating the expression of the enzyme telomerase which adds nucleotides to the ends of DNA. It, in turn, permits unlimited multiplication of descendant cells.

(d) Evading apoptosis. Apoptosis is programmed cell death. Apoptosis is necessary to remove damaged cells and to keep mitosis in check. Tumors can develop resistance to apoptosis effector mechanisms, allowing defective cells to survive and proliferate.

(e) Sustained angiogenesis. Tumors can develop an increased angiogenic ability to grow larger. A common feature of tumor cells is augmented levels of the vascular endothelial growth factor (VEGF), which promotes angiogenesis.

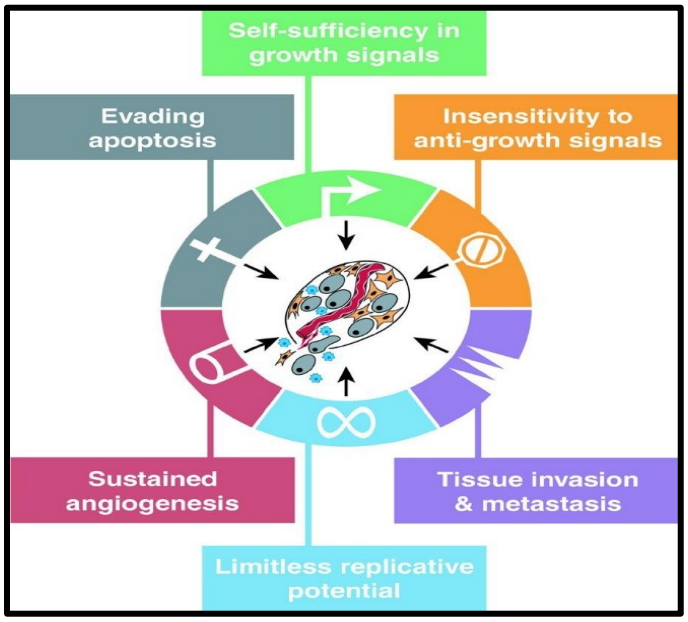

Figure 1.1: Acquired Capabilities of Cancer by Douglas et al.

Douglas Hanahan, Robert A Weinberg The hallmark of Cancer Cell, Volume 100, Issue 1, 2000, 57–70 [10] Reproduce with permission.

(f)Tissue invasion and metastasis. As a tumor mass grows, the cells spread to distant tissues and organs, a process called metastasis. Metastasis requires alterations of proteins involved in cell-cell adhesion (e.g., E-cadherin).

Tumors have to evolve strategies to progress by escaping immune responses. In the late 90s, "immunoevasion" was proposed as new hallmark of tumors. Its include production of immunosuppressive cytokines, apoptosis of activated T cells, or loss of costimulatory and Human leukocyte antigen [11] and will be discussed in section 1.3.2

1.3.2 Cancer immune editing

In humans, our immune system protects us against invasive threats. How can our immune system also promote tumor growth? It is theorized that three phases of immunoediting—elimination, equilibrium, and escape—can both prevent and permit the dissemination of defective cells (Figure 1.2).

(a) Elimination phase: Anti-tumor immune responses

Immunoediting integrates responses from both innate and adaptive branches of the immune system in a four-stage elimination phase. Initially, a growing tumor produces stromal damage and inflammation which alerts the innate immune system to send lymphocytes to the tumor site where they produce IFN-γ inducing tumor cezll death. In the second stage, small protein molecules that help to prevent angiogenesis (chemokines) are produced. Macrophages and natural killer cell activate each other by reciprocal production of IL-12 and IFN-γ in the third step of elimination phase followed by apoptosis of tumor cells. In the last step, the remaining antigen bearing tumor cells are destroyed by the tumor-specific CD4+ and CD8+ T lymphocytes [12].

(b) Equilibrium phase: Tumor persistence

Despite the potent immune response, tumors can survive the elimination phase via immunoediting. The survivors continue to be bombarded by lymphocytes and cytokines from the host immune system, but the tumors remain resistant to immune-mediated killing. This dynamic equilibrium can sometimes be maintained for many years 10-20 years. [13,14]

(c) Escape phase: Tumor progression

Tumor cells that manage to survive the human immune response at one site are free to travel to other sites, where they are likely to repeat their subversion of immune responses [15]. Such malignant tumors can directly or indirectly impede immune responses. Direct mechanisms include (a) Irregularities in antigen processing [16] (b) lowering in tumor antigen expression [17] (c)

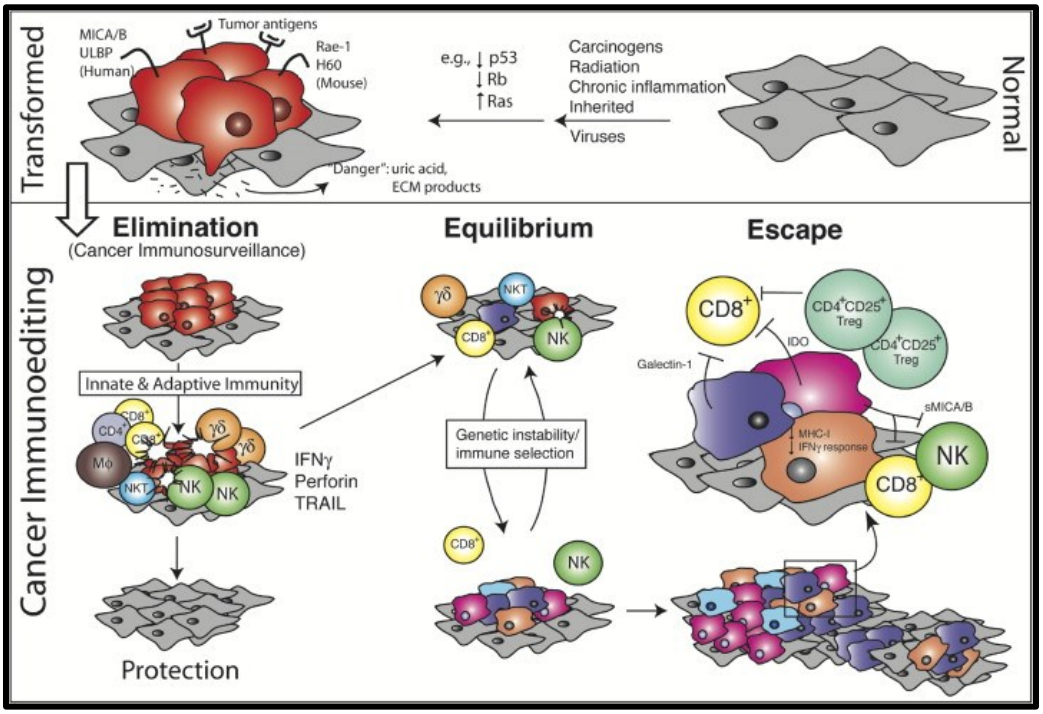

Figure 1.2: Cancer immunosurveillance and immunoediting. (Dunn et al. Immunity 2004; 21: 137-148) [12] (1) Elimination of cancer (2) Equilibrium (tumor cells and immune cells reach a

state that keeps tumor expansion in check) (3) Escape (tumor growth even in the presence of an antitumor immune response). (Reproduce with permission).

modified expression level of MHC class I/II and costimulatory molecules. Indirect mechanisms are associated with (a) tolerance of T cells to tumor-specific antigens (b) suppression of immune effector cells via immunosuppressive cytokines such as TGF-β or IL-10 (c) secretion of soluble ligands that block lymphocyte activation [18].

The complexity of cancer immunoediting provides opportunities to harness specific aspects of the immune response to induce tumor regression. For example, inhibition of tumor escape mechanisms could render tumor cells visible to the immune system, enabling immune-mediated destruction. Understanding of the role of polarized macrophage at the elimination and escape phases of cancer immunoediting also help to control the tumor progression and will be discussed in section 1.3.3.

1.3.3 Macrophage polarization

Monocytes are formed in bone marrow and then travel in blood stream for three days before infiltrating to different parts of the body where they mature into tissue resident phagocytosis cells called macrophages [19]. Tissue-resident macrophages are mostly named according to the tissue of residence such as alveolar macrophage in the lungs, osteoclast in the bone or microglia in the brain but their primary function are that of macrophages. These resident tissue macrophages proliferate to generate the mature macrophage and cover nearly all the body tissues as shown in figure 1.3[20].

These resident tissue macrophages can undergo polarization to fine tune its function based on the signal present in the tissue. Depending upon the stimuli macrophages polarized themselves

into M1 (classically activated macrophages) or M2 macrophages (alternatively activated macrophages) and discussed below and summarized in Table 1.1 [21].

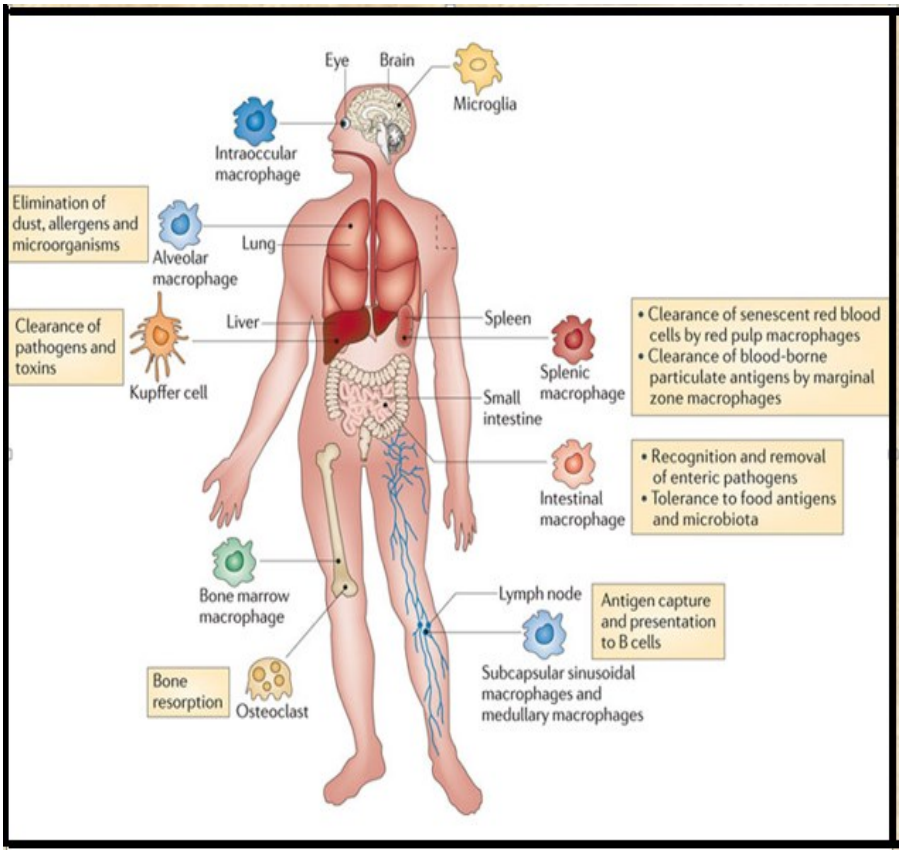

Figure 1.3: Development and differentiation of Macrophages.

Murry and Wynn, 2011

Nat Rev Immunol 11(11). 723-37[20] (Reproduce with permission).

M1 polarization is induced by microbial products like LPS or proinflammatory or Th1 cytokines like IFN-γ and GM-CSF. M1 macrophage has microbicidal and inflammatory properties (secreting IL-1β, TNF-α, IL-12, IL-6). They also produce toxic intermediates (reactive nitrogen intermediate, reactive oxygen intermediate) that kill tumor cells or microorganisms. When exposed to signals such as LPS and IFN-γ, they express opsonic receptors like Fcγ (CD16) and overexpressing the IL-1 receptor, major histocompatibility complex-II (MHC class II) and Toll-like receptor TLR2 and 4) [22].

M2 polarization is induced by anti-inflammatory or Th2 cytokines (IL-4, IL-13, IL-10), and have regulatory properties with no microbicidal activity. They contribute to tissue remodeling and repair, promotion of angiogenesis, and suppression of inflammatory responses. They suppress Th1 adaptive immune responses directly through the secretion of immunosuppressive cytokines (have low IL-12 and high IL-10 phenotype) and indirectly through the release of chemokines [22]. Mantovani and colleagues demonstrated that they were poor antigen presenting cells but showed great potential to suppress T cell activation and proliferation via TGF-β and IL-10. [23].

Table 1.1: Polarized macrophage induction, cytokine production, and function.

	M1 (Classical activation)	**M2 (Alternative activation)**
Induction	LPS, IFN-γ, GM-CSF	IL-4, IL-13, IL-10
Cytokine Production	IL-1β, TNF-α, IL-6, IL-12, RNI, ROI,	IL-10 TGF-β
Functions	Intracellular microbicidal activity Tumor suppression Th1 type response (pro-inflammatory) Immunostimulation Efficient Antigen Presenting Capacity	No microbicidal activity Tumor promotion Th2 type response (anti-inflammatory) Immunoregulation Angiogenesis Tissue remodeling

The composition of solid tumor mainly contains neoplastic cells, fibroblasts, endothelial cells, and immune cells. The only immune cells that infiltrate the tumor are usually macrophages. These macrophages are known as Tumor-associated macrophages (TAM) often representing up to 50% of the tumor mass [24]. Depending upon the tumor microenvironment and signaling the TAM polarized themselves into either M1 or M2 like macrophages and played a critical role in tumorigenesis.

1.3.4 Therapeutic targeting of TAMs

TAM mainly express the M2 polarization and perform a fundamental role in the tumor progression. To date, three different strategies, exist to counter the tumor progression.

(a) Inhibition of TAM recruitment to the tumor site: Trabectedin, a natural product derived from the marine organism *Ecteinascidia turbinata*, exhibited antitumor activity with cytotoxic effects on monocytes and macrophages, including TAMs. [25].

(b) Blockage of TAM proangiogenic functions: Vascular endothelial growth factor (VEGF) contributes to monocyte recruitment to a tumor and the neovascularization of tumors. Therefore, blocking of VEGF and its receptor is a promising strategy for blockage of TAM proangiogenic function. Specific inhibition of VEGF reduced macrophage infiltration into tumors, [26] thus VEGF neutralizing antibody therapies could decrease tumor metastasis.[27]

(c) Reversal of the TAM suppressive phenotype toward proinflammatory macrophages: Shifting the macrophage balance toward the anti-tumor phenotype is a third strategy to circumvent the pro-tumoral features of TAMs. Multiple studies indicated that the activation of Toll-like receptors (e.g., TLR9) stimulated polarization of macrophages toward anti-tumor activity by inducing an inflammatory mediator [28]. Indeed, therapy combining CpG, the ligand of TLR9, and the anti-

IL-10R antibody shifted infiltrating macrophages toward the anti-tumor phenotype and triggered innate immune responses.[29]

1.3.5 Importance of macrophage in tumor

All these attempts in above section were made to control the tumor by directly targeting the TAM progression toward the tumor or antagonizing the tumorigenesis effect produced by them. However, the effective targeting and delivering of the drug in the tumor vicinity is quite challenging. Inefficient targeting also leads to the undesirable effect to the normal cells. The current study focus on the efficient delivery of drug to these macrophages using the advantage of colloidal drug delivery system (nanoparticles) and its secondary toxicity effects. They are discussed in detail in the proceeding section.

1.4 Tuberculosis

Mycobacterium tuberculosis (M.tb) is a highly efficient pathogen, killing millions of infected people annually. The capacity of *M. tuberculosis* to survive and to cause disease is strongly associated with its ability to escape from the immune system of the host. Particularly, it possess the remarkable survival capacity in the hostile environment of macrophages. The deep understanding of its virulance strategies will help to develop the novel drug target strategies against infectious disease.

1.4.1 Mycobacterium tubercle pathogenesis

M.tb is the type of bacteira that can survive and replicate inside macrophage phagosomes. Upon infection of a host, *M.tb* is phagocytosed primarily by alveolar macrophages and can grow logarithmically for approximately two weeks until the adaptive immune response is activated and Interferon (IFN-γ) contributes to restricting mycobacterial growth. [30] *M.tb* continues to survive

as a successful pathogen avoiding complete clearance from the host by interfering with the infected macrophages, altering the cytokine and cytokine receptor expression profile and protecting its endosome from exposure to various innate antimicrobial activities. *M.tb* can persist comfortably for months, years or decades within the host. The infection can be divided into three different interrelated stages briefly describe below:

Ist Stage. The first stage is the aerosol transmission of *M.tb* containing droplets from an infected individual to a healthy individual. Once within the lungs, *M.tb* enters and resides within alveolar macrophages. The bactericidal capacity of the alveolar macrophages often kills but not completely eradicate the ingested bacilli. In most cases, macrophage contained the bacilli, and this initial suppression of infection partially depends upon the genetics of humans and on the inhaled *M.tb* strains. Primary infection involves the multiplication of M.tb in lungs and cause mild inflammation. Although, the alveolar macrophages are considered as effective barrier against pathogens but M.tb has evolved such mechanisms that evade the host immune response, thus survive in the macrophages. These survival mechanisms mainly include the blocking the reactive oxygen and nitrogen intermediates (RNIs and ROIs), triggering the anti-inflammatory response and production [31] and reducing the acidification of the *M.tb*-containing phagosome. [32,33]

2nd Stage: The next stage of infection is characterized by the emergence of cell-mediated immunity and the formation of granulomas. *M.tb* bacilli that are escaped from the bactericidal effects of alveolar macrophages will multiply and result in the destruction of alveolar macrophages. It will, in turn, attract blood monocytes and other inflammatory cells (i.e. neutrophils) to the site of infection. Monocytes mature to become antigen presenting alveolar macrophages and dendritic cells (DCs). They ingest, but not effectively kill the bacteria. At this step, *M.tb* grows and cause limited tissue damage. After 6–8 weeks of infection, antigen presenting

DCs travele to lymph nodes where it cause the activation of T lymphocytes. These activated T lymphocytes migrate to the site of infection, proliferate and form an early stage granuloma, where macrophages are activated and kill the intracellular *M.tb* [34].However, continuing T cell activation leads to the formation of granulomas and leads to that stage in which the infection (latency) persist and cause growth of bacteria and its spread to the surrounding tissue sites. At this juncture, more than 90% of infected people remain asymptomatic, but *M.tb* may survive within the alveolar macrophage. [35]

3rd Stage The final stage starts when latent and controlled *M.tb* infection is activated again. The two factors involved in this process include a decline in the immunity of host due to the genetic and environmental changes; and failure to develop immune signals. These circumstances cause the disruption of granuloma structure which eventualy results in lung cavitation [35-38]. The reactivation of this infection might also be due to the alterations in host chemokine/cytokines networks, stress, medication, and old age. [39,40]

1.4.2 Cytokines in the Immune response to M. tuberculosis

Innate immune recognition of *M.tb* by phagocytic cells leads to rapid production of pro- and anti-inflammatory cytokines. Janeway defines cytokines as "proteins released by cells that affect the behavior of other cells that bear receptors for them" [39]. These cytokines and chemokines recruit inflammatory cells to areas of infection, activate transmigrated cells, and coordinate the inflammatory and adaptive immune response to *M.tb*. Clearance of mycobacterial infections depends on cytokine networks established and maintained by macrophages. There are many cytokines involved in the immune response to *M.tb* and are describe as and tabulated in Table 1.

Tumor necrosis factor-α

Tumor necrosis factor-a (TNF-α) is a prototypic proinflammatory cytokine released from macrophages after interaction with *M.tb* or its derived components. After macrophage exposure, TNF-α undergoes cleavage by TNF-α-converting enzyme and is released from the cell as a trimeric surface molecule. In combination with IFN-γ, they play a crucial role to activate the macrophage to produce nitric oxide synthase 2 to generate nitric oxide which kill the intracellular harboring *M.tb* inside the macrophage.[41,42].

Mice shows an increased susceptibility to *M.tb* infections when they have a deficiency in TNF-α production and or lack TNF-α receptors [43,44]. In other studies, the absence of TNF-α in mice leads to a delay or deficient granuloma formation which eventually lead to a wide dissemination of *M.tb* [45].

In humans, there is proof that TNF-α plays a major role in host defense to *M.tb.* The significance of TNF-α in controlling human *M.tb.* was realized when anti-TNF-α therapy in rheumatoid patients led to reactivation of latent TB infections [40].

Interleukin-1β

IL-1β is a proinflammatory cytokine that is produced by infections and proinflammatory conditions [46]. IL-1β is released in the cell in an inactive precursor form (pro-IL1β- IL-1β) and activated after cleavage by Caspase-1 Conversion of pro-IL-1β to IL-1β can occur with numerous bacterial stimuli, including *M.tb* and its bacterial products within the cytoplasm. Once secreted, IL-1β acts primarily through IL-1R type I receptor, which further activates the expression of other proinflammatory cytokines. The importance of IL-1β in *M.tb* infection is established by knockout

mice studies. Animals that have both IL-1β and IL-1α deleted, form larger granulomas after infection and are not capable of removing the mycobacteria as efficiently as wildtype mice [47].

IFN-γ and IFN-γ Receptors

IFN-γ activates macrophages, enhances their production of proinflammatory cytokines, and up-regulates their surface expression of cytokine and chemokine receptors and enhances its antigen presentation [48].

IFN-γ deficient mice disseminate the *M.tb* infection faster when infected via intravenous or aerosolized route [49]. In another study mice deficient in IFN-γ failed to produce nitric oxide due to low iNOS expression and exhibited unrestricted *M.tb* growth and tissue necrosis with mice go though *M.tb* infection faster [50].

The patients with clinically active tuberculosis report a low level of IFN-γ when compared with latent tuberculosis [51].

Interleukin-10

IL-10 is a cytokine produced by activated macrophages, monocytes, DC and other T- cell subsets [52], IL-10 is known to suppress proinflammatory cytokine responses by the innate immune and adaptive immune system.IL-10 is also thought to play a major role in many bacterial infections [53]. Studies carried out in mice have identified that IL-10 may not be critical for susceptibility to the initial infection with *M.tb* but may play a role in reactivation of the latent disease [54,55].

Mouse model showed that IL-10 alone played a pivotal role during the chronic/latent stage of pulmonary tuberculosis. [56]. Recent study suggest that IL-10 may interfere with *M.tb* persistence by stalling phagosome maturation in human macrophages [57]. Under these

circumstances, the benefits of IL-10 are controversial, as IL-10 seems to limit tissue damage by suppressing inflammation along with its contribution towards the host environment that allows *M.tb* to persist, and thus IL-10 directly cause the reactivation of TB.

Table 1.2: Cytokine production and function in the immune response to Mycobacterium Tuberculosis. Summarize from [58,59].

Cytokine	**Producer**	**Functions**
TNF-α	Macrophages, Dendritic Cells and T-lymphocytes	Synergize with IFN-γ to enhance NOS2 activity
IL-1β	Macrophages, Monocytes Dendritic Cells	Essential for the acute phase response Facilitates T lymphocyte expression of IL2R and IL-2 release
IFN-γ	T-lymphocytes and Natural killer cells	Stimulates Th1 response Activates macrophages Sufficient to control *M.tb* infection
IL-10	Macrophages, T-lymphocytes	Macrophage deactivation and downregulation of IL-12 and IFN-γ Reduces CD4+ T-cell response

1.4.3 Importance of macrophage in tuberculosis

Macrophages resident in lung tissue phagocytose extracellular bacteria and secrete cytokines, chemokines, and proteases to regulate the proinflammatory response and counter the intracellular *M.tb* infection. Mice lacking such secreted entities (e.g., IL-1β, IFN-γ, IL-12, TNF-α) quickly succumb to infections [60]. The same cytokines help to control human Mtb infections, and their downregulation through the production of IL-10 or TGF-β can be detrimental for the spread of *M.tb* infection [61].

Proinflammatory cytokines are necessary for a host response to *M.tb* infection. The chemokines RANTES, MIP1-α, MIP2, MCP-1, MCP-3, MCP-5, and the IFN-γ-induced protein are also released upon macrophage infection with *M.tb*, and the receptors for chemokines CCR5, RANTES, MIP1-α, and MIP1-β are expressed. Some of these entities have been found to be essential for protection against Mtb infection as well as for granuloma formation [61].

Th1 cytokines are also thought to be necessary for a potent response to *M.tb* infection. Reactivation of latent tuberculosis has also been associated with a switch from a Th1 response to a Th2 response [62]. In *M.tb* infection mice, Th2 cytokine treatment deprives macrophages of their killing mechanisms leading to increased *M.tb* replication [63].

1.5 Targeted drug delivery

A major goal in the pharmaceutical industry is to synthesize or discover chemical entities that will target a specific region in the body with high precision and accuracy. In late 1970, one approach that has drawn lots of attention for targeted drug delivery were colloidal drug delivery system. They are further classified to nanoparticles, nanocapsules, micelles, liposomes, branched polymers and layer by layer assemblies as shown in figure 1.4.

Figure 1.4: Classification of colloidal drug delivery system, adapted from [64] (Reproduce with permission).

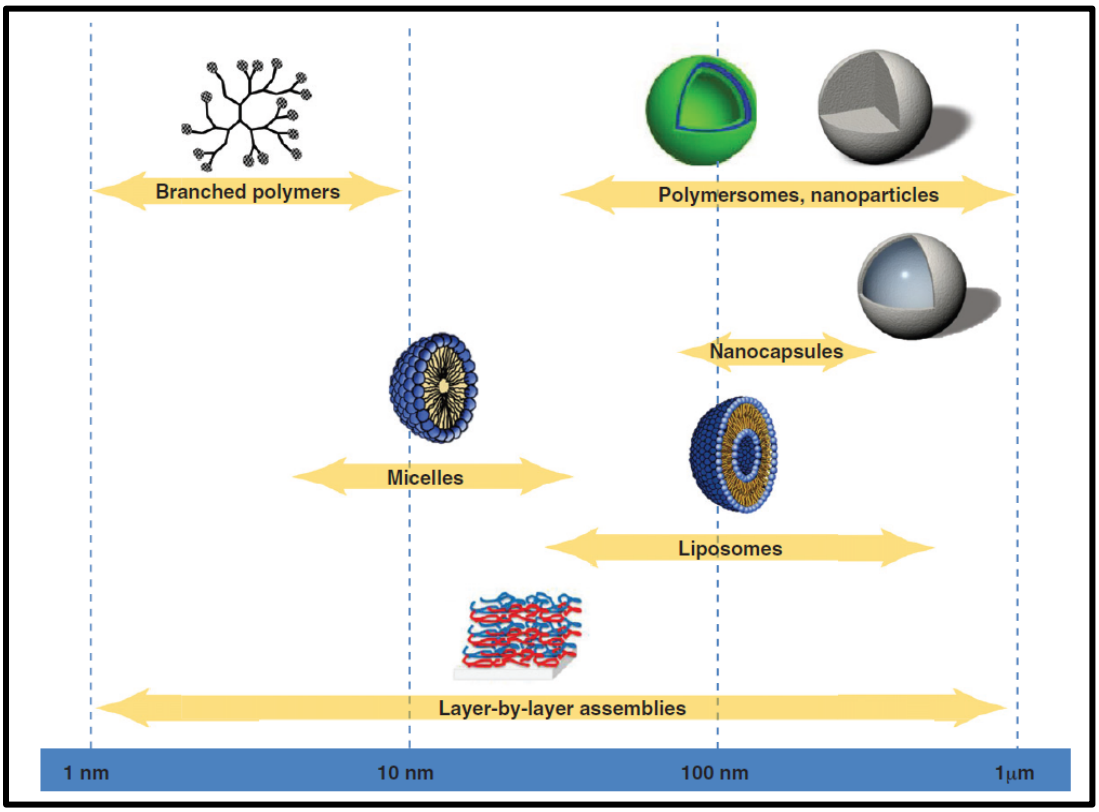

Particle Size ⟶

Nanoparticles are more frequently studied in the last few decades for targeted drug delivery. In 1984, it was found that nanoparticles end up in the liver cell after intravenous injection to rabbits [65]. The associated of nanoparticles is 100 times greater in the Kupfer cell (macrophage in the liver) than the primary liver parenchyma cells [66]. In another study following intravenous injection, nanoparticles are cleared rapidly from the blood (usually within a minute) by Kupfer cells (macrophage in the liver) [67]. These finding challenged the use of nanoparticle as target drug delivery system. Different attempts were made afterward to escape the macrophage uptake

and enhance the nanoparticles circulation. Briefly, these attempts include the understanding of macrophage cellular uptake mechanism and nanoparticles characteristics such as charge, size, and coating [67]. By modifying this parameter, the scientist can effectively achieve long circulating nanoparticles [67].Stealth nanoparticles circulate for prolonged time in plasma from 2 to 24 hours in mice and rats, and this can be extended for up to 45 h in human depending upon the particle size and coating materials [68].

However, with the advancement of science and the significance of macrophages in tumor and tuberculosis (discuss earlier), the decade-old belief that nanosized drug delivery systems need to be protected from phagocytosis needs to be reassessed [67]. The focus of the current study has been macrophage targeting with nanocarriers. This approach is taking advantage of the disadvantages of colloidal drug delivery system and its interaction with macrophage. The targeting mode can be active or passive according to the physiological environment of the disease, and will be discussed in section 1.5.1 and 1.5.2.

1.5.1 Active targeting

Active targeting systems can be achieved by the surface decoration of the delivery vehicle with a ligand that selectively interacts with receptors on the surface of target macrophages. Naher et al. reported that surface factionalized gelatin nanoparticles showed efficient amphotericin delivery to macrophages for effective treatment of leishmaniasis [69]. Al-Hallak et al. reported macrophage nanoparticle interaction using isothermal microcalorimetry method using four different nanoparticles. Mannosylated decorated gelatin nanoparticle showed the maximum interaction and cellular uptake among the nanoparticles [70]. Nimje et al. reported that the macrophage cellular uptake of rifabutin loaded mannose decorated solid lipid nanoparticles was six times higher than the rifabutin loaded solid lipid nanoparticles that were not decorated with

mannose [71]. Nahar and Jain developed different mannose-decorated, engineered PLGA Poly (lactic-co-glycolic acid) nanoparticles for efficient delivery of amphotericin B to macrophages. The mannose decorated PLGA nanoparticles showed good uptake and more disposition in macrophage-rich organs, delivering an anti-leishmanial drug efficiently to macrophages compared to plane PLGA nanoparticles [72].

1.5.2 Passive targeting

Due to an abnormal rate of cellular division and growth, cancer is associated with enhanced vascularization via angiogenesis [73]. Tumor vasculature results in leaky vessels with gaps that can range from 100 nm to 2 μm depending on the type and the size of the tumor [74]. Tumors also suffer from poor lymph drainage due to a lack of a well-defined lymphatic system [75]. This leaky vasculature combined with poor lymphatic drainage results in an enhanced permeability and retention (EPR) effect [76] at the tumor site. Nanoparticles with a mean size of around 100-200 nm are attractive candidates for tumor targeting. Moreover, the poor lymph drainage also contributes towards the significant retention of nanoparticles at the tumor site.

Bhardwaj et al. synthesized Paclitaxel-loaded PLGA nanoparticles stabilized with cationic surfactants and applied this formulation to increase the oral bioavailability of the drug to treat chemical-induced breast cancer in rats. Their studies showed that nanoparticles of 120 nm used for the rats experiment had improved efficacy compared to IV native paclitaxel. EPR explain the effectiveness of these nanoparticle formulations [77]. Danhier et al. reported that nanoparticles loaded with paclitaxel could reach a tumor site and maintained an effective therapeutic concentration for an extended period. The authors postulated that the efficient migration and stasis of the nanoparticles were due to EPR of nanoparticles at the tumor site. These paclitaxel nanoparticles were more effective than Taxol® at delaying tumor growth [78].

1.6 Primary and Secondary toxicity

1.6.1 Primary toxicity

Primary toxicity (PT) is defined as the immediate effect produced by a foreign substance including nanoparticles after interaction with a cell or its components. For example, inorganic nanoparticles (silver nanoparticle) have shown a primary toxicity effect after interaction with HepG2 human hepatoma cells by interfering with mitochondrial functions, lactate dehydrogenase levels (cause membrane leakage) and DNA function. PT is characterized by induction of abnormal cellular morphology (micronucleus formation, bi-nucleated cells), displaying cellular shrinkage, and acquisition of an irregular shape depending upon dose [79].

Silica nanoparticles have also shown primary toxicity effects by decreasing the cell viability of A-549 cells in a dose-dependent manner. The effect is mainly produced by elevated reactive oxygen species (ROS), reduced glutathione and increased lipid peroxidation levels that leads to an increase in oxidative stress and damage in the cellular membrane [80].

1.6.2 Secondary toxicity

In contrast to primary toxicity, secondary toxicity effects are produced in a delayed manner in response to biodegradation of nanoparticles in the macrophages. These effects are characterized by the release of different cytokines and chemokines i.e. (TNF-α, IFN-γ, IL-1β, IL-10) [81,82] which play a significant role in acute and chronic stages of inflammation.

1.7 Rationale and Hypothesis

Illum and Davis, in 1984, found that nanoparticles mostly accumulate in the liver and spleen cells after intravenous injection to rabbits [65]. The accumulation of nanoparticles is 100 times greater in the Kupfer cell than the primary liver parenchyma cells [66]. Another study has shown that, following intravenous injection, nanoparticles are rapidly cleared from the blood (usually within a minute) by Kupfer cells [67]. These finding challenged the use of nanoparticle as target drug delivery system. Various stealth nanoparticles were synthesised to overcome this drawback to increase the duration of nanoparticle in blood circulation. It includes different coating techniques, modification in the surface charge and size or decorating the nanoparticles surface with various ligands. [67]

Paul Ehrlich first proposed the ability of the immune system to identify and destroy tumor cells in 1909 [6]. After 50 years, in 1957, Burnet and Thomas introduced the concept of cancer immune surveillance by predicting that lymphocytes were responsible for the elimination of continuously arising cancer cells [7]. In late 20^{th} century, the idea of immune surveillance was substituted with a new term of cancer immuno-editing by Schreiber and colleagues who proposed that immunity, not only protects a host from tumor development but also promotes tumor growth [8,9]. In 1992, Montovani et al for the first time highlighted the significance of macrophage in neoplastic cells and proposed "macrophage balance hypothesis". He defined the complex dual functionality of tumor associated macrophages (TAMs) and its role in tumor progression depending upon inflamed microenvironment [83,84]. Since then, different attempts were made to revert the polarization of macrophages from pro-tumor response to anti-tumor response in cancer microenvironments. [28,29]

Historically, the role of macrophages in immune activation is well known since 1960 when Mackaness et al reported an enhanced antimicrobial activity of macrophages in mice after infecting them with mycobacterium bovis bacillus Calamette Guerin (BCG) as compared to non treated mice [85]. In tuberculosis, mycobacterium tubercle invades and logarithmically replicate inside of macrophages. Mycobacterium survival inside the macrophage primarily depends on the host immune response (i.e. the intrinsic microbicidal capacity of host macrophage) as well as the virulence of the mycobacterium strain. At the initial infection phase, macrophages cause mild inflammation in lungs to overcome the mycobacterium infection. However, the mycobacterium also evolved a different method to revert the inflammatory responses by inhibiting the production of reactive oxygen and nitrogen intermediate species [31] and reducing the acidification of the mycobacterium-containing phagosome. [32,33]

The current study utilised these two unique features of macrophages. Firstly, the ability of cellular uptake of nanoparticles by macrophages (a well-known disadvantage) was used as an advantage to target macrophages with drug-loaded nanocarriers in murine alveolar macrophages. Two different nanocarriers (micelles and nanoparticles) were investigated in the study. HA-TS and RIF-HA-TS micelles were synthesized and studied for both cellular uptakes as well as active targeting while Gelatin and PIBCA drug-loaded nanoparticles were studied only for cellular uptake by macrophages.

Secondly, the phagocytosis of nanocarriers by macrophage was characterized by the release of variety inflammatory mediators in the microenvironment, including type 1 cytokines or type 2 cytokines (secondary toxicity) which play a significant role in acute and chronic stages of inflammation.

Hypothesis:

Nanocarriers trigger secondary toxicity, an inflammatory response, in macrophages - Is there a benefit?

The study is primarily taking advantage of macrophage phagocytosis property and its secondary toxicity effect after interaction with the nanocarrier. It investigated the macrophage's ability to uptake nanocarriers by active or passive transport mechanisms. The study investigated the secondary toxicity effects to produce proinflammatory and anti-inflammatory responses and its implication on disease conditions like tuberculosis or cancer.

1.8 Objectives

The study covers the following objectives

(i) To study if two different colloidal drug carriers with active and passive transport mechanisms (micelles/nanoparticles) can trigger secondary toxicity in macrophages.

(ii) To analyze what possible consequences secondary toxicity effects (cytokine profiling: proinflammatory vs. anti-inflammatory) might have on the infection of macrophages with mycobacteria tuberculosis.

(iii) Investigate the effect of secondary toxicity in macrophages cocultured with lung cancer cells mimicing tumor microenvironment.

(iv) To study the effect of different anti-inflammatory drugs on the microenvronment between macrophages and cancer cells.

Chapter 2 discusses in detail the synthesis and characterization of a new colloidal drug delivery system (micelles) and **Chapter 3** covers the application of these micelles after interaction with macrophages to induce the secondary toxicity effect. Both these chapters try to achieve the our **first objective**. The data of these chapters has already been published in ***Journal of biomedical nanotechnology*** with the title of ***Hyaluronic Acid-Tocopherol Succinate-Based Self-Assembling Micelles for Targeted Delivery of Rifampicin to Alveolar Macrophages.*** *June 2015, 11:1283-1311.*

In **Chapter 4**, the synthesis and characterization of two different biodegradable nanoparticles are discussed. It also covers the cell viability studies and explores nanoparticles-macrophage interactions to induce secondary toxicity. The chapter briefly cover our **first and second objective**. The data of these chapters has already been published in ***Journal of Therapeutic Delivery*** with the title of ***Immune Response to Anti-tuberculosis Drug loaded Gelatin and Polyisobutyl-cyanoacrylate Nanoparticles in Macrophages.*** *April 2016, 07:04: 213-228*

In **Chapter 5** we synthesized and characterized two different biodegradable nanoparticles. The role of secondary cytotoxic in a macrophage-lung cancer co-culture model was investigated. The contents of this chapters accomplish our **third objective** i.e. to analyze the secondary toxicity effects in a microclimate of a lung cancer model. Additionally, **Chapter 5** also explores the secondary toxicity effect trigger by nanoparticles in the presence and absence of anti-inflammatory drugs. It completes our **fourth objective**. The data of these chapters has been publication in ***Journal of Molecular Pharmaceutics*** with the title of ***Inflammation caused by nano-sized delivery systems: Is there a benefit?*** *August* 2016, *13* :9: :3270–3278

Chapter 2

Synthesis and *in vitro* characterization of Hyaluronic acid tocopherol succinate-based self-assembling micelles.

This study has already been published as Yuan Gao, Muhammad Khan Sarfraz et al. Hyaluronic Acid-Tocopherol Succinate-Based Self-Assembling Micelles for Targeted Delivery of Rifampicin to Alveolar Macrophages in Journal of Biomedical Nanotechnology. June 2015, 11:1283-1311

Abstract

The *in vitro* synthesis and characterization of new hyaluronic acid–tocopherol succinate based micelles was completed. These new amphiphilic conjugates were synthesized by chemical conjugation of hydrophobic α-tocopherol succinate (TS) to hydrophilic hyaluronic acid (HA). The micelles were characterized by FTIR and NMR to reconfirm the incorporated chemical structural changes during synthesis of micelles. Morphological changes were studied by Zetasizer, TEM, DSC and X-ray diffraction techniques. Colloidal stability of micelles in PBS and serum, rifampicin drug loading and *in vitro* drug release from micelles at different pH were also assessed. The results showed that HA-TS conjugates form self-aggregating micelles in an aqueous medium via hydrophobic interactions between TS subunits. Both the FTIR and NMR results indicated that TS-NH_2 were successfully grafted onto the HA chain. The TEM studies revealed the morphology of HA-TS_7 micelles and observed spherical micelles with a narrow distribution of particle size (PDI < 0.5). Mean particle size was in the range of 212–294.6 nm with various degree of substitution (DS) of the hydrophobic moiety. The DS of HA-TS micelles, made the inner core of the micelle more hydrophobic with TS and lead to an improved drug loading capacity. The DSC analysis showed that RIF was incorporated in RIF-HA-TS_7 micelles. The X-ray diffraction spectrum revealed that there was no RIF crystal in RIF-HA-TS_7 micelles. The micelles were stable for two weeks at 37 °C. The HA-TS micelles were efficiently encapsulated with rifampicin (RIF) with drug loadings of 70.7–79.1% (w/w). The *in vitro* release curves showed that the incorporated RIF was sustained released from RIF loaded HA-TS (RIF-HA-TS) micelles.

2.1 Introduction

Macrophages are the key cells in the immune response against mycobacteria and also provide a niche for Mycobacterium tuberculosis (MTB) multiplication [86]. Thus, anti-MTB drugs that target the macrophage can be more efficient in the treatment of MTB. Currently, nanotechnology is one of the most promising approachs for targeted drug delivery. Due to their nano-size dimensions and ability to display a targeting moiety to ligands, a nano delivery system can deliver therapeutic moieties more selectively with better efficiency for the treatment of MTB [87-91].

Hyaluronic acid (HA) containing micelles as a drug carrier for MTB treatment has not been reported. Macrophages are known to express HA receptors such as CD44 [92,93], which is also a macrophage binding site for MTB [94]. Due to CD44 receptors on its outer membrane, a macrophage becomes a target cell for MTB treatment using an HA modified nano-carriers. HA is also shown to induce inflammatory gene expression in the alveolar macrophages [92]. Due to unique properties of HA in the activation process of alveolar macrophages, the aim is to develop a hydrophobic hyaluronic acid α- tocopherol succinate (HA-TS) nano-carriers. TS is a well-known hydrophobic vitamin analog composed of three domains, including a hydrophobic domain [95] that accounts for its solubilization capacity.

In this chapter, we discuss in detail the synthesis of HA-TS micelles and its characterization and morphology studies using Zetasizer, TEM, DSC and X-ray diffraction techniques. Colloidal stability of micelles had also been discussed in PBS and serum. The RIF-HA-TS micelles were evaluated for drug loading and *in vitro* drug release at different pH.

2.2 Materials and Methods

2.2.1 Materials

Sodium hyaluronate (HA-Na) (average Mn = 16900) was obtained from Lifecore Biomedical (Chaska, MN). Dimethylformamide (DMF), acetone, 1-ethyl-3(3-dimethylaminopropyl), carbodiimide hydrochloride (EDC), formamide, dichloromethane (DCM), α-tocopherol succinate (TS), *N*-hydroxysuccinimide (NHS), 3-(4,5-dimethylthiazol-2-yl)-2,5-diphenyl tetrazolium bromide (MTT), cytochalasin B and ethylenediamine (EDA) were obtained from Sigma-Aldrich (Ontario, Canada). RIF was purchased from PCCA (Houston, TX).

2.2.2 Methodology: Synthesis and characterization

2.2.2.1 Synthesis of HA-TS

The carboxyl group of α-tocopherol succinate (TS) was first converted to the amine group in the presence of ethylene-di-amine (EDA), resulting in the formation of amino ethyl tocopherol succinate (TS-NH_2). Then, the HA-TS conjugate was synthesized by coupling the acid of HA with the terminal amine of TS-NH_2 in the presence of carbodiimide hydrochloride (EDC) and (*N*-hydroxysuccinimide) NHS. The detailed procedure was described below in Fig. 2.1.

First, tocopherol succinate, TS (0.2 mmol), was dissolved in 2 mL of DCM (dichloromethane) and mixed with EDC (0.24 mmol) in 1 mL DCM and NHS (0.24 mmol) in 0.5 mL of DMF. The three solutions were mixed and stirred for 12 h at room temperature (RT) under a nitrogen atmosphere in the absence of light. The reaction solution was slowly added into a solution of EDA (6 mmol) in 2 mL DMF. The molar ratio between succiniimido-TS and EDA was approximately 1:30. After being stirring for eight hours, the mixture was washed several times

with excess ddH_2O. The organic layer was dried over anhydrous sodium sulfate for 1 h, filtered and concentrated under a vacuum at RT to obtain TS-NH_2.

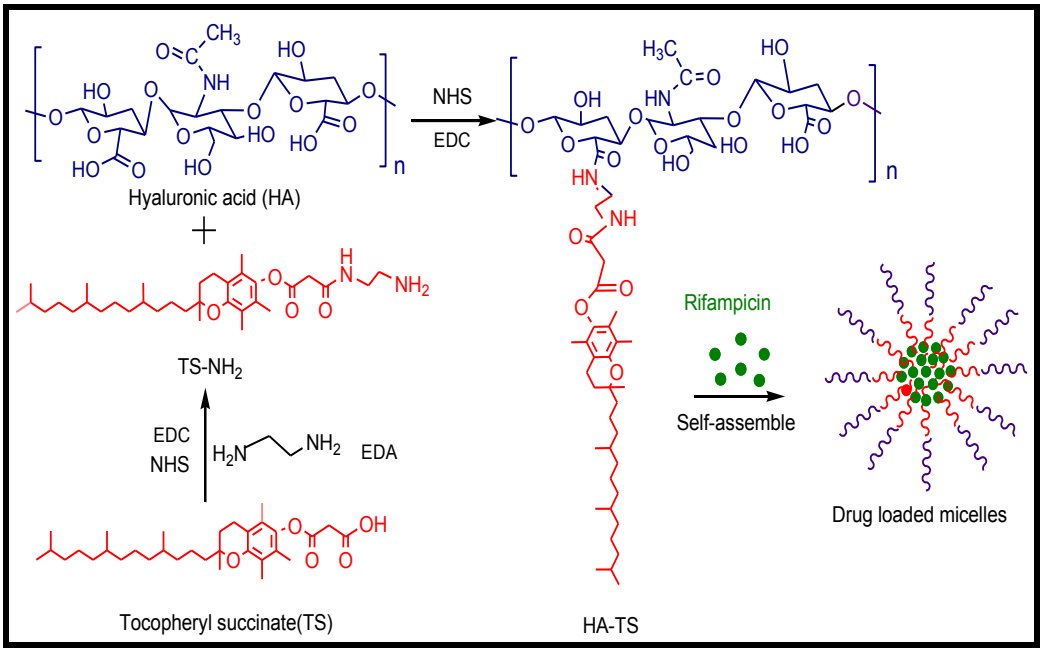

Figure 2.1: Synthesis of HA-TS conjugates and structure of RIF-loaded HA-TS micelles in aqueous solution.

HA-Na (5 μmol) was then dissolved in formamide in the presence of EDC (90 μmol–210 μmol) and NHS (90 μmol–210 μmol) for 30 min. Then, a solution of TS-NH_2 (75 μmol–175 μmol) in DMF was added slowly and the reaction mixture was stirred for 24 h at RT under a nitrogen atmosphere in the absence of light. Furthermore, the reaction mixture was extensively dialyzed with ddH_2O /methanol (1:3 *v/v*) and ddH_2O in dialysis bags with a MW cut-off of 12–14 kDa (Spectrum, CA) for two days. The resulting solution was filtered through a membrane filter (pore size: 0.45 μm, Millipore) and lyophilized.

The structure of the product HA-TS was confirmed by a Nicolet Magner 550 infrared (IR) spectrophotometer (Thermo Electron Co.Waltham, MA) in the wavelength range 500–4000cm^{-1} and ^{1}H HMR at 300 MHz (Varian, CA).

2.2.2.2 Preparation of self-assembled micelles

RIF-HA-TS micelles were prepared using the following procedure. Briefly, HA-TS conjugates (1 mg) were dissolved in 1 mL of methanol/ddH_2O (1:1 *v/v*). A predetermined amount of RIF (2-5 mg) in methanol solution was added slowly to the HA-TS solution. The resulting mixture was dialyzed for 2 h with ddH_2O or PBS using dialysis bags (MWCO 12–14 kDa). After that, the solution was filtered through a 0.45 μm membrane filter. The blank HA-TS micelles were prepared by dissolving the HA-TS conjugate in methanol/H_2O (1:1 *v/v*), followed by dialysis with ddH_2O or PBS for 2 h, and later on filtration through a 0.45 μm membrane filter.

2.2.2.3 Characterization of HA-TS micelles

2.2.2.3.1 Fluorescence spectroscopy

The *critical micelle concentration (CMC).* The CMC of amphiphilic HA-TS micelles was determined by fluorescence spectroscopy using pyrene as the probe. Briefly, 1 mL of 6.0×10^{-7}M pyrene solution in acetone was added to a series of 10 mL volumetric flasks and the acetone was evaporated. HA-TS conjugate solutions (10 mL each) of various concentrations (1×10^{-4} to 0.5 mg/mL) were added to the volumetric flasks and sonicated for 30 min. The samples were incubated at 50 °C for 1 h and left to cool at RT. Pyrene excitation fluorescence spectra were recorded from 300-400 nm by using a MP-1 fluorescence spectrophotometer (Photon Technology International, London, UK) with an emission wavelength of 390 nm. The slit-width of both excitation and emission was 3 nm. The fluorescence intensities of the peaks at 336 nm (I_1) and 347 nm (I_3) were

extracted from the spectra. The CMC was estimated as the cross-point by extrapolating the intensity ratio I_3/I_1 (I_{347}/I_{336}) at low and high concentration regions**.**

2.2.2.3.2 Dynamic light scattering (DLS) and TEM

The particle size and distribution of micelles were measured by DLS using a Malvern Zetasizer HSA 3000 (Worcestershire, England). All DLS measurements were performed at 25 °C at a scattering angle of 90°. The morphology was observed by a JEM-2010 transmission electron microscopy (TEM, JEDL, Japan) at an accelerating voltage of 200 KV. Briefly, samples were mounted on a copper grid coated with carbon thin film and observed by TEM after air-drying.

2.2.2.3.3 Differential scanning calorimetry (DSC)

DSC patterns of the free RIF, blank HA-TS_7 conjugate and freeze dried RIF-HA-TS_7 micelles along with a physical mixture of free RIF and blank HA-TS_7 conjugate (RIF/HS-TS_7) were performed using a DSC Star system (Mettler Toledo, Schwerzenbach, Switzerland). The physical mixture was prepared by mixing free RIF with blank HA-TS7 conjugate (7:3 *w/w*) thoroughly in the motor. The temperature of the DSC module was equilibrated at 400 °C.

2.2.2.3.4 X-ray diffraction (XRD)

The X-ray diffraction (XRD) spectra of free RIF, blank HA-TS_7 conjugate and freeze dried RIF-HA-TS_7 micelles were determined using an Ultima-IV X-ray diffractometer (Rigaku Americas, Woodlands, TX).

2.2.2.3.5 Colloidal stability

The stability of the HA-TS and RIF-HA-TS micelles were studied using PBS and bovine serum albumin (BSA) as reported by Yang *et al.* [96]. At pH 7.4 PBS, the micelles (1mg/mL) were prepared as described in the previous section. The stability of the micelles in the presence of proteins was assessed. In brief, HA-TS micelles in pH 7.4 PBS (2 mg/mL) were mixed with an

equal volume of 10% *w/w* BSA dissolved in PBS. The mixture was incubated at 37 °C. The average diameter of the resulting samples was measured as discussed earlier.

2.2.2.4 Drug loadings

The amount of RIF encapsulated in HA-TS was determined by HPLC experiments. We used a reversed-phase C18 column (LiChrocart–LiChrospher 100 RP-18.5 μm, Merck, Darmstat, Germany). The mobile phase comprised of a mixture of methanol and 10 mM ammonium acetate (60:40 *v/v*) and was delivered in 20 μL injections at a flow rate of 1.00 mL/min [97]. A 2 mg sample of RIF-HA-TS was dissolved in 50 mL of methanol/ddH_2O (1:1 *v/v*) followed by filtration through a 0.45 μm membrane filter. The column effluent was detected at 337 nm with an ultraviolet detector (Dynamax UV-1, Rainin). The drug loading was defined as the amount of drug encapsulated per gram of drug-loaded sample.

2.2.2.4.1 In vitro drug release

The *in vitro* drug release profiles of RIF-HA-TS micelles were evaluated using a membrane diffusion system [98]. In detail, RIF-HA-TS micelles with nearly 5 mg RIF were placed into a 2 mL flat-bottomed plastic cell (with an internal diameter of 2 cm) mounted with a 12–14 kDa molecular weight membrane at the bottom. The cells were fixed on the motor shaft of USP dissolution apparatus I (VanKel, NC). *In vitro* release was performed under sink conditions at 37 °C and 100 rpm in 100 mL of buffer. The buffer pH values were selected to simulate the physiological pH (7.4) and endosomal pH of alveolar macrophages (5.2) [99]. At designated time intervals, 1 mL of the sample was collected, and the medium was replenished. The released drug was measured by HPLC and the experiments were performed in triplicate.

Similarity factor was used to compare the difference of dissolution profile of RIF from HA-TS at different data point as below.

$$f_2 = 50\mathrm{Log}\left\{\left[1+1/n\sum_{t=1}^{n}(R_t - T_t)^2\right]^{-0.5} \times 100\right\}$$

Where n is the number of dissolution samples taken, R_t and T_t are the individual percentages dissolved at each time point for the references and test dissolution profiles respectively and f2 value between 50 and 100 suggests that the data of two dissolution profiles are similar.

2.2.2.5 Statistical analysis

The results were shown as the mean ± S.D. Differences were considered statistically significant at $p < 0.05$. A student's t test was used for the statistical analysis.

2.3 Results and Discussion

2.3.1 Characterization of HA-TS conjugates - IR and HNMR

In an attempt to prepare the amphiphilic HA conjugates, hydrophilic HA was chemically conjugated to hydrophobic TS via an EDA linker (Fig. 2.1). The three conjugates (HA-TS_7, HA-TS_8, and HA-TS_{10}) with different ratios of TS to HA were synthesized and structures were confirmed by ^{1}H NMR and IR analyses.

FTIR: The characteristic IR bands of HA and HA-TS are shown in Fig. 2.2. In Fig.2.2 (A) the absorption bands at 3365 cm^{-1} correspond to the OH of HA. Two bands at approximately 1617 cm^{-1} and 1407 cm^{-1} are attributed to the COO^{-1} of HA and bands at 1017 cm^{-1} are attributable to the stretching of the C-O group of HA [100]. The spectrum of HA-TS shows an amide C=O bond at approximately 1635 cm^{-1} Fig.2.2 (B). This band demonstrates the formation of an amide C=O bond between HA and TS-NH_2. The broad band centered at 3376.7 cm^{-1} corresponds to the OH of HA, NH of HA and NH of TS-NH_2. Also, the bands at 2926.7 cm^{-1} and 2868.4 cm^{-1} represent asymmetric and symmetric stretching vibrations of $–CH_2–$ and $–CH_3$ of TS, respectively [95,101]. These results suggest that TS-NH_2 was conjugated with HA. The chemical structures of HA-TS conjugates were also confirmed using ^{1}H NMR. The spectra of native HA in D_2O and HA-TS in DMSO-D_6/D_2O (1:1 *v/v*) are presented in Fig. 2.3 (A). The peak at 2.0 ppm corresponds to the methyl protons of the *N*-acetyl group (3H, $NHCO–CH_3$) of HA and broad multiplex between approximately 3.2 and 3.9 ppm corresponds to the signals of the protons in the sugar rings [102]. Compared with the spectrum of HA (Fig. 2.3(A)), HA-TS (Fig. 2.3(B)) clearly shows additional signals at 0.7 ppm, 1.3 ppm, 2.2 ppm, 2.7 ppm and 3.3 ppm. These signals can be attributed to the methyl protons (12H, $–CH_3$) on the chain of TS, the

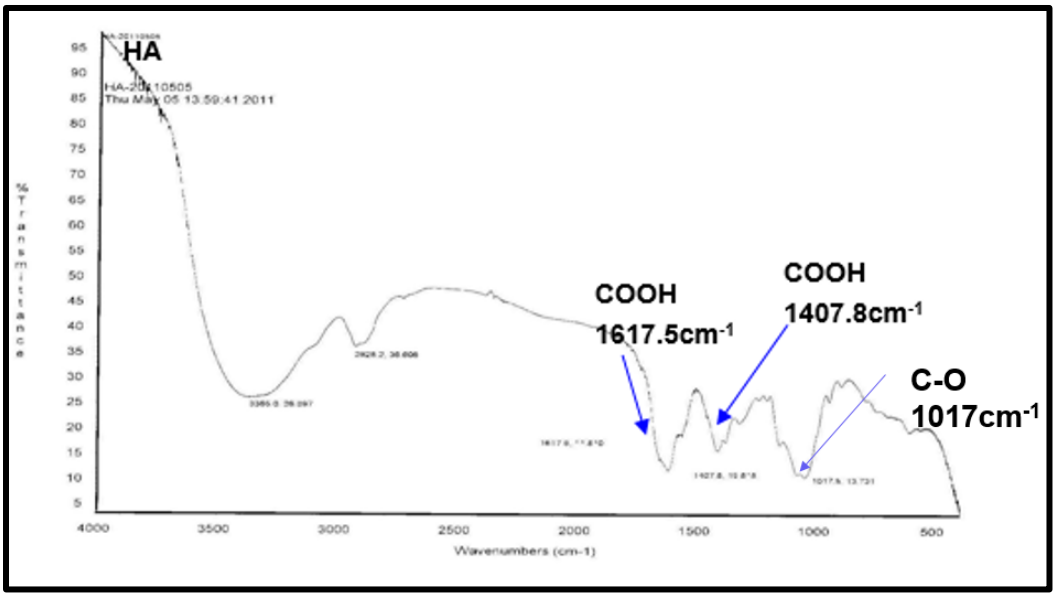

Figure 2.2: (A) FTIR Spectra of HA

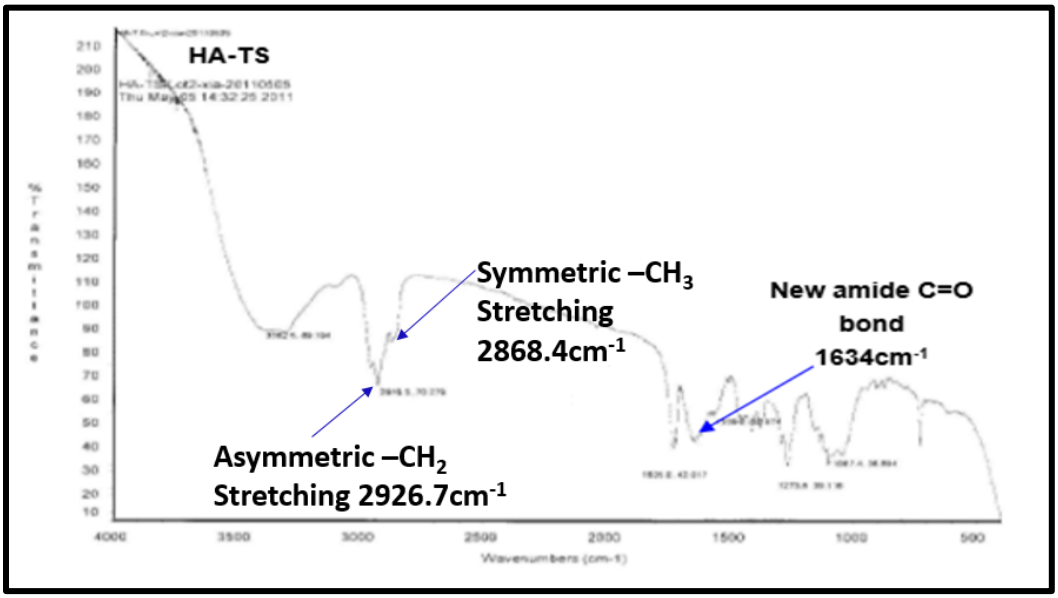

Figure 2.2: (B) FTIR Spectra of HA-TS conjugate.

^{1}H NMR

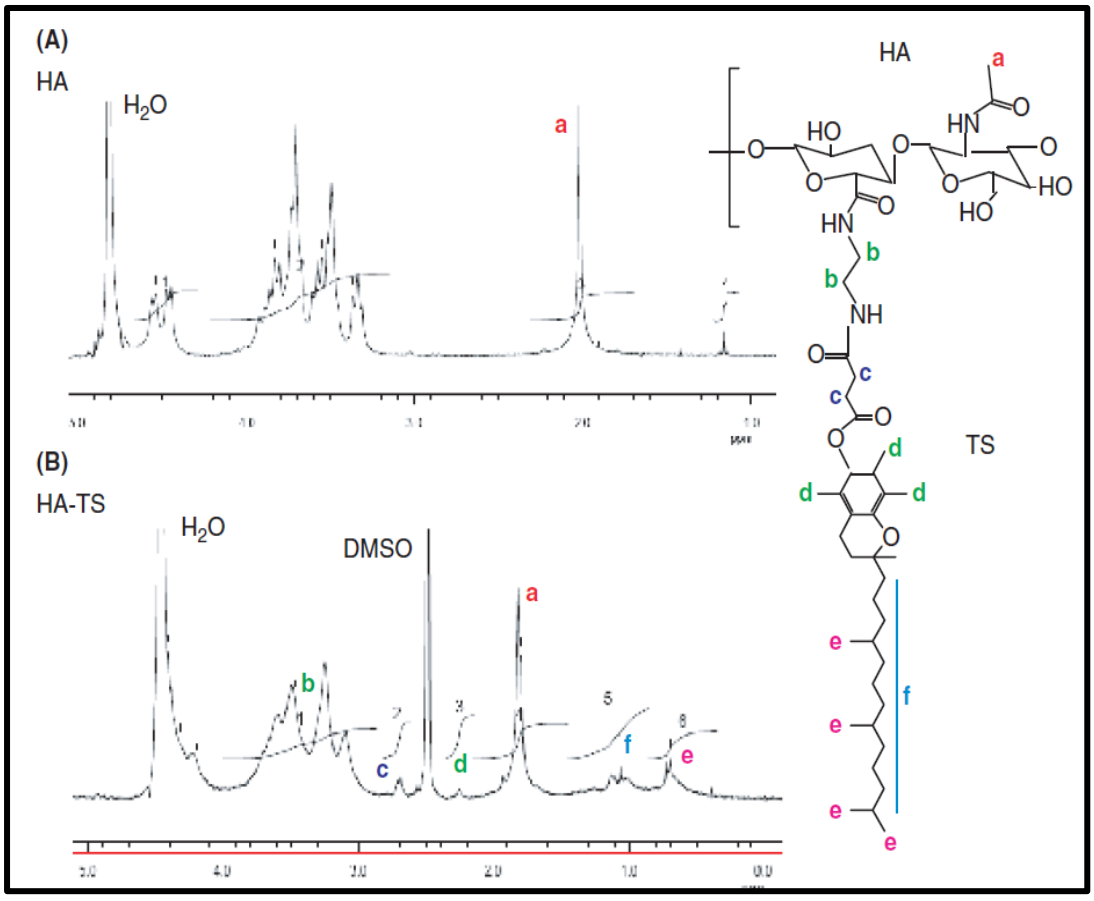

Figure 2.3: ^{1}H NMR spectra of (A) HA in D_2O and (B) HA-TS in DMSO-D_6/D_2O (1:1 *v/v*).

methylene proton on the chain of TS, the methyl protons (9H, -CH_3) of the benzene ring the methylene protons (4H, CH_2-CO) of TS and the methylene protons (4H, –CH_2NH) of EDA, respectively. The results indicate that TS-NH_2 was successfully grafted onto the HA chain.

The DS of the HA derivatives that corresponds to the number of grafted molecules per 100 disaccharide units was calculated from the integration ratio between the methyl group in TS-NH_2 (δ = 0.7 ppm [12H, –CH_3]) and the characteristic peak of the N-acetyl group in HA (δ = 1.8 ppm [3H, –$COCH_3$–]). Table 2.1 summarizes the features of the HA-TS conjugates. The DS of the HA-TS conjugates is 7.39–9.89%, which increases as the molar ratio of TS–NH_2 to HA increases.

Table 2.1: Characteristics of HA-TS conjugates.

Sample[a]	Feed ratio[b]	Mn[c]	DS[d]	CMC (mg/mL)[e]	Particle sizes (nm)	_ ζ (mV)[f]
HA-TS7	15:1	18651	7.39	0.013	294.6±3.12	−30.9±1.22
HA-TS8	25:1	18874	8.33	0.008	255.7±7.08	−27.3±0.60
HA-TS10	35:1	19243	9.89	0.005	212.0±1.88	−23.7±0.10

Notes: [a] HA-TS conjugates with different DS values; [b] Molar feed ratio of TS-NH_2 to HA; [c] Number-average molecular weight, estimated from the ^{1}H NMR Spectrum, [d] Degree of substitution of the TS-NH_2 moiety, [e] Critical micelle concentration, [f] ζ potential.

2.3.2 Critical micelle concentration

TS was used as the hydrophobic moiety to make an amphiphilic polymer that can form stable micelles in an aqueous environment. Due to these amphiphilic properties, HA-TS micelles might have a core–shell structure. The hydrophilic HA domain forms the outer segment of the micelles, while a hydrophobic TS main forms the inner core of the micelles. The *CMC* values were calculated using fluorescence spectroscopy as reported in section 2.2.2.31. *CMC* values increased from 0.005 to 0.013 mg/mL as the DS of the TS group decreased (Table 2.1 and Fig.2.4). This effect resulted in higher hydrophobicity induced by the presence of additional TS, enabling the inner core of HA-TS micelles to assemble more readily.

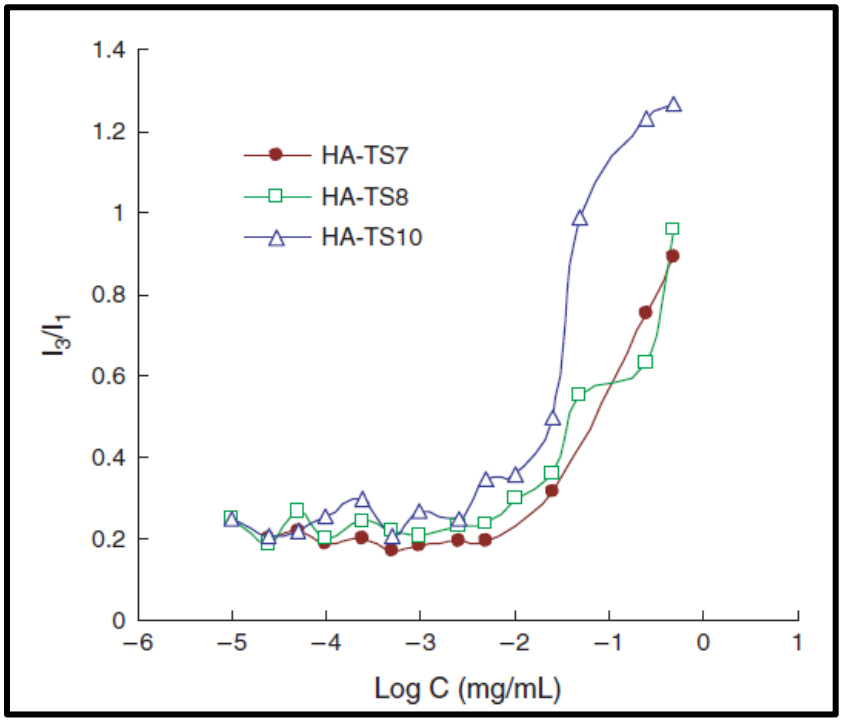

Figure 2.4: Intensity ratios I_3/I_1 from pyrene excitation spectra as a function of HA-TS micelle concentration in ddH_2O.

2.3.3 Particle size, morphology and drug loadings

Table 2.1 shows the particle size of blank HA-TS micelles with various DS. As DS values increase, the particle sizes of HA-TS micelles decrease from 294.6 to 212.0 nm. The hydrophobic RIF can be incorporated into the core of the micelles via hydrophobic interactions. The presence of RIF in the core of micelles had increased the volume of the hydrophobic block, leading to larger micelles (Table 2.2).

The TEM morphology and size distribution of HA-TS_7 micelles are shown in Fig. 2.5A and 2.5B. Spherical HA-TS_7 micelles were observed, with a narrow distribution of particle size (PDI < 0.5). These results indicated that the HA-TS conjugate formed micelles in an aqueous environment. The data showed that the micelles particle sizes by TEM were slightly smaller than those determined by DLS measurements. This difference was due to the fact that TEM measured the micelles in a dry condition, while DLS measured the micelles particle size in solution. Similar results had been reported in other studies indicating the HA-TS conjugate formed slightly larger micelles in an aqueous environment [103,104].

The drug loadings of HA-TS micelles with various DS were 70.01 ± 0.85%, 72.85 ± 3.44% and 79.09 ± 2.59%, respectively (Table 2.2). A higher DS of the HA-TS conjugate had resulted in higher drug loading. An increase of hydrophobic TS might enhance the hydrophobicity of micelles, thus increasing the loading of the hydrophobic drug RIF. The HA-TS conjugates showed an excellent ability to encapsulate the RIF drug. These conjugates had similar drug loading capacities compared with RIF-solid lipid NPs [105] and were superior to RIF-gelatin NPs [90]

Table 2.2: Characteristics of RIF-HA-TS micelles.

	RIF-HA-TS$_7$	**RIF-HA-TS$_8$**	**RIF-HA-TS$_{10}$**
Size (nm)	299.6±12.1	273.1±7.66	238.5±10.7
PDI [a]	0.302±0.05	0.464±0.09	0.282±0.04
(%) Drug loading (w/w)	70.01±0.85	72.85±3.44	79.09±2.59

Note: [a] Polydispersity index of micelles size.

(A) (B

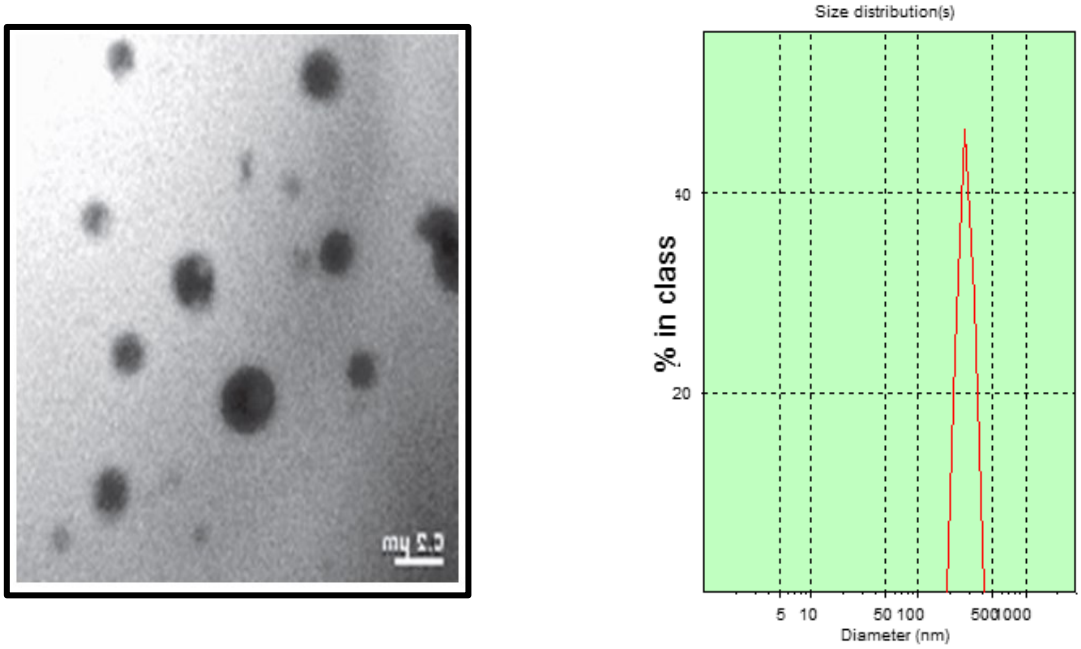

Figure: 2.5: TEM images (A) and size distribution (B) of HA-TS.

2.3.4 DSC

The curves of DSC shown in Fig. 2.6 suggest that RIF-HA-TS_7 do not exist as a physical mixture. One exothermic peak near 228 °C was found for HA-TS_7 Fig. 2.6 (A). Upon heating to 260°C, RIF undergoes an exothermic transition Fig.2.6 (B) [106]. The characteristic peak of RIF almost disappears in the curve for RIF-HA-TS_7 Fig. 2.6 (C), suggesting that RIF was molecularly incorporated into HA-TS_7. On the other hand, in the DSC curve of the physical mixture, the RIF/HA-TS_7 was also different from that of RIF-HA-TS_7 in which there was an exothermic peak for RIF in the curve Fig. 2.6 (D). The results concluded that that RIF was incorporated in RIF-HA-TS_7 micelles.

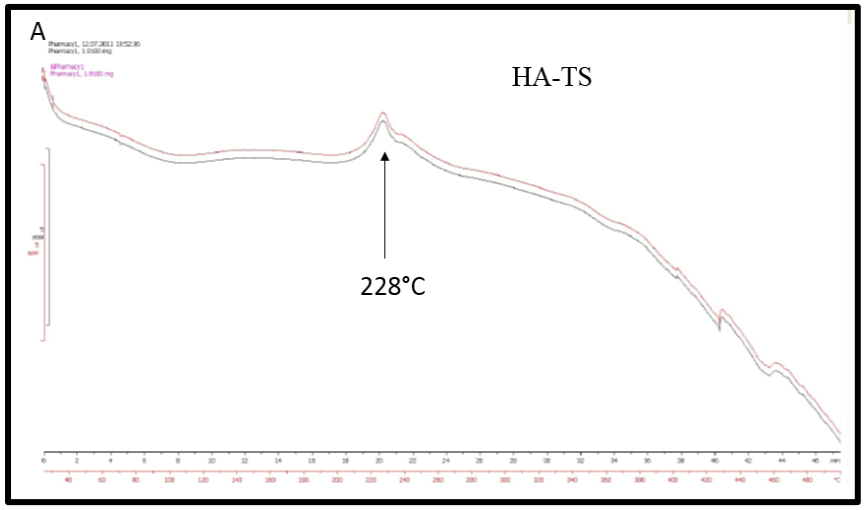

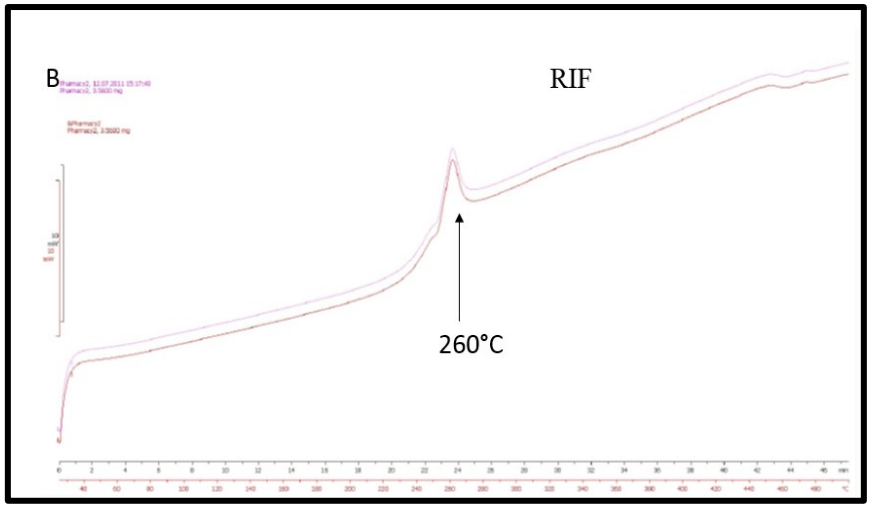

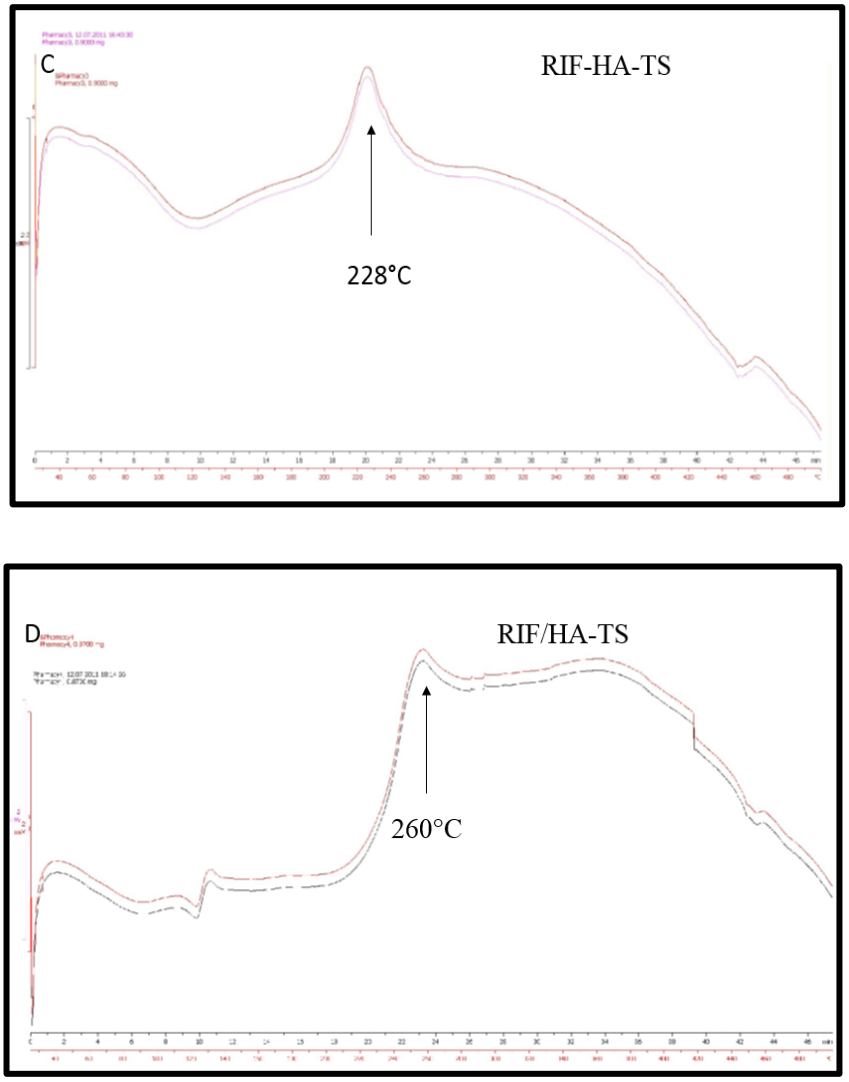

Figure 2.6: Curves of differential scanning calorimetry: (A) HA-TS; (B) RIF; (C) RIF-HA-TS; (D) HA-TS + RIF physical mixture.

2.3.5 X-ray

Fig.2.7 shows the XRD spectra of RIF, blank HA-TS_7 and RIF-HA-TS_7. The characteristic X-ray diffraction peaks of RIF were dispersed in contrast to HA-TS and RIF-HA-TS with glossy peaks, respectively. These XRD spectrum results concluded that there were no RIF crystals in the RIF-HA-TS_7 micelles.

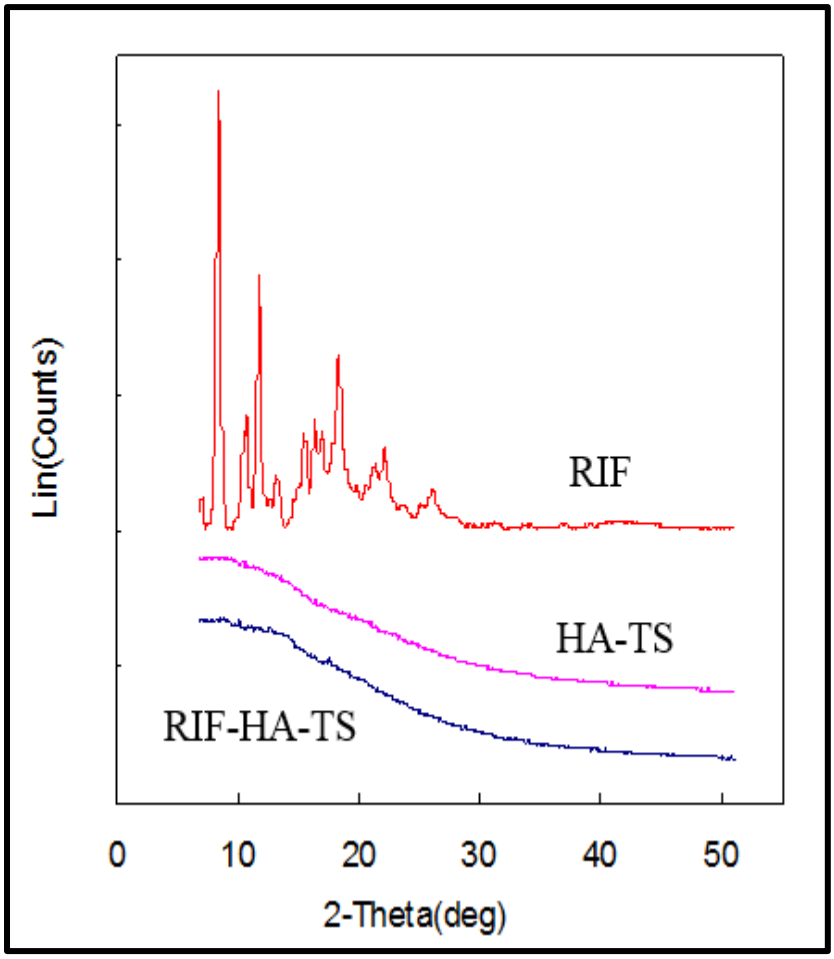

Figure 2.7: Powder X-ray diffraction patterns for RIF, blank HA-TS and RIF-HA-TS.

2.3.6 Colloidal stability

Colloidal stability of nano-carriers micelles under physiological conditions is an important factor for biological applications. The particle size distributions of HA-TS and RIF-HA-TS micelles were monitored for two weeks. The results showed that the HA-TS, as well as RIF-HA-TS micelles, maintained their sizes in PBS without aggregation for two weeks at 37 °C (Fig. 2.8 (A)). The micelle surface was shown to be negatively charged and therefore might provide long-term stability in PBS conditions (Table 2.1). For *in vivo* application, it is imperative for the micelles to be stable in the presence of BSA. As shown in Fig. 2.8 (B), the particle size of the HA-TS micelles did not change significantly within 24 h of incubation with 10% BSA, and no precipitation or aggregation was observed.

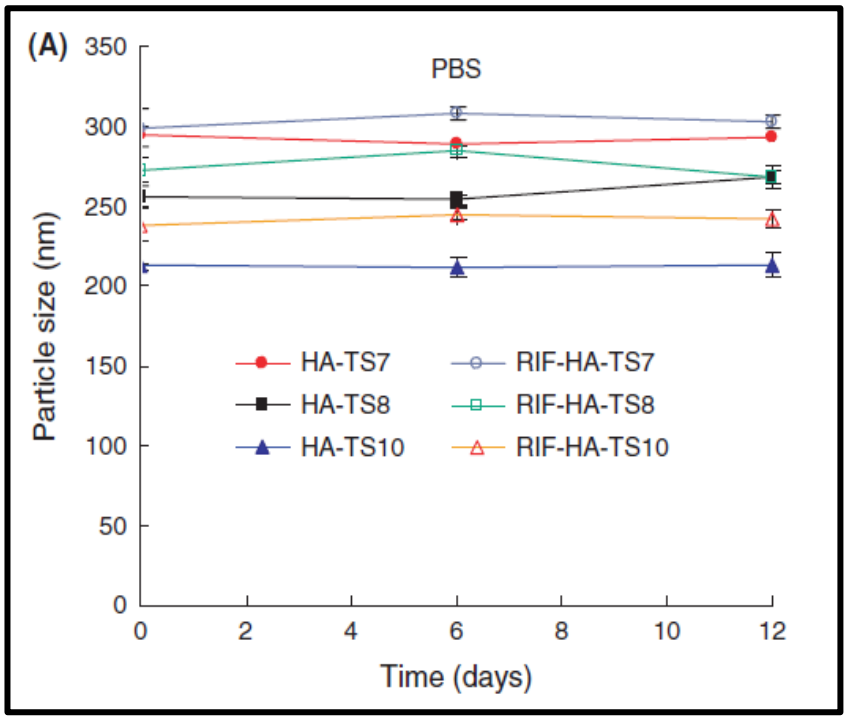

Figure 2.8: (A) Hydrodynamic radius (nm) of HA-TS micelles and RIF-HA-TS micelles at 37°C in PBS pH (7.4). Data shown are the means ± S.D. (n = 3).

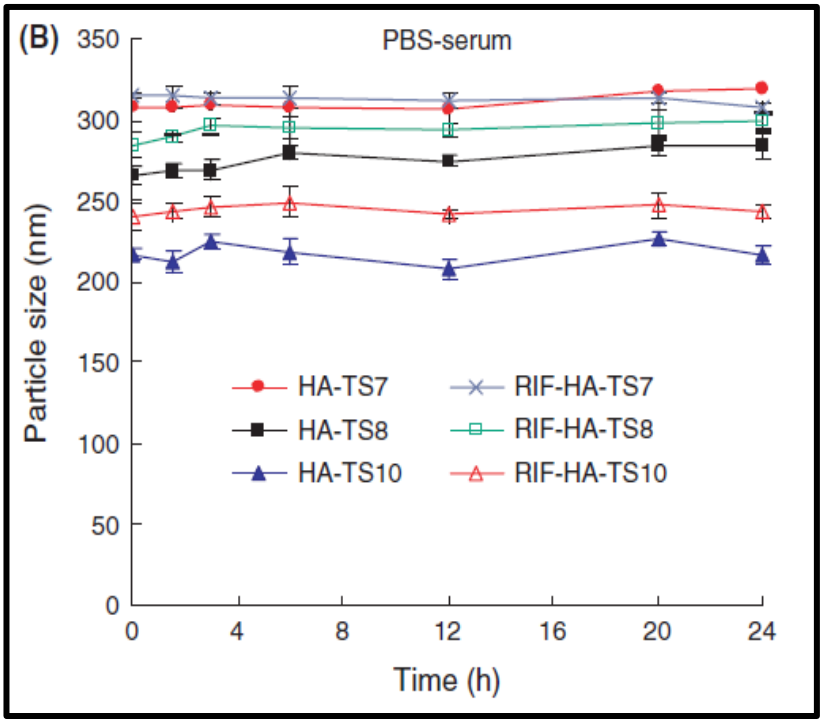

Figure 2.8: (B) Hydrodynamic radius (nm) of HA-TS micelles and RIF-HA-TS micelles at 37°C in PBS pH (7.4) with 10% BSA. Data shown are the means ± S.D. (n = 3).

2.3.7 In vitro drug release

The *in vitro* release of RIF from HA–TS micelles was carried out in buffer (PBS pH 7.4 and acetate buffer pH 5.2). The buffer pH values were selected to simulate the physiological pH (7.4) and endosomal pH of alveolar macrophages (5.2) [99]. The amount of RIF released after 13 h from the RIF-HA-TS_7, RIF-HA–TS_8 and RIF-HA–TS_{10} micelles was found to be 79.82%, 76.16%, and 55.62%, respectively, in PBS (pH 7.4) (Fig. 2.9(A)), whereas the amount of RIF released after 13 h is shown to be 57.95%, 55.97%, and 53.55% in acetate buffer (pH 5.2) (Fig. 2.9(B)). f_2 Similarity factor (f2) was used to determine the release rate of RIF from HA-TS

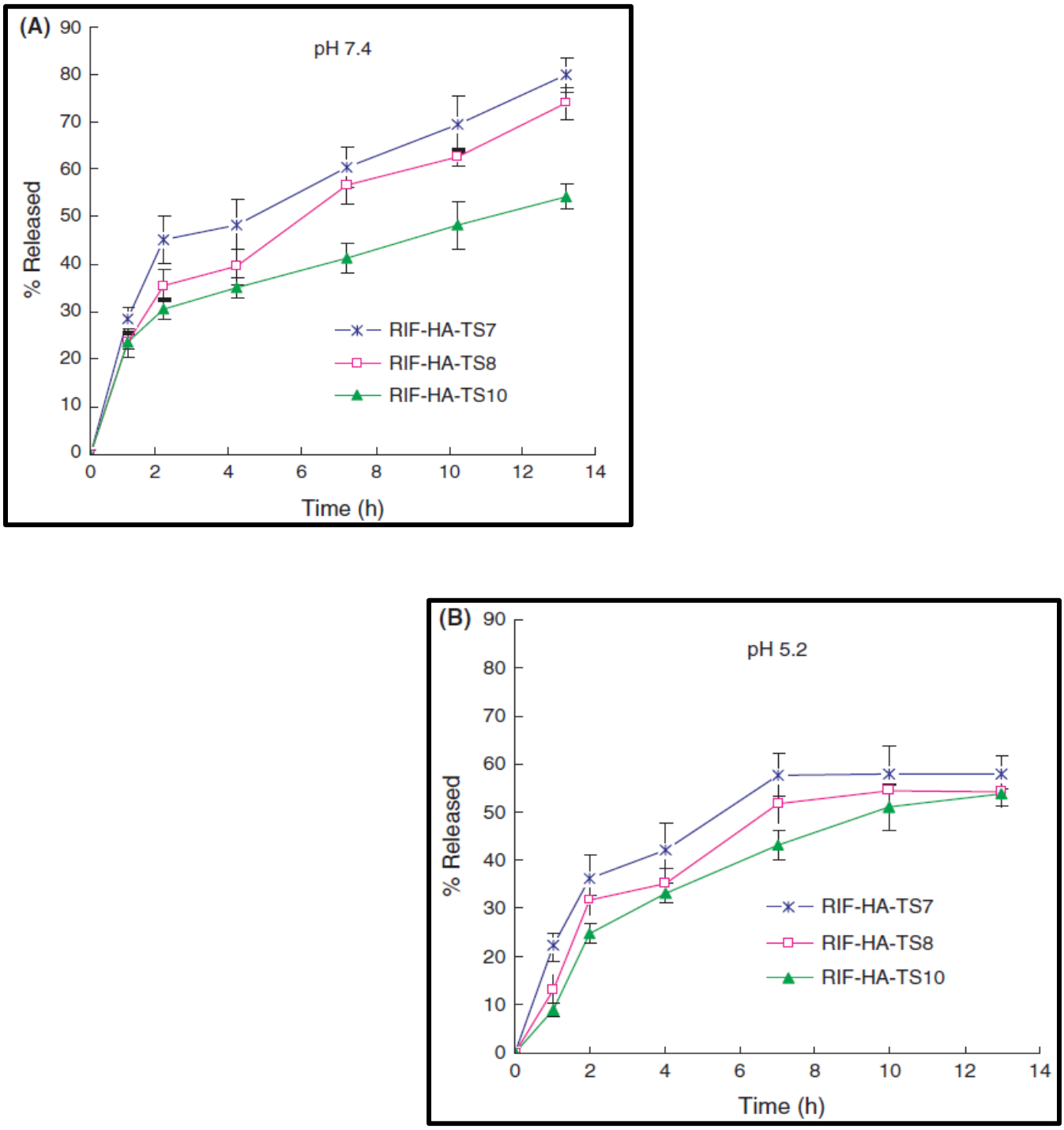

Figure 2.9: In vitro release curves of RIF-HA-TS micelles with different DS in buffers. (A) buffer with pH 7.4. (B) Buffer with pH 5.2. Data shown are the means ± S.D. (n = 3).

micelles. A significant decrease in the release rate of RIF from HA-TS micelles was observed in the acetate buffer as compared to pH 7.4 for all micelles (RIF-HA-$TS_{7,}$ RIF-HA–TS8 and RIF-HA–TS_{10} micelles). The difference might be due to the higher solubility in PBS with (pH 7.4) than the pH 5.2 [107]. Similar results had been reported by Esmaeili et al. [99]. Also, increased hydrophobicity of the HA-TS core results in slower sustained drug release might be due to hydrophobic interactions between the RIF and conjugate.

2.4 Discussion

The characteristic peaks of RIF-HA-TS micelles were evaluated using the FTIR and ^{1}H NMR. Using FTIR, the COO^{-1} group of HA, an amide bond between the HA and TS-NH_2 and the bands at 2926.7 cm^{-1} and 2868.4 cm^{-1} represent asymmetric and symmetric stretching Infra-red vibrations of $–CH_2–$ and $–CH_3$ of TS, suggesting that the TS-NH_2 was conjugated with HA. Fig.2.2 (A & B) [95,101].

In addition to FTIR, the chemical structure was further reconfirmed using the ^{1}H NMR. The HA-TS showed additional signals at 0.7 ppm, 1.3 ppm, 2.2 ppm, 2.7 ppm and 3.3 ppm (Fig 2.3 B) in comparison to the HA signal (Fig 2.3 A). These signals were attributed to the methyl protons (12H, $–CH_3$) on the chain of TS, the methylene protons on the chain of TS, the methyl protons (9H, $–CH_3$) of the benzene ring, the methylene protons (4H, CH_2-CO) of TS and the methylene protons (4H, $–CH_2NH$) of EDA, respectively. Both the FTIR and ^{1}H NMR results indicated that TS-NH_2 was successfully grafted onto the HA chain. The DS of the HA-TS conjugates was 7.39–9.89%, which increased as the molar ratio of TS–NH_2 to HA increased. (Table 2.1).

The HA-TS had formed the stable micelles in aqueous environments, *i.e*. the hydrophilic domain formed the outer segment of the micelles, while a hydrophobic TS formed the inner core of the micelles. The *CMC* values were increased with the decrease in DS of TS in HA-TS micelles. The decrease in *CMC* values were due to higher hydrophobicity induced by the additional TS, enabling the inner core of HA-TS micelles to assemble more readily.

The DLS studies showed the particle sizes distribution of blank HA-TS micelles with various DS in Table 2.1. As DS values were increased, the particle size of HA-TS micelles was decreased, from 294.6 to 212.0 nm. The hydrophobic RIF was incorporated into the core of the

micelles via hydrophobic interactions. The presence of RIF in the core of micelles increased the volume of the hydrophobic block leading to larger micelles (Table 2.2). The TEM studies revealed the spherical morphology of HA-TS_7 micelles with a narrow distribution of particle size (PDI < 0.5) observed. The mean particle size of micelles by TEM was slightly smaller than that determined by DLS measurements. The difference was due to the fact that the TEM measured the micelles in a dry condition, while DLS measured the micelles in solution. Similar results had been reported in other studies indicating the HA-TS conjugate formed slightly larger micelles in an aqueous environment [103,104].

The micelles showed the increase in drug loading capacity with an increase in DS of HA-TS. The increased DS led to growing in hydrophobicity of micelles and this hydrophobic core help to load the hydrophobic drug like RIF. These HA-TS micelles had shown similar drug loading capacities as compared with RIF-solid lipid NPs [105] and were superior to RIF-gelatin NPs [90]. The DSC analysis revealed that RIF was incorporated in RIF-HA-TS_7 micelles. Moreover, the X-rays diffraction spectrum showed that there were no RIF crystals in RIF-HA-TS_7 micelles.

Colloidal stability data showed that the micelles were stable for two weeks at 37 °C. The surface of micelles was shown to be negatively charged, a condition that might have provided long-term stability in PBS conditions (Table 2.1). For *in vivo* application, it is imperative for the micelles to be stable in the presence of serum. As shown in Fig. 2.8 (B), the particle size of the HA-TS micelles was not changed significantly within 24 h of incubation with 10% serum, and no precipitation or aggregation was observed.

The *in vitro* release of RIF from HA–TS micelles was carried out in buffer (PBS pH 7.4 and acetate buffer pH 5.2) to simulate the physiological pH (7.4) and endosomal pH of alveolar macrophages (5.2) [99]. There was a significant decrease in the release of RIF from RIF-HA-TS

micelles at pH 5.2 as compared to pH 7.4. This difference might be due to the higher solubility of RIF in PBS with (pH 7.4) than with the pH 5.2 [107]. Similar results have been reported by Esmaeili et al. [99]. Also, increased hydrophobicity of the HA-TS core led to the slower release of the drug that might be due to hydrophobic interactions between the RIF and conjugate. The *in vitro* release curves showed that the incorporated RIF was a sustained released from RIF loaded HA-TS (RIF-HA-TS) micelles.

2.5 Conclusion

We have synthesized a new HA-TS conjugate which can self-assemble in aqueous solution into micelles with good colloidal stability and biocompatibility. The hydrophobic drug RIF was incorporated in HA-TS micelles with high drug loading and sustained release pattern from RIF-HA-TS micelles.

Chapter 3

Macrophage Behaviour after Cellular Uptake and Intracellular localization of micelles.

This study has already been published as Yuan Gao, Muhammad Khan Sarfraz e al. *Hyaluronic Acid-Tocopherol Succinate-Based Self-Assembling Micelles for Targeted Delivery of Rifampicin to Alveolar Macrophages in Journal of Biomedical Nanotechnology June 2015, 11:1283-1311*

Abstract

The behavior of alveolar macrophages after cellular uptake of micelles was evaluated. Macrophage cellular uptake was investigated depending upon the DS of micelles, concentration of micelles, optimum time and temperature. Moreover, cellular uptake was also studied after activation with LPS and HA-TS. Furthermore, the recognition of CD44 receptors on the cellular surface was done by anti-mouse CD44 mAb IMF7 and its mechanism of cellular uptake was investigated with phagocytosis inhibitor, Cytochalasin B. The secondary toxicity of macrophages after cellular uptake and release of cytokines was measured using cytokines array kits. The results showed that the cellular uptake of RIF-HA-TS micelles was more efficiently taken up by MH-S cells than the free RIF solution via phagocytosis and receptor-mediated endocytosis. Cellular uptake of RIF-HA-TS micelles was time-dependent and dose-dependent. The HA-TS micelles retained the biological recognition of HA receptor that interact with a CD44 receptor on macrophage surface. Furthermore, the HA-TS micelles could induce the proinflammatory cytokine release (secondary toxicity effect) which could enhance the anti-tuberculosis activity of RIF-HA-TS micelles. The RIF-HA-TS micelles deliver the drug more efficiently to macrophage. Both effects might increase the efficiency of the new treatment.

3.1 Introduction

Immunological activities play a major role in the fight against TB infection [108]. During *Mycobacterium tuberculosis* (MTB) infection, a strong CD44+ T-type response is considered critical for the containment of MTB using activation of infected macrophages by proinflammatory Th_1 type cytokines. This activation of infected macrophages plays an essential role in the development of T-cell-mediated immune response. T-cells can display at least two phenotypes, proinflammatory Th_1 and anti-inflammatory Th_2 depending upon the pattern of cytokine secretions.

Th_1 proinflammatory cytokines (secondary toxicity effects) including TNF-α, IFN-γ, IL-1β and IL-12 have a protective role in the immunology of TB [109]. TNF-α, a crucial proinflammatory cytokine that activates the macrophages to liberate nitric oxide synthase-2 which is responsible for killing the intracellular MTB [110]. IFN-γ is a major macrophage-activating factor which is associated with the generation of macrophage killing activity and important in the host response to MTB infection [111]. IL-1β plays a significant role in pathways and production of proinflammatory cytokines required to control MTB infections [112].

T-helper type 2 (Th2) cell activation leads to the release of anti-inflammatory cytokines like 1L-10 [113] that can undermine Th1-mediated immunity and drive alternative activation (secondary toxicity effect) of macrophages. IL-10 cytokine plays a significant role in immune regulation during MTB infection [114]. Its anti-inflammatory response to MTB infections helps the progression of Mycobacterium by down-regulating the production of proinflammatory cytokines [115]. It also inhibits the production of proinflammatory interferon-gamma IFN-γ from T-cells [116] which in turn prevent the phagosome maturation in mycobacterium-infected macrophages, one of the main antimicrobial mechanisms expressed by macrophages [117]. IFN-γ

plays a central role in resistance to MTB infection and a decrease in IFN-γ production leads the individuals susceptible to tuberculosis [118].

In the previous chapter, we successfully synthesized and *In vitro* characterized the RIF-HA-TS_7 micelles. The current chapter investigates the targeted drug delivery of micelles to CD44+ receptor on macrophage surface. It also covers the various factors affecting the cellular uptake of micelles and its internalization. Furthermore, it also investigates the activation of macrophage to produce proinflammatory and anti-inflammatory (secondary toxicity) responses and its profiling.

3.2 Material and Methods

3.2.1 Materials

The alveolar macrophage cell line (MH-S) were purchased from the American Type Culture Collection (Manassas, VA). Rat anti-mouse CD44 antibody (mAb) IMF 7 and PE-labeled anti-mouse CD44 mAb IM7 were obtained from BD Biosciences (Franklin Lakes, NJ). Radio-Immunoprecipitation Assay (RIPA) lysis buffer was from Thermo Scientific (Rockford, IL). Alexa-Fluor® 488 succinimidyl ester was purchased from Invitrogen (Burlington, Canada). Raybio cytokine antibody array was from Ray Bio-tech Inc (Norcross GA). All media were purchased from Gibco BRL (Gaithersburg, MD). BIO-Rad protein assay agent (Bio-Rad, Hemel Hempstead, UK).

3.2.2 Methodology

3.2.2.1 Cell Uptake Studies - cell lines, cell extract and HPLC analysis methods

The murine alveolar macrophage cell line MH-S was cultured in RPMI 1640 medium supplemented with 10% fetal bovine serum and 1% penicillin-streptomycin mixture at 37°C under a 5% CO_2 atmosphere.

The cellular uptake of RIF by MH-S cells was studied as follows. For each experiment, upon completion of the treatment, the incubation media was removed and cells were washed 3 times with cold PBS (pH 7.4) followed by lysis with 200µL RIPA lysis buffer for 1 h. Each of the lysates was centrifuged at 8000 rpm for 5 min and the supernatant was collected. The collected samples were added to an equal volume of acetonitrile and then vortexed for 2 min to solubilize the RIF and precipitate the protein. The samples were further centrifuged for 5 min at 8000 rpm and the concentration of RIF in the supernatant was determined by HPLC. The concentration of RIF taken up by MH-S cells was normalized to the amount of cellular protein, which was determined using a BIO-Rad protein assay agent (Bio-Rad, Hemel Hempstead, UK) as per manufacturer protocol. The experiments were performed in triplicate for each time point.

3.2.2.2 Effect of degree of substitution (DS) of the conjugate on cellular uptake

MH-S cells were seeded evenly into a 6-well plate (Coring) at a concentration of 5×10^5 cells/well. After 24 h, the medium was changed with serum-free medium. Then confluent cells were exposed to 500 µg/mL RIF-HA-TS micelles with various DS (7.39%, 8.33%, and 9.89%) for 2 h at 37 °C before performing any further analysis as described above.

3.2.2.3 Effect of RIF-HA-TS micelles concentration on cellular uptake

MH-S cells were seeded in a 6-well plate (Corning) at a density of 5×10^5 cells/well and incubated for 24 h. After incubation, these confluent cells were exposed to different concentration of 200-500 µg/mL RIF-HA-TS_7 micelles in serum-free medium for 2 h at 37°C before performing any further analysis as described above.

3.2.2.4 Time course of RIF content after the administration

To investigate the time, for maximum intracellular RIF concentration, MH-S cells (5×10^5 cells/well) were seeded in a 6-well plate (Corning) at a density of 5×10^5 cells/well and incubated for 24 h. After 24 h, these confluent cells were exposed to 500 μg/mL RIF–HA-TS_7 micelles for up to 24 h at 37 °C before analysis. The samples were collected at different time points up to 24 h and analyzed as described above.

3.2.2.5 Effect of temperature on cellular uptake

In order to confirm the energy dependent uptake (active transport) of micells by macrophages, the cells were studies at at 37°C and 4°C. MH-S cells (5×10^5cells/well) were incubated in the six-well plate for 24 h. After 24 h, a confluent cell in each well was treated with the 500 μg/mL RIF-HA-TS_7 micelles and free RIF solution respectively for 2 h at 37°C and 4 °C in serum-free medium before any further analysis. The free RIF solution was administered from a stock solution (4mg/ml in 1% DMSO in PBS).

3.2.2.6 Cellular uptake on un-activated and activated MH-S cells

To study the effect of un-activated and activated macrophages on cellular uptake, the following experiments were carried out. MH-S cells were seeded in 6-well plates at 5×10^5 cells/well for 24 h. After 24 h, these confluent cells were treated with LPS 100 ng/mL in serum free medium for 2 h at 37 °C. Cells without LPS pre-treatment were used as a control. These un-activated and activated macrophages were further treated with RIF-HA-TS_7 micelles to achieve RIF final concentration of 500 μg/mL for another 2 h in serum-free medium before any further analysis.

In another experiment, the activation of macrophages by HA-TS was studied. MH-S cells were seeded in 6-well plates at 5×10^5 cells/well for 24 h. After 24 h, these confluent cells were treated with HA-TS_7 micelles (215 μg/mL) in serum-free medium for 3 h at 37 °C. Cells without HA-TS_7 micelles pre-treatment were used as a control. Then, after 3 h, these macrophages were further treated with RIF-HA-TS_7 micelles to achieve RIF final concentration of 500 μg/mL for another 2 h in serum-free medium before any further analysis.

3.2.3 HA, antibody and cytochalasin B blocking cellular uptake

3.2.3.1 Study the effect of HA

The following experiment was conducted to investigate the effect of HA on cellular uptake. The goal was to saturate the CD44 receptors on macrophage surface by increasing the concentration of HA and study its effect on cellular uptake of RIF-HA-TS_7 micelles. Two different concentrations 50-150 μg/mL of HA were co-incubated in six-well plates with MH-S cell (5×10^5 cells/well) at 4 °C for 1 h. Then RIF-HA-TS_7 micelles were added to achieve a RIF final concentration of 500 μg/mL in serum-free medium and the cells were continued to be incubated at 37 °C for another 2 h before any further analysis. Cells without any co-incubation were used as positive control.

3.2.3.2 Study the effect of Antibody

The following experiment was conducted to investigate the effect of antibody on cellular uptake. The gaol was to investigate that whether the cellular uptake of micelles was due to the recognition of CD44 receptor on macrophage surface by HA. Blocking of CD44 receptors on macrophage surface was done by anti-mouse CD44 mAb IMF7 (Anti-CD44 mAb) before treatment with RIF-HA-TS_7 micelles. Two different concentrations 50-150 μg/mL of HA were co-incubated in six-well plates with MH-S cell (5×10^5 cells/well) at 4 °C for 45 min. Then RIF-HA-

TS_7 micelles were added to achieve a RIF final concentration of 500 μg/mL in serum-free medium and the cells were continued to be incubated at 37 °C for another 2 h. Cells without any co-incubation were used as positive control.

3.2.3.3 Study the effect of cytochalasin B

The mechanism of cellular uptake was investigated by the following experiment. The gaol was to investigate the macrophage cellular uptake mechanism of micelles by blocking cellular phagocytosis process. Phagocytosis inhibitor cytochalasin B was used as phagocytosis inhibitor on macrophage surface. Different concentrations of cytochalasin B (2 μM -13.3 μM) were co-incubated in six-well plates with MH-S cell (5×10^5 cells/well) at 4 °C for 1 h. Then RIF-HA-TS_7 micelles were added to achieve a RIF final concentration of 500 μg/mL in serum-free medium and the cells were continued to be incubated at 37 °C for another 2 h before any further analysis. Cells without any co-incubation were used as positive control.

3.3 Imaging of Alexa 488-HA-TS micelles internalization

Macrophage internalization of micelles was studied using confocal laser scanning microscopy (CLSM). Alexa 488-HA-TS_7 micelles and DAPI were used to investigate the internalization of micelles. Alexa-488 was a fluorescence dye with cyan green color and extensively used in cell biology studies using fluorescence microscope. DAPI is also a fluorescent dye with blue color and binds strongly to DNA [119]. MH-S cells were seeded on a cover slip in a 12-well culture plate with a seeding density of 1×10^5 cells/cover slip and incubated at 37 °C until they reached sub-confluent levels. At confluency, the complete growth medium was replaced with serum-free medium. After a change of medium, these cells were treated 50 μg/mL Alexa 488-HA-TS_7 micelles. The treatment with Alexa 488-HA-TS_7 micelles was given for 2 h. After 2 h, the cover slips were removed, washed with PBS. After washing, coverslips were fixed with 4%

formaldehyde and stained with DAPI (100 ng/mL) for 10 min. Furthermore, the cover slips were washed with PBS, mounted on a glass slide and sealed with glycerol in PBS (pH 9.0). The slides were visualized under the CLSM (Zeiss 510 NLO, Berkochen, Germany).

3.4 CD44 expression by confocal and flow cytometry

3.4.1 Flow cytometry: The confirmation of CD44 receptors on macrophage cell surface was done using the flow cytometry as reported by Belitsos *et al.* [120]. MH-S Cells were collected at 1×10^6 cells/mL and suspended in cold PBS containing 1% FBS. The cells were incubated with PE-anti-CD44 mAb IM7 or PE-isotype control at 16 ng/mL on ice for 45 min. Following incubation, the cells were washed, collected, centrifuged and re-suspended in cold PBS containing 1% FBS twice. Then the cells were analyzed on an automatic flow cytometer (FAScan; Beckman Instruments, Inc., Fullerton, CA). The negative control was set using cell without treatment. In each test, 1×10^4 cells were analyzed per run on an automatic flow cytometer. A single argon-ion laser beam was used for excitation (488 nm). The data analysis was performed using FCS software.

3.4.2 Confocal laser scanning microscopy (CLSM)

In another experiment, MH-S cells were grown on cover slips for 24 h. The cells were incubated with a PE-labeled anti-CD44 mAb (25 μg/mL) for 30 min at 4 °C in serum-free medium, followed by incubation with Alexa 488-HA-TS_7 micelles (50 μg/mL) for another 2 h. Then, each well was aspirated, washed with PBS and examined under a CLSM.

3.5 Cell viability

The cytotoxicity of RIF-HA-TS_7 micelles and blank HA-TS_7 micelles to MH-S cells were evaluated in a MTT assay. MH-S cells were seeded evenly into 96-well plates at a concentration of 5000 cells/well and incubated for 24 h in a humidified atmosphere of 5% CO_2 at 37 °C. Various

concentrations of blank HA-TS_7 micelles were added to achieve final concentrations of 25–250 μg/mL and were incubated for 48 h.

In another experiment, samples of RIF-HA-TS_7 micelles and free RIF solution were added to each well to achieve final concentrations of 0.01 to 0.5 mg/mL respectively. After 48 h incubation, the medium was replaced by 180 μL fresh complete medium and 20 μL MTT solution (5 mg/mL) respectively. Cells were incubated for an additional 4 h. The medium was carefully removed and 200 μL DMSO was added to dissolve the formazan. Absorbance was measured at 490 nm using a microplate reader (VMax® Kinetic, Molecular Devices, CA) at 25 °C. Cell viability was expressed as a percentage of absorbance with respect to that of untreated cells. The experiment was replicated 6 times for each time point.

3.6 Cytokine analysis

Before an experiment, MH-S cells were plated at a density of 5×10^6 cells/well. After 24 hours, the medium was replaced with fresh medium and the following treatments were added:

(i) LPS (100 ng/mL),

(ii) Blank HA-TS micelles (215 μg/mL),

(iii) RIF-HA-TS micelles (500 μg/mL) and

(iv) Free RIF solution (500 μg/mL).

Control wells consisted of cells incubated with medium only. After 6 h, the supernatants were collected, centrifuged at 8000rpm for 5 min to remove cellular debris and stored at −80 °C for determination of cytokine content. The experiment was performed in triplicate.

Raybio ® Mouse Cytokine antibody array II (RayBio-tech, Inc., Norcross, GA, Cat# AAM-CYT-2-8) was used to assess the changes of cytokine secreting profiles. The Th1 inflammatory cytokines and chemokines including IL-12p70, IL-12-p30p70, IFN-γ, TNF-α, IL-1β, IL-2

macrophages inflammatory protein-1 (MIP-1α), (MIP-2) and (MIP-3β) and secreted (RANTES), keratinocyte-derived chemokine (KC), leptin, monocytes chemoattractant protein-1 (MCP-1) and MCP-5. The Th2 anti-inflammatory cytokines IL-4, IL-5, IL-6, IL-9, IL-10 and IL-13 were also assayed according to the manufacturer protocols. In brief kits were removed from storage and equilibrate at room temperature. The antibody membrane was placed carefully into a well of incubation tray. Each well was incubated with 2ml of blocking buffer for 30 minutes before aspiration. Now each well was treated with collected sample for 5 h. Afterward each well was treated with 2ml of each wash buffer 1 and 2 (thrice) for 5 minutes. After the antibody–cytokine complexes were formed, membranes were incubated with biotinylated secondary antibodies and then with labeled streptavidin for 2 h. The wells were washed with washing buffer as discussed above. Now membrane was treated with 500 µl of detection buffer for 2-3 minutes before chemiluminescence imaging. The membranes were exposed to X-ray film for 5-10 s. The film was developed and intensity of the signal of each spot representing a specific cytokine was evaluated using Image J software (http://rsb.info.nih.gov/ij/). The relative protein levels were obtained by subtracting the background staining and normalizing to the positive controls on the same membrane.

3.7 Statistical analysis

The results were shown as the mean ± S. D. Differences were considered statistically significant at $p < 0.05$. Student's t test was used for the statistical analysis.

3.8 Result and Discussion

3.8.1 Effect of DS of conjugate on uptake

The targeting efficiency of HA modified micelles to the site of interest might significantly depend on the DS of the hydrophobic moiety. This property could affect numerous physicochemical properties of HA modified micelles including particle size, stability in an aqueous medium and the binding affinity of HA to the tumor cells. Therefore, the cellular uptake of various HA-TS micelles with different DS (HA-TS_7, HA-TS_8 and HA-TS_{10}) by MH-S cells was evaluated.

We had already discussed in detail in the previous chapter that degree of substitution of TS-NH_2 was increased from 7.39, 8.33 and 9.89 respectively as we move from (HA-TS_7 > HA-TS_8> HA-TS_{10}) Table 2.1. The cellular uptake of these micelles was shown in (Fig. 3.1). The amount of RIF-HA-TS micelles taken up by MH-S cells decreases by increasing DS of TS to HA (HA-TS_7 > HA-TS_8> HA-TS_{10}) indicating that HA-TS conjugates with low DS (i.e., HA-TS_7) were more readily taken up by cells than those with high DS (HA-TS_8, HA-TS_{10}). Depending upon the micelles cellular activity, RIF-HA-TS_7 micelles were chosen for further studies.

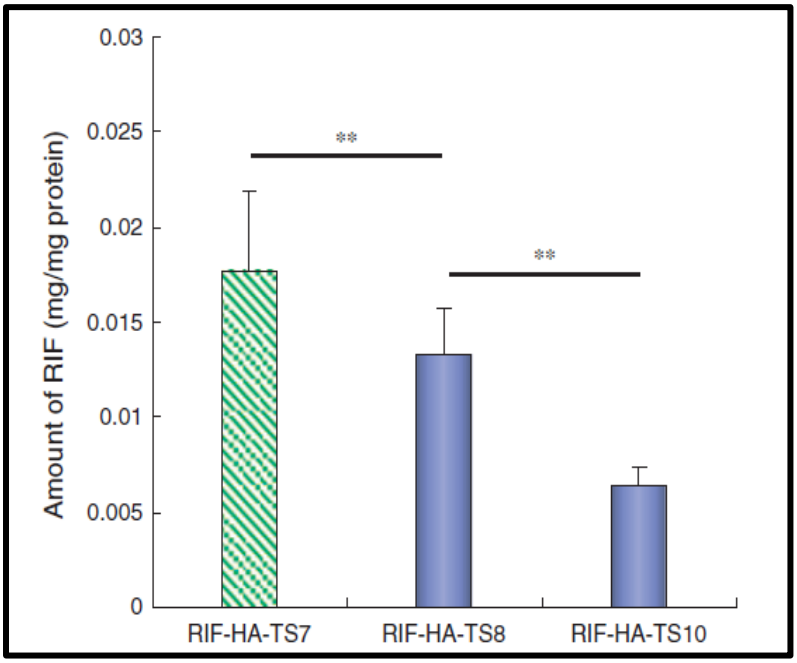

Figure 3.1: Uptake of RIF by MH-S cells from HA-TS micelles with different DS at 2 h. Data shown are the means ± S.D. (n = 3). ** $p < 0.01$.

3.8.2 Effect of concentration of RIF-HA-TS on uptake

Different concentrations of RIF-HA-TS_7 from 200 to 500 µg/mL were investigated for cellular uptake by macrophages. The goal was to find the underlying mechanism that how the cellular uptake was affected by different RIF-HA-TS_7 micelles concentration. The results of different RIF-HA-TS_7 micelles concentration on cellular uptake were shown in Fig. 3.2. The data demonstrated that the intracellular uptake of RIF by MH-S cell was directly dependent on the cellular uptake concentration of RIF-HA-TS_7 micelles. It demonstrated that intracellular uptake of RIF by MH-S cell increases as we increase the RIF-HA-TS_7 micelles concentrations from 200 to 500 µg/mL. Depending upon the maximum intracellular RIF concentration, 500 µg/mL of RIF-HA-TS_7 micelles were selected for further studies.

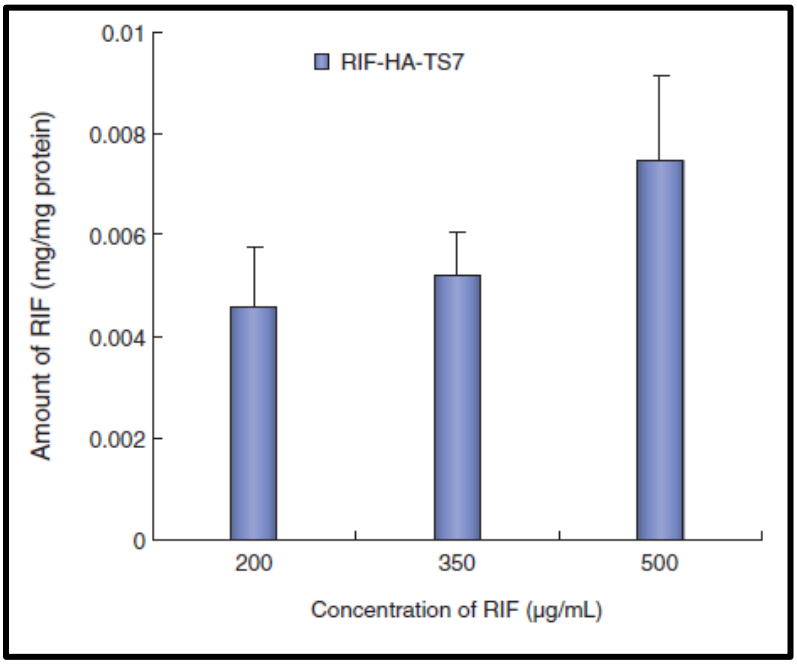

Figure 3.2: Relationship between the RIF-HA-TS_7 micelles concentration and the RIF uptake amount.

3.8.3 Time course of RIF content

To investigate the optimum time for maximum cellular uptake activity, free RIF and RIF-HA-TS_7 micelles were treated with MH-S cells at the concentration of (500 μg/mL) respectively. The samples were collected at different time interval up till 24 h. The results of intracellular uptake of RIF at a various time point were shown in Fig. 3.3. The data showed that after administration of free RIF and RIF-HA-TS_7 micelles with a RIF concentration of (500 μg/mL) to MH-S cells, the amount of intracellular RIF increased and reached a peak at 12 h, then decrease gradually between 12 and 24 h. Furthermore, intracellular uptake of RIF by MH-S cells was 2-3 fold greater from

RIF-HA-TS$_7$ micelles than free RIF solution. The results demonstrated that HA-TS micelles facilitate drug uptake with maximum uptake at 12 h.

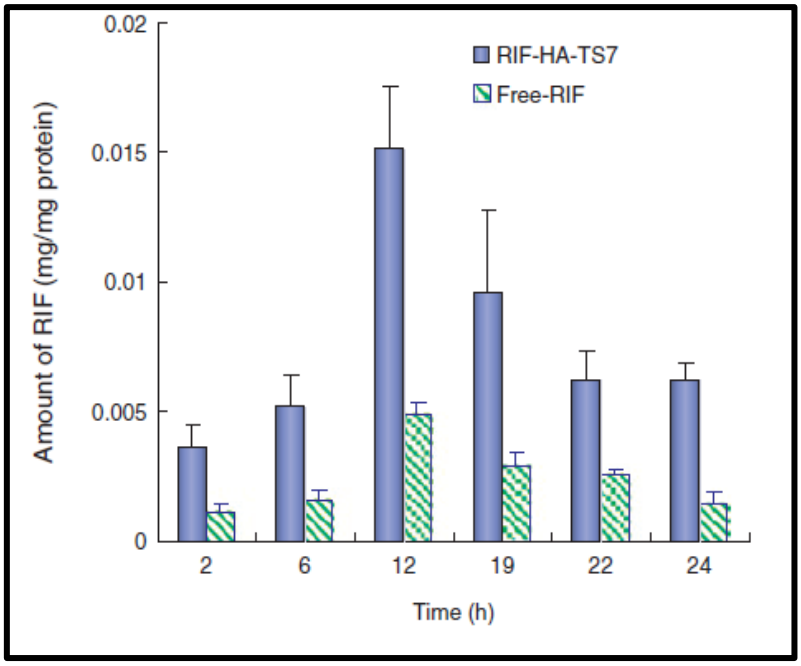

Figure 3.3: Time course of the amount of RIF in MH-S cells after the administration of RIF-HA-TS$_7$ micelles and free RIF (500 μg/ml) within 24 h.

3.8.4 Temperature-dependent uptake

To investigate the energy dependent uptake of micells by macrophages, RIF-HA-TS7 micelles and free RIF solution were added to MH-S cells at at 4 °C or 37 °C respectively. The uptake of RIF-HA-TS7 micelles and free RIF solution at 4 °C was reduced to about 60% and 87% of the uptake observed at 37 °C as shown in Fig. 3.4 Thus, both of the RIF-HA-TS7 micelles and free RIF solutions are taken up by MH-S cells via an energy-dependent pathway.

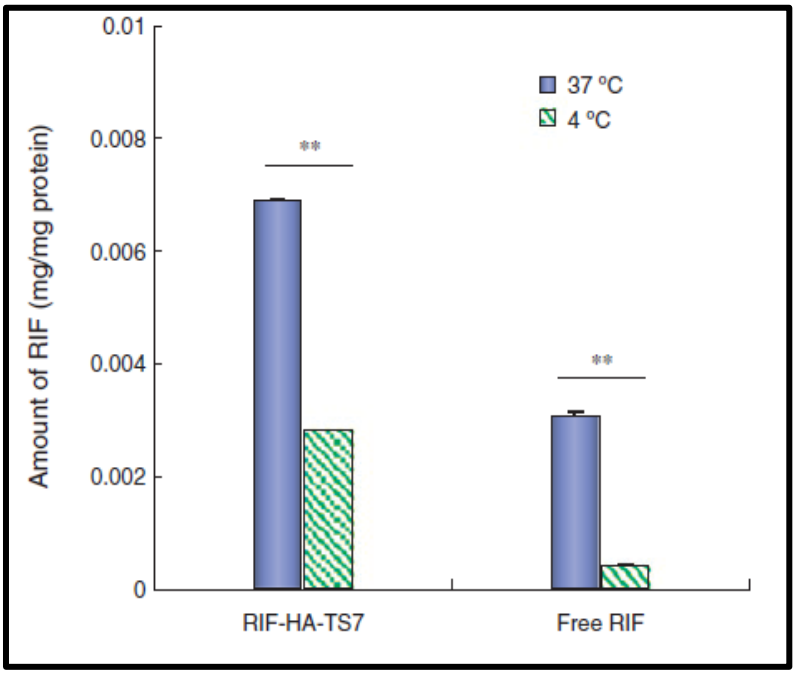

Figure 3.4: Temperature-dependent uptake of RIF-HA-TS$_7$ and free RIF (500 μg/mL) by MH-S macrophage at 4°C and 37°C, monitored after 2 h incubation. Data shown are the means ± S.D. (n=3). ** $p < 0.01$.

3.8.5 Cell uptake by un-activated and activated MH-S cells

The experiment was carried out to investigate the effect of activation of macrophage on cellular uptake of micelles. Macrophages were activated by treating them with LPS for 2 h and then further with RIF-HA-TS_7 micelles to achieve RIF final concentration of 500 µg/mL for another 2 h in serum-free medium. The results of intracellular uptake of RIF after activation with and without LPS were shown in Fig. 3.5. The data demonstrated that the intracellular uptake of RIF by MH-S cells was directly dependent on the cellular uptake of RIF-HA-TS_7 micelles. The data indicated that the amount of intracellular RIF concentration was 1.9 folds greater in activated MH-S cells as compared to un-activated cells. The result indicated that LPS could activate MH-S macrophages.

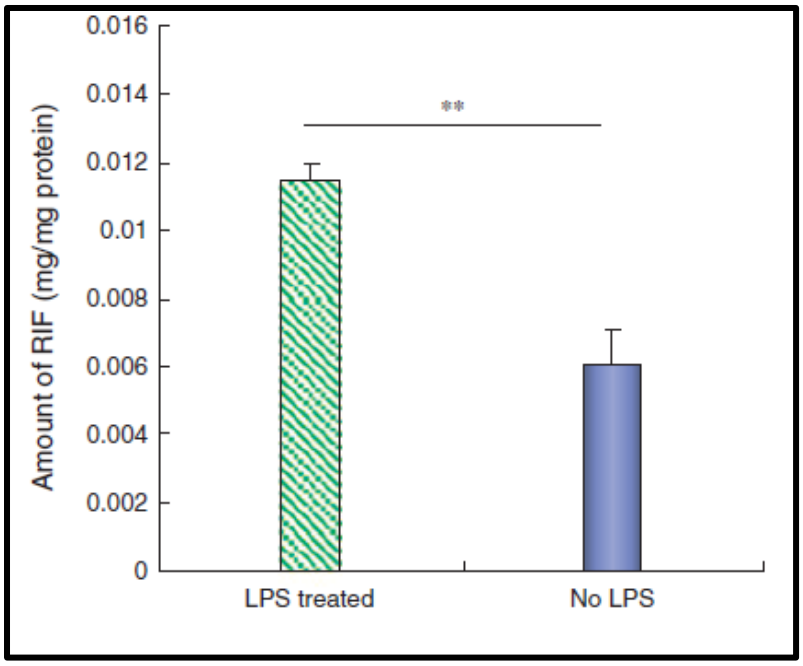

Figure 3.5: Uptake of RIF-HA-TS_7 micelles by MH-S at 2 h incubation after pre-treatment with LPS (100ng/ml for 2 h at 37ºC. Data shown is the means ± S.D. (n = 3). ** $p < 0.01$, * $p < 0.05$.

In another experiment, the macrophages were activated by HA-TS micelles (215 μg/mL) for 2 h and then treated with RIF-HA-TS_7 micelles to achieve RIF final concentration of 500 µg/mL for another 2 h in serum-free medium. The results of intracellular uptake of RIF after activation with and without HA-TS were shown in Fig. 3.6. The data demonstrated that the intracellular uptake of RIF by MH-S cells was directly dependent on the cellular uptake of RIF-HA-TS_7 micelles. Moreover, the amount of intracellular RIF in HA-TS pre-incubation macrophages were higher as compared to cells without pretreatments. The result indicated that HA-TS micelles could activate MH-S macrophages.

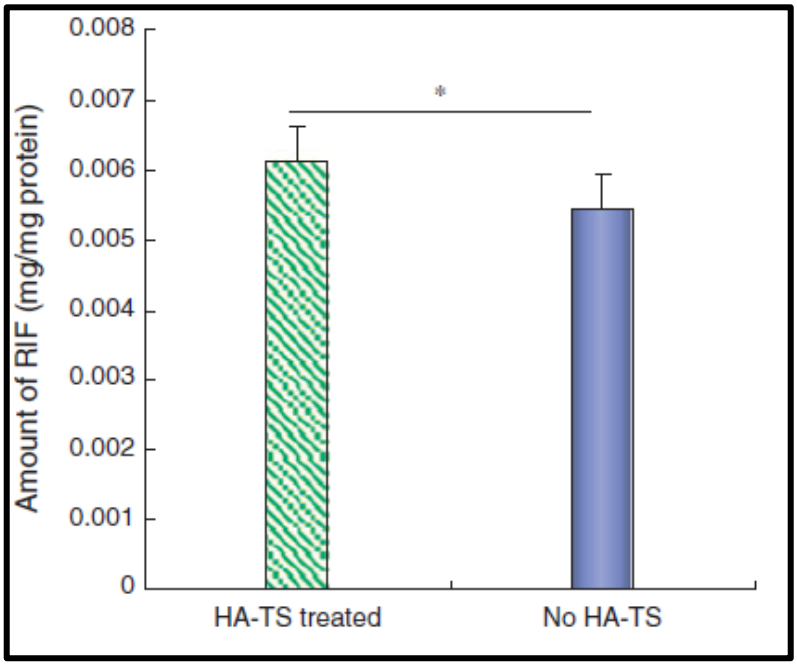

Figure 3.6: Uptake of RIF-HA-TS_7 micelles by MH-S at 2 h incubation after pre-treatment with HA-TS7 micelles (215μg/ml) for 3 h at 37ºC. Data shown is the means ± S.D. (n = 3). ** $p <$ 0.01, * $p < 0.05$.

3.8.6 Uptake mechanism studies

3.8.6.1 Uptake inhibition by HA

The experiment was carried out to investigate the cellular uptake of RIF-HA-TS_7 micelles after saturation of CD44 receptors on macrophage surface by increasing concentration of HA. The results of intracellular uptake of RIF were shown in Fig. 3.7. The data demonstrated that in comparison to control, HA at 50 μg/mL caused a lower uptake of RIF-HA-TS_7 micelles which might be due to the inhibition of CD44 receptor on MH-S cells. In contrast, HA with higher HA concentration of 150 μg/mL, improved the uptake of RIF-HA-TS micelles, which might be related to the activation of MH-S cells induced by higher HA concentration [92].

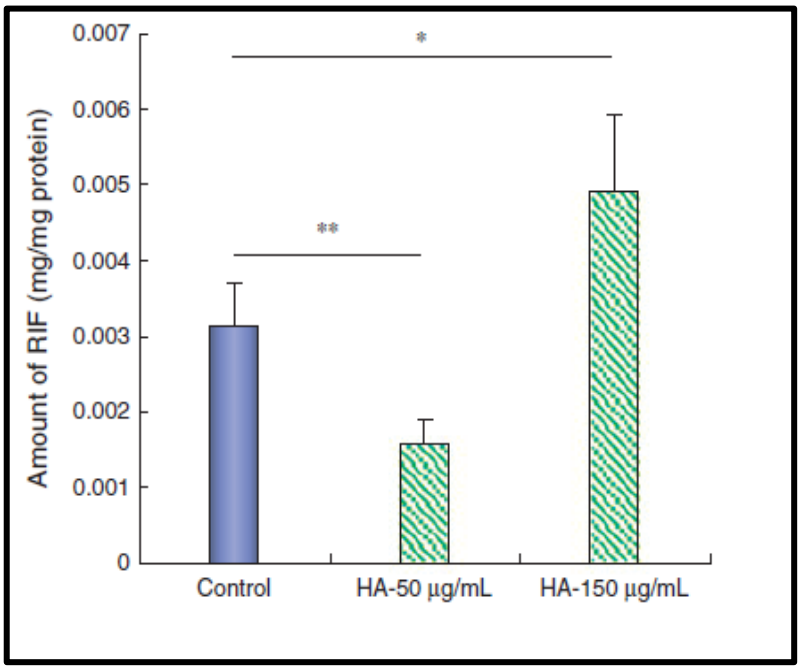

Figure 3.7: Uptake of RIF-HA-TS_7 micelles by MH-S after various treatment, followed by 2 h incubation with RIF-HA-TS (500µg/mL) covered HA at 4°C (50-150 µg/ml) for 1 h. Data shown is the means ± S.D. (n = 3). ** $p < 0.01$, * $p < 0.05$.

3.8.6.2 Uptake inhibition by antibody

The experiment was conducted to re-confirm that the cellular uptake of micelles was due to the recognition of CD44 receptor on macrophage surface by HA. Blocking of CD44 receptors on macrophage surface was done by anti-mouse CD44 mAb IMF7 (Anti-CD44 mAb) before treatment with RIF-HA-TS_7 micelles. The results of intracellular uptake of RIF were shown in Fig. 3.8. The data demonstrated that in comparison to control, the cells treated with anti-CD44 mAb showed a significant decrease in cellular uptake of RIF. The cellular uptake of RIF-HA-TS_7 micelles was decreased with increasing concentration of Anti-CD44 mAb. These findings have suggested the important role of CD44 receptors in cellular uptake of RIF-HA-TS_7 micelles.

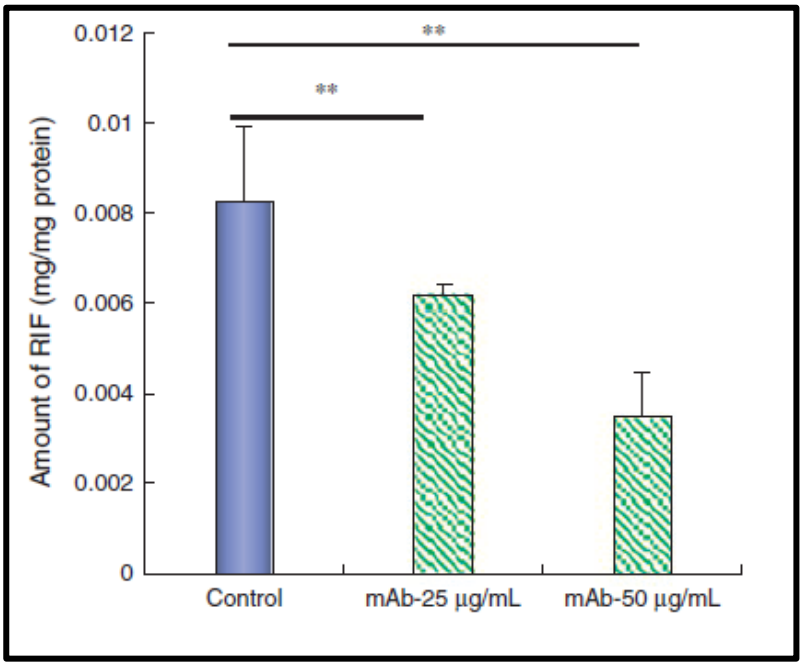

Figure 3.8: Uptake of RIF-HA-TS_7 micelles by MH-S after various treatment, followed by 2 h incubation with RIF-HA-TS (500µg/mL) anti-CD44 mAb IM7 (25 – 50 µg/mL) at 4°C for 45min. Data shown is the means ± S.D. (n = 3). ** $p < 0.01$, * $p < 0.05$.

3.8.6.3 Uptake inhibition by cytochalasin B

The experiment was conducted to investigate the mechanism involved in cellular uptake of micelles. The macrophages were treated with phagocytosis inhibitor, Cytochalasin B, before treatment with RIF-HA-TS_7 micelles [121]. The results of intracellular uptake of RIF were shown in Fig. 3.9. The data demonstrated that in comparison to control, the cells treated with cytochalasin B showed significant decreased in cellular uptake of RIF. The cellular uptake of RIF-HA-TS_7 micelles was decreased by increasing concentration of cytochalasin B (2 to 13.3 μM). The observed significant reduction in the cellular uptake of RIF-HA-TS_7 micelles demonstrated that phagocytosis was mainly responsible for the uptake of RIF-HA-TS_7 micelles.

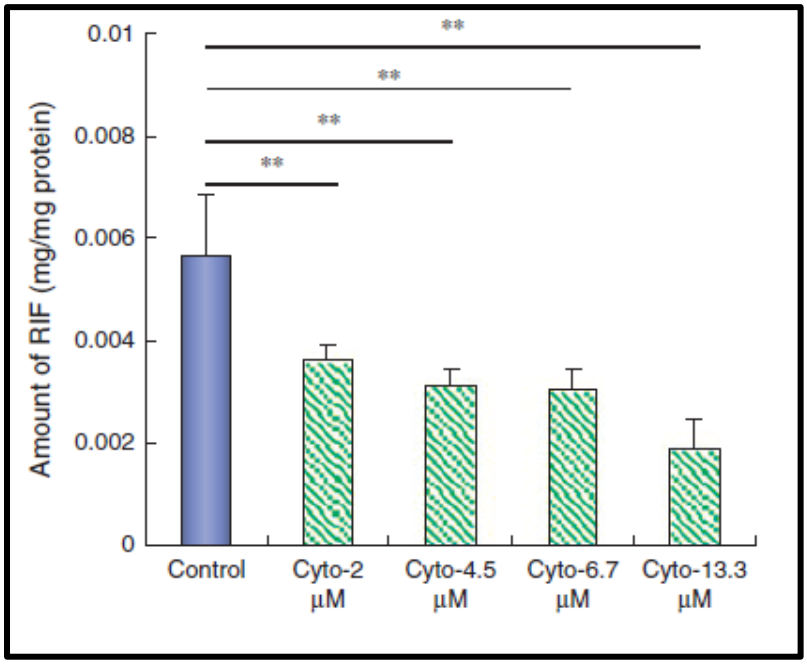

Figure 3.9: Uptake of RIF-HA-TS_7 micelles by MH-S after various treatment, followed by 2 h incubation with RIF-HA-TS (500µg/mL) cytochalasin B (2 to 13.3µM) at 4°C for 45 min. Data shown is the means ± S.D. (n = 3). ** $p < 0.01$, * $p < 0.05$.

3.8.7 Intracellular localization

The interaction between cells and micelles had been studied using confocal laser scanning microscopy (CLSM). Macrophage cells stained with DAPI were shown in Fig. 3.10 (A). It also shows the blue stained nuclei in each macrophage cells. HA-TS_7 micelles were labeled with a green fluorescence marker Alexa 488 and were shown in Fig. 3.10 (B). It also shows the high concentration of micelles accumulates in the cytoplasm of macrophage.

Furthermore, micelles accumulation and nuclei staining of the macrophage were shown in Fig. 3.10 (C). It showed us that most of Alexa 488-HA-TS_7 micelles were evenly internalized into the cytoplasm. It was in accordance with the reported study that the macrophages can internalize nanoparticles into a phagosome after phagocytosis [122] which will carry the nanoparticles throughout the cytoplasm. This cellular localization was in good agreement with other nano-carriers [123].

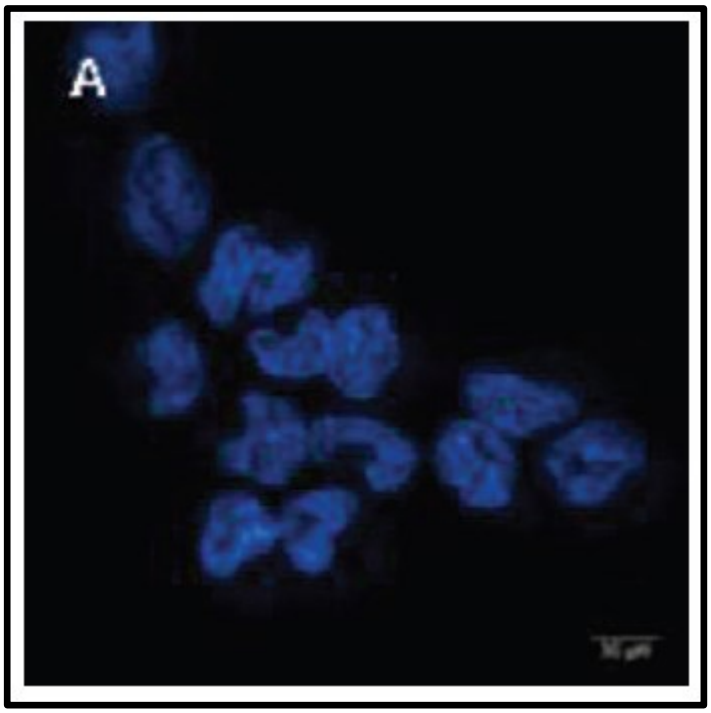

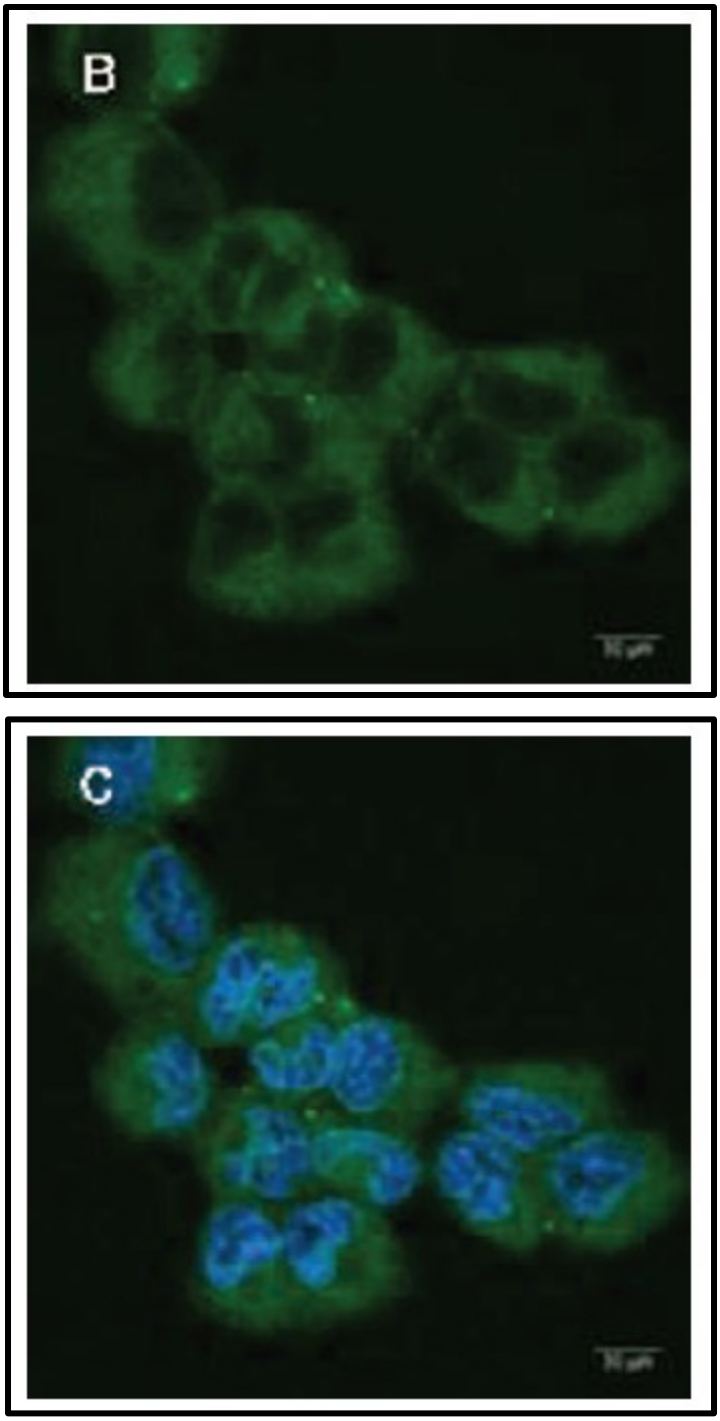

Figure 3.10: Confocal images (A) Nuclei of cells were identified using DAPI (blue). (B) HA-TS_7, micelles were visualized using conjugate Alexa 488 (green); and (C) merge of A and B (Scale bar is 30μm).

3.8.8 CD44 expression in the MH-S cells

Two independent methods were used to investigate the CD44 expression on the MH-S cells. The detail description of both these methodologies was discussed above i.e. Flow Cytometry and Confocal laser scanning microscopy (CLSM). The flow cytometry data showed that MH-S cells treated with PE-anti-CD44 mAb IM7 had strong red intensity, demonstrating high expression of CD44 on the cell membranes of the MH-S cells (Fig 3.11).

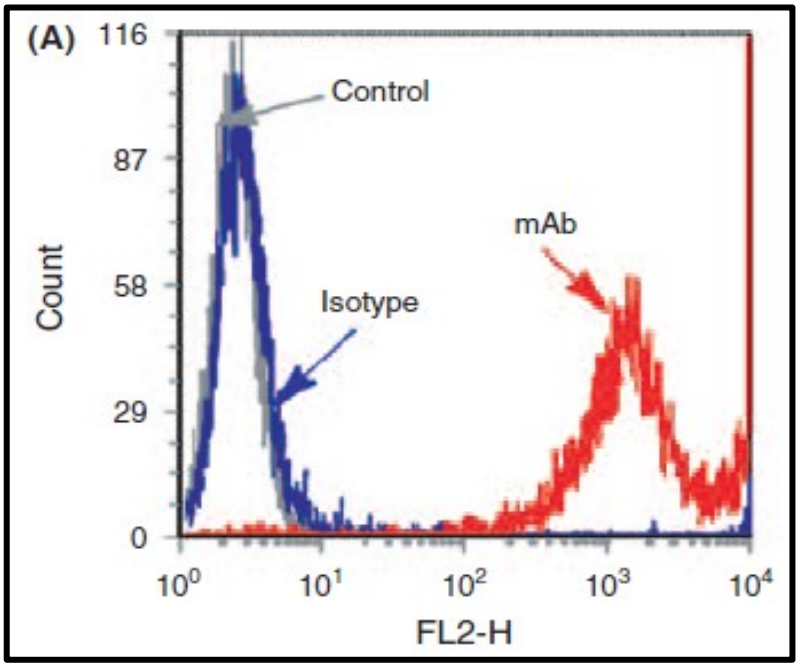

Figure 3.11: Flow cytometry analysis of MH-S cells upon incubation with PE-isotype control, PE-anti-CD44 mAb IM7 for 45 min at 4ºC respectively as compared with cells without treatment.

The confocal images of MH-S cells used as a positive control and treated only with Alexa 488-HA-TS_7 micelles were shown in Fig. 3.12 (A). The green fluorescence at the surface of MH-S cells confirms the presence of Alexa 488-HA-TS_7 micelles having an affinity for CD44 receptors. However, the confocal images of MH-S cells treated with PE-anti-CD44 mAb IM7 for 30 min at 4 °C were shown in Fig 3.12 (B). The red fluoresce on the macrophage membrane confirm the presence of CD44 receptors on the cell surface as CD44 mAb IM7 only binds with CD44 receptors. However, the MH-S cells treated with PE-anti-CD44 mAb IM7 for 30 min at 4 °C, followed by incubation with Alexa 488-HA-TS_7 micelles for 2 h were shown in Fig 3.12 (C). As expected, the Alexa 488-HA-TS_7 micelles exhibit a less intense green fluorescence as compared with that in the cells without antibody pretreatment (Fig. 3.12 A), indicating that the PE-anti-CD44 mAb IM7 can bind the CD44 receptor competitively thus inhibit uptake of Alexa 488-HA-TS_7 micelles. This was confirmed with the co-localization of Alexa 488-HA-TS_7 with PE-anti-CD44 mAb IM7, which produces the yellow fluorescence in the merged images.

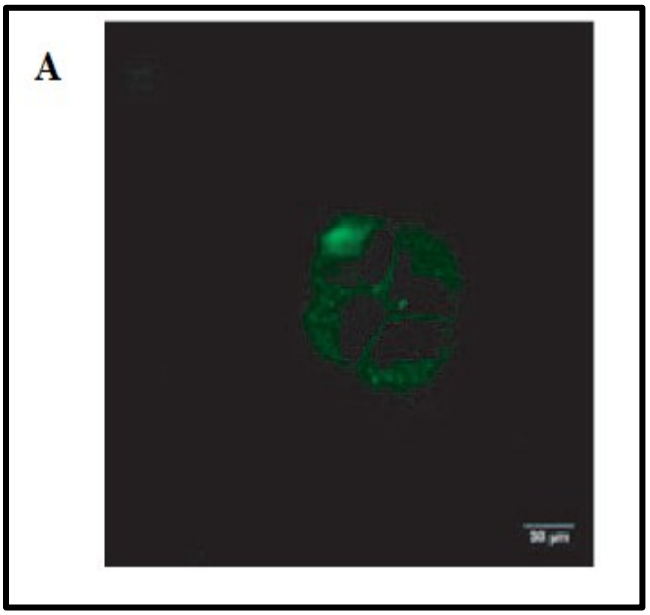

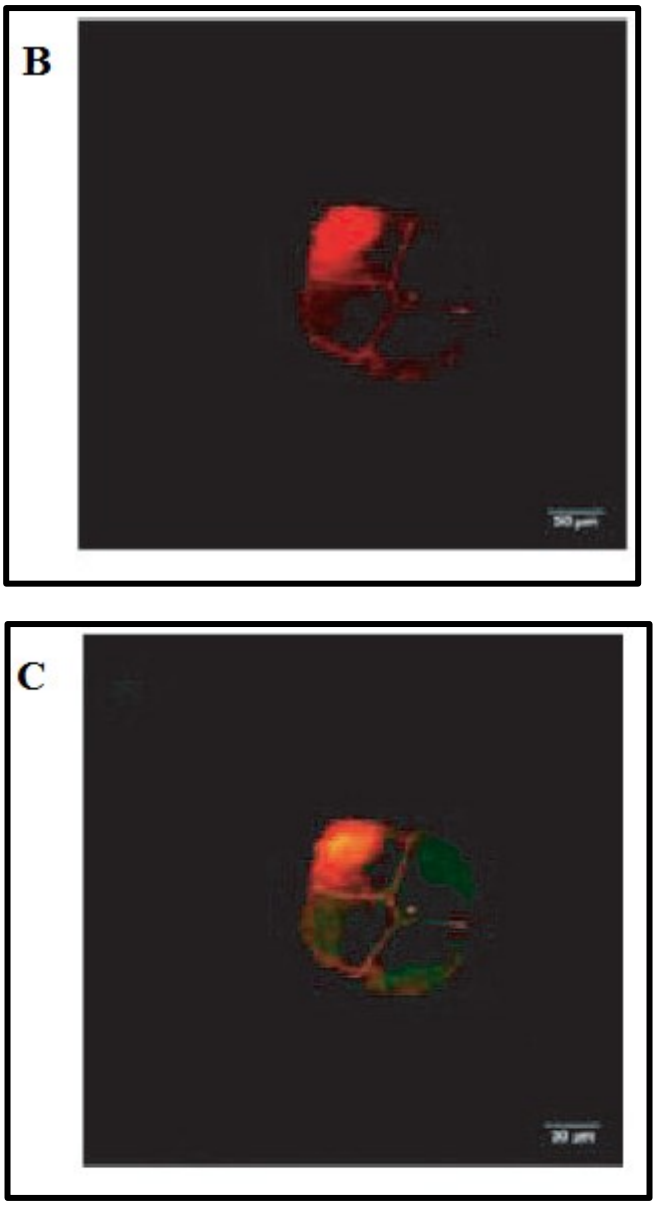

Figure 3.12: Confocal images of MH-S cells (A) HA-TS_7 micelles was visualized using conjugate Alexa 488 (green). (B) PE-anti-CD44 mAb IM7 was visualized as (red) (C) Uptake of HA-TS_7 micelles after pre-treating them with PE-anti-CD44 mAb IM7 (Scale bar is 30 μm).

3.8.9 Cell viability

The MH-S cell cytotoxicity was determined using the MTT assay. Blank HA-TS_7 micelles, RIF-HA-TS_7 micelles and free RIF solution were evaluated using the MTT assay. The MTT results using different concentrations of RIF-HA-TS_7 micelles and RIF-solutions were shown in Fig. 3.13. In general, by increasing the concentration, there was an increase in cellular toxicity for both RIF-HA-TS_7 micelles and RIF-solutions. However, RIF-HA-TS_7 micelles significantly exhibit higher cytotoxicity to MH-S cells than to free RIF solution within 48 h, which might be due to higher uptake of RIF-HA-TS_7 micelles.

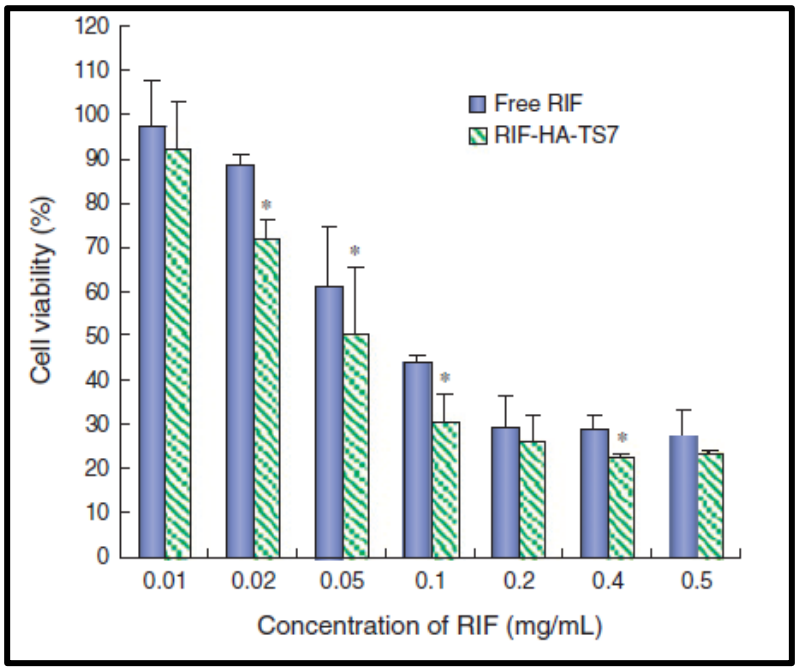

Figure 3.13: Viability assays of MH-S cells by treatment with free RIF solution versus RIF-HA-TS_7 micelles. Data shown is the means ± S.D. (n = 6) * $p < 0.05$.

The MTT results using different concentrations of blank HA-TS_7 micelles were shown in Fig. 3.14. In general, by increasing the concentration range from 25-250 µg/mL, there was no obvious cytotoxicity observed over 48 h for blank HA-TS_7 micelles which showed the favorable biocompatibility of blank HA-TS7 to MH-S cells.

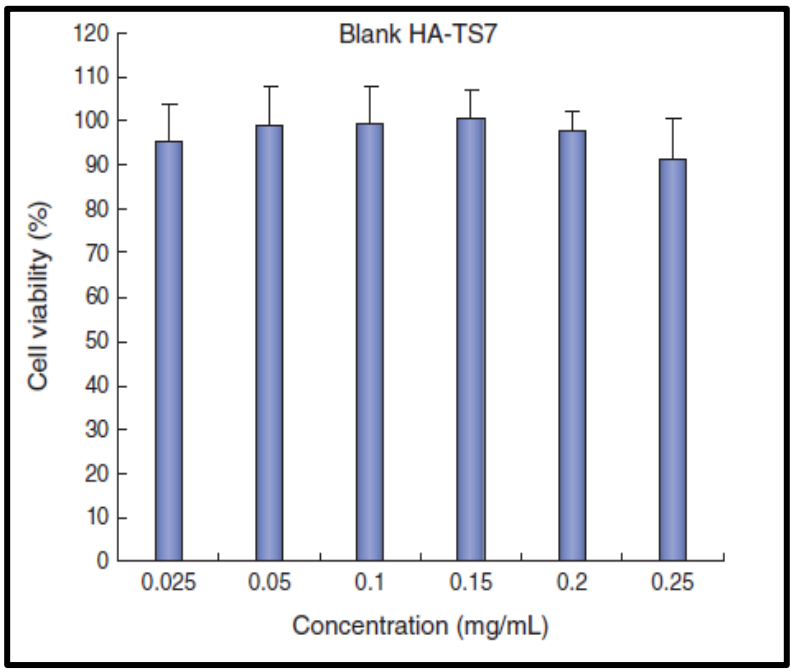

Figure 3.14: Viability assays of MH-S cells by treatment with Blank-HA-TS_7 micelles. Data shown is the means ± S.D. (n = 6) * $p < 0.05$.

3.8.10 Cytokine secretion assay

Elimination of MTB infection mainly depends on the success of the interaction between infected macrophages and T lymphocytes [109].Differentiated T- cells can be divided into proinflammatory Th1 and anti-inflammatory Th2 subsets based on their cytokine production [124]. Macrophage infected with MTB uses a Th1 response to fight the infection in the early stage [125]. Thus various cytokines (IL-12p70, IL-2, IL-1β, IL-12p40p70, IFN-γ, TNF-α, IL-4, IL-5, IL-6, IL-9, IL-10, IL-13) and chemokines (MIP-1α, MIP-2, MIP-3β, RANTES, leptin, KC, MCP-1 and MCP-5) were investigated after macrophages were exposed to different treatments.

To determine a qualitative estimation of cytokine, LPS, blank HA-TS micelles, RIF-HA-TS micelles and free RIF solution were tested using mouse cytokine protein array II membranes. The results were shown in Fig. 3.15 and 3.16

.

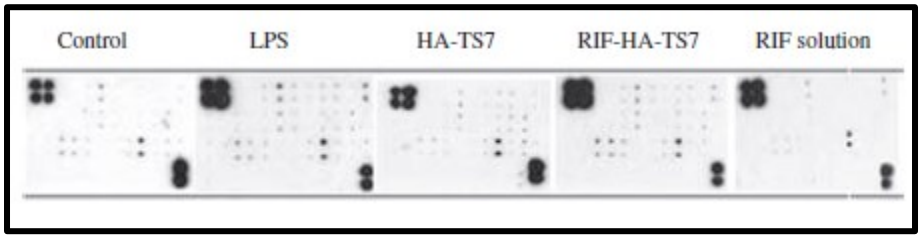

.

Figure 3.15: Images of mouse cytokine protein array II membranes that were assayed with the conditioned media obtained after incubation with multiple treatments for 6 h.

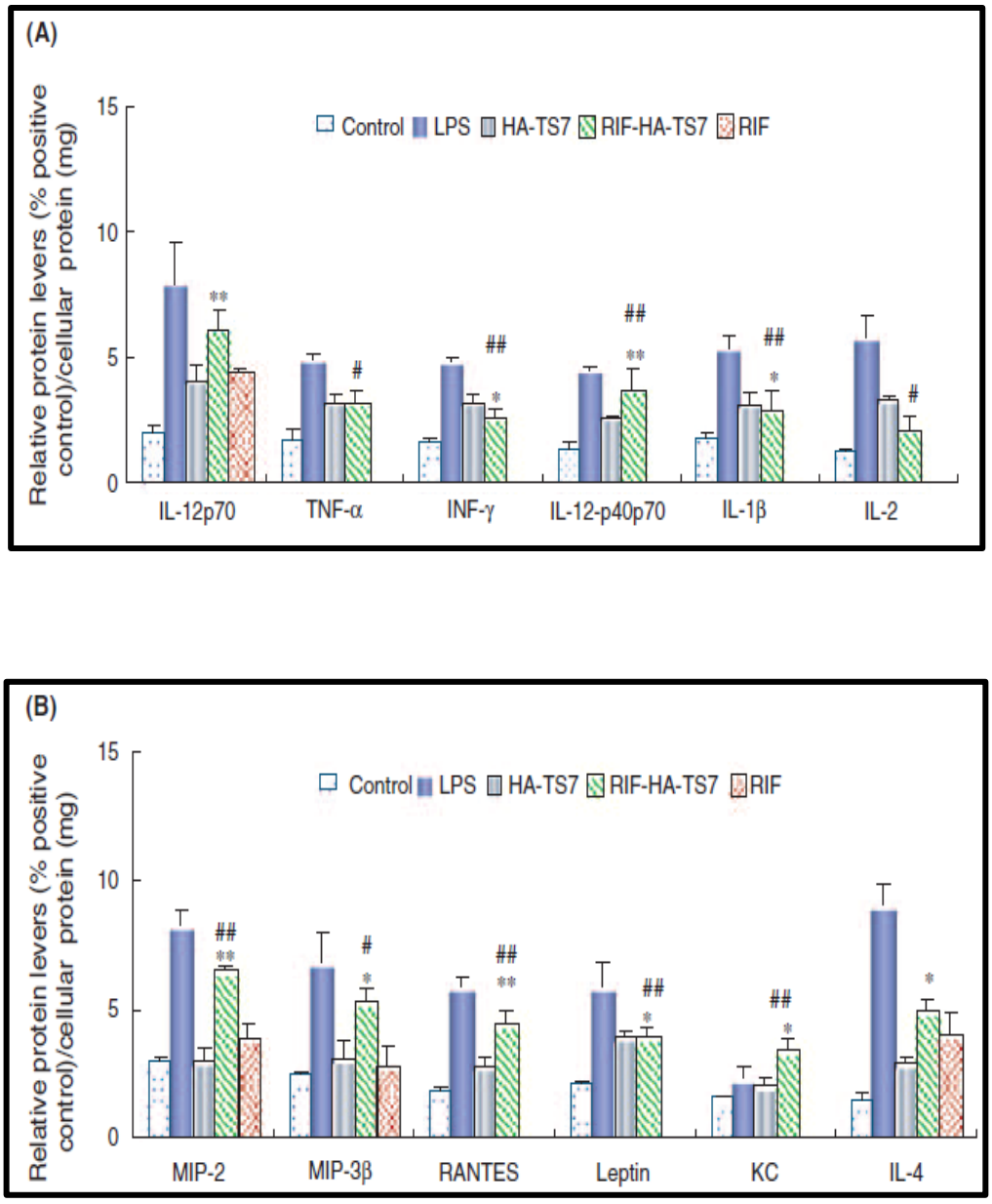

Figure 3.16: (A-B) Cytokines and chemokines release from MH-S cells following exposure to LPS, blank HA-TS_7 micelles, RIF-HA-TS_7 micelles and free RIF solution, which was determined using the microarray at 6h. Untreated cells were used as a control. *Significant of RIF-HA-TS versus control, # Significant of RIF-HA-TS vs. free RIF solution. **, ## $p < 0.01$, *, # $p < 0.05$.

Our results showed a significant increase in Th1 cytokines and chemokines (IL-12p70, IL-12p40p70, MIP-2, MIP-3β, RANTES, IFN-γ, leptin, KC and IL-1β) at 6 h, in macrophages exposed to RIF-HA-TS_7 micelles as compared to untreated macrophages (controls) (Fig 3.15 & 3.16).

Furthermore, a significant increase of proinflammatory cytokine and chemokines including TNF-α, IFN-γ, MIP-2, MIP-3β, IL-12p40p70, RANTES, leptin, KC, IL-1β and IL-2 was detected in MH-S cells when exposed to RIF-HA-TS_7 micelles as compared to those treated with free RIF solution only. In-significance difference was observed for the secretion of anti-inflammatory cytokine IL-4.

Also, the immune response from MH-S cells after LPS treatment was significantly higher than that when MH-S cells were treated with the RIF-HA-TS_7 micelles as shown in appendix -I. Finally, there was no production of cytokine and chemokines such as IL-3, IL-5, IL-6, IL-9, IL-10, IL-13, MCP-5, MCP-1 and MIP-1α in MH-S cells treated with RIF-HA-TS micelles as well as RIF solution.

3.9 Discussion

In our study, we developed RIF-HA-TS micelles which had targeting tag leading to the efficient cellular uptake of the RIF in MH-S cells. We examined the cellular uptake behavior of RIF-HA-TS micelles by MH-S cells by measuring intracellular RIF concentration under various conditions. The results showed that the cellular uptake of RIF-HA-TS micelles was dependent on the degree of substitution, dose, time and temperature.

The data revealed that DS had some effect on the cellular uptake of HA-TS micelles (Fig 3.1). HA-TS conjugates with low DS (i.e., HA-TS_7) were more readily internalized than those with high DS. It might be due to hydrophilic HA moieties on the surfaces of HA-TS conjugates, which might interact with the CD44 receptor and subsequently enhance the ability of RIF-HA-TS micelles to enter MH-S cells. It was in accordance with a reported study where nanoparticles that exhibit a high grafting density of HA show a significantly higher uptake [126]. Another possible reason may be the size of the micelles. It has been reported that particle size is an important factor for the phagocytosis of particles by macrophages [127,128]. Our data showed that lower DS leads to a larger size RIF-HA-TS_7 micelles (~300 nm) that were taken up more significantly than the smaller micelles (Fig. 3.1 and Table 3.2).

The data showed that there was a delay before a significant increase in total RIF concentration occurred at 12 h (Fig 3.3). The RIF concentration decrease between 12 and 24 h that might be due to the diffusion of RIF outside of the cells. A similar result was reported by Hirota et al. who studied RIF-PLGA microsphere in NR8383 cells [87]. Onoshita et al. indicated that the highest uptake of RIF-PLGA microsphere occurred at 12 h and then decreased rapidly between 12 and 24 h [97].

The high uptake of RIF-HA-TS micelles following LPS treatment could be explained by LPS turning CD44 into its high-affinity HA binding form (Fig. 3.5). Similar results were reported by Kamat et al. that the uptake of HA covered nanoparticles was increased upon LPS stimulated [129].

Low-molecular-weight of HA plays a major role in macrophage activation which could activate an innate immune response via Toll-Like Receptor TLR2 and TLR4 [92,130]. Our studies showed that HA (50 μg/mL) could block the RIF-HA-TS micelles uptake on MH-S cells while HA with a higher concentration of 150 μg/mL improves the uptake of RIF-HA-TS micelles (Fig. 3.7). The activation causes a 1.5-fold higher cellular uptake by MH-S as compared to no treatment. This might be due to the excretion of a cytokine such as TNF-α by the HA-treated cells [92,131] which change the morphology of CD44 receptor thus increase the binding of HA to CD44 [44].

LPS is a potent stimulator of innate immune response. It was used as a positive control in this study at a concentration range of 100 ng/ml. LPS treatment showed significant increases in Th1 cytokines production (secondary toxicity) for 6 h incubations compared with that of untreated cells. This showed the high sensitivity of macrophage to LPS. Beside LPS, the data also revealed that the HA could also induce the activation of macrophage as compared to the control [132]. The results showed that HA-TS micelles at a concentration of 215 μg/mL could activate macrophage and induce proinflammatory cytokines and thus enhance the uptake of RIF-HA-TS micelles (Fig. 3.6).

The data showed the secretion of cytokine (secondary toxicity effect) in response to RIF-HA-TS or free RIF solution (Fig. 3.16). Our results showed a significant increase in Th1 cytokines and chemokines (TNF-α, IFN-γ, MIP-2, MIP-3β, IL-12p40p70, RANTES, leptin, KC, IL-1β and IL-2) in macrophages after 6 h, exposed to RIF-HA-TS micelles as compared to those treated with

free RIF solution. There was no significant difference of Th2 cytokine such as IL-4 between these treatment groups. Furthermore, other Th2 cytokines IL-3, IL-5, IL-6, IL-9, IL-10 and IL-13 were not observed in both treatments. It indicates that RIF loaded into micelles increase the Th1 response of cells. This might be key to enhance rifampicin therapy against TB infection. Similar results have been reported by other authors using micro-particles [133]. Additionally, although cultures exposed to both blank HA-TS micelles and RIF-HA-TS micelles trigger cytokine produvtion, but their level was lower as compared to those for LPS.

Based on all above finding, RIF-HA-TS micelles enhance cellular uptake while concomitantly stimulating an innate immune response (i.e. stimulation of proinflammatory cytokines (secondary toxicity effect)), thus demonstrating the suitability of HA-TS micelles as potential drug delivery nanocarriers for TB treatment.

3.10 Conclusion

Compared to the free RIF solution, the RIF-HA-TS micelles were more efficiently taken up by MH-S cells via phagocytosis and receptor-mediated endocytosis. The cellular uptake of RIF-HA-TS micelles was time as well as dose-dependent on MH-S cells. The HA-TS micelles retained the biological recognition of HA receptor that interact with a CD44 receptor on macrophage surface. Furthermore, the HA-TS micelles could induce the proinflammatory cytokine release (secondary toxicity effect) that might enhance the anti-tuberculosis activity of RIF. The RIF-HA-TS micelles delivered the drug more efficiently to macrophage and concomitantly stimulate an innate immune response. Both effects might increase the efficiency of the new treatment.

Chapter 4

Immune Response to Anti-tuberculosis Drug Loaded Gelatin and Polyisobutyl-Cyanoacrylate Nanoparticles in Macrophages

This study has already been published as Muhammad Sarfraz, Wenjun Shi et al. *Immune response to anti-tuberculosis drug-loaded gelatin and polyisobutyl-cyanoacrylate nanoparticles in macrophages in Journal of Therapeutic Delivery. April 2016, 07:04: 213-228*

Abstract

Background: Secondary toxicity of nanoparticles in macrophages is a well-known phenomenon. The aim of the study was to investigate the immune-response of macrophages after nanoparticle treatment.

Methods & Results: Antituberculosis drugs moxifloxacin and rifampicin were loaded into gelatin and polyisobutyl-cyanoacrylate nanoparticles. The nanoparticles were physicochemical characterized. Cellular immune responses and cellular viability were determined. The drug release kinetics vary depending on the type of nanoparticle, size and loading capacity. IC50 values of polyisobutyl-cyanoacrylate nanoparticles were lower than for gelatin nanoparticles. Nanoparticles treatment induced the higher release of Th1 type cytokines compared to free drug.

Conclusion: Nanoparticles together with chemotherapeutic drugs might be able to trigger an immune response in macrophages. The combined effect might be able to overcome mycobacteria infections.

Keywords: Nanotechnology, Rifampicin, Moxifloxacin, Macrophage, Immuno-stimulation, Tuberculosis.

4.1 Introduction

The success of any drug therapy depends upon its ability to overcome challenges like poor solubility, alteration in pharmacokinetics, cytotoxicity and delivery to the site of action. In the past decades, the use of nanoparticles (NPs) to deliver drugs has shown potential to overcome problems with solubility, hydrophobicity and poor bioavailability. NPs can be used for controlled release or targeted drug delivery [134,135]. Drugs contained in NPs might also show reduced systemic toxicity [136]. However, drug targeting can be challenging, for example, polystyrene NPs of 60 nm are quickly removed from the blood [137].Other injectable NPs show even shorter half-lives due to macrophage uptake [138]. Macrophages play a major role in interrupting drug targeting strategies. However, NPs are an ideal drug carrier if the macrophage is itself the target cell [139,140].

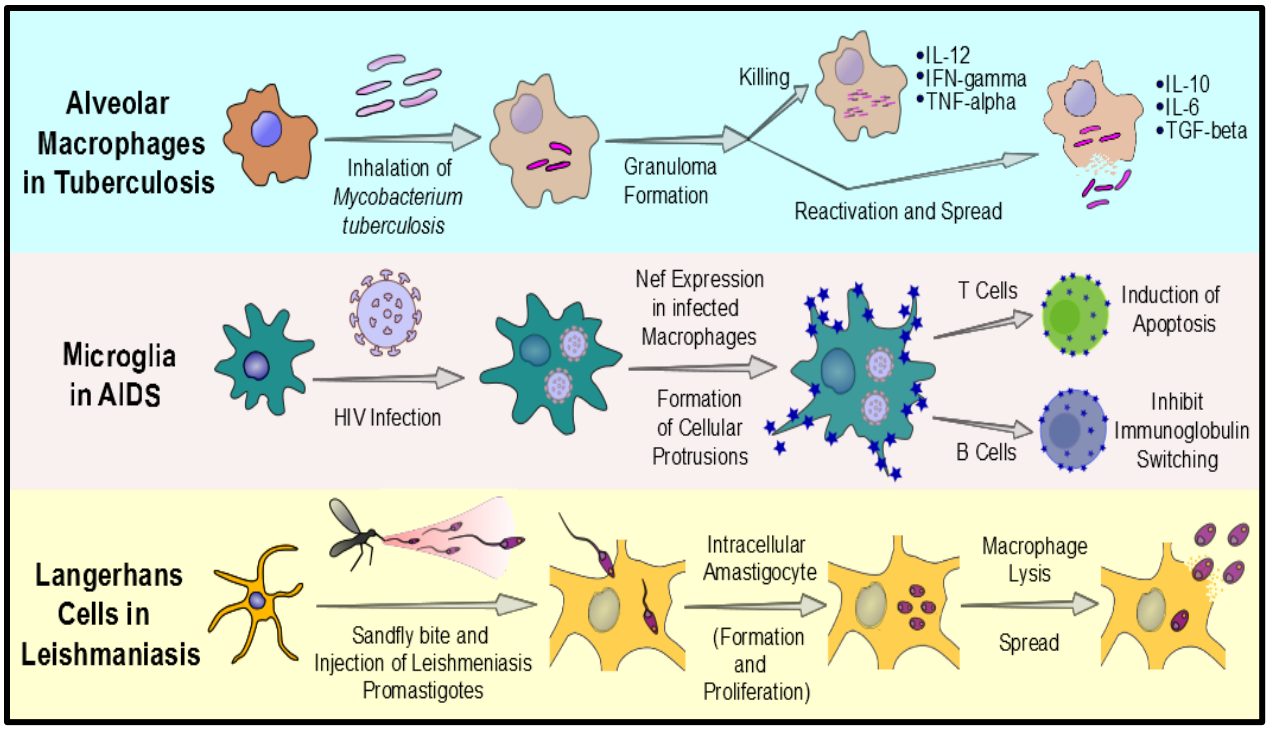

Figure 4.1: The role of the macrophage in different diseases. Adapted from ref [125,141,142].

Macrophages play a major role in the progression of diseases like tuberculosis [125], acquired immune deficiency syndrome (AIDS) [141] and leishmaniasis [142], as outlined in Fig. 4.1. Tuberculosis (TB) is reported to kill more than 3500 people daily globally and leading to 1.3 million deaths yearly [143]. Alveolar macrophages are host cells for the mycobacterium tubercle [144]. The mycobacterium multiplies in macrophages and triggers a cascade of immune responses. These immunological activities are necessary for the fight against a TB infection [145,146]. In *Mycobacterium tuberculosis* infections, a strong CD4+ T type 1 helper (Th_1) like the immune response is considered critical for the containment of the disease. The immune response activates infected macrophages with the Th1-type cytokine tumor necrosis factor (TNF-α) [147], interlukin-10 (IL-10) [114,148], and interleukin-1β [112,149], as shown in Fig. 4.2.

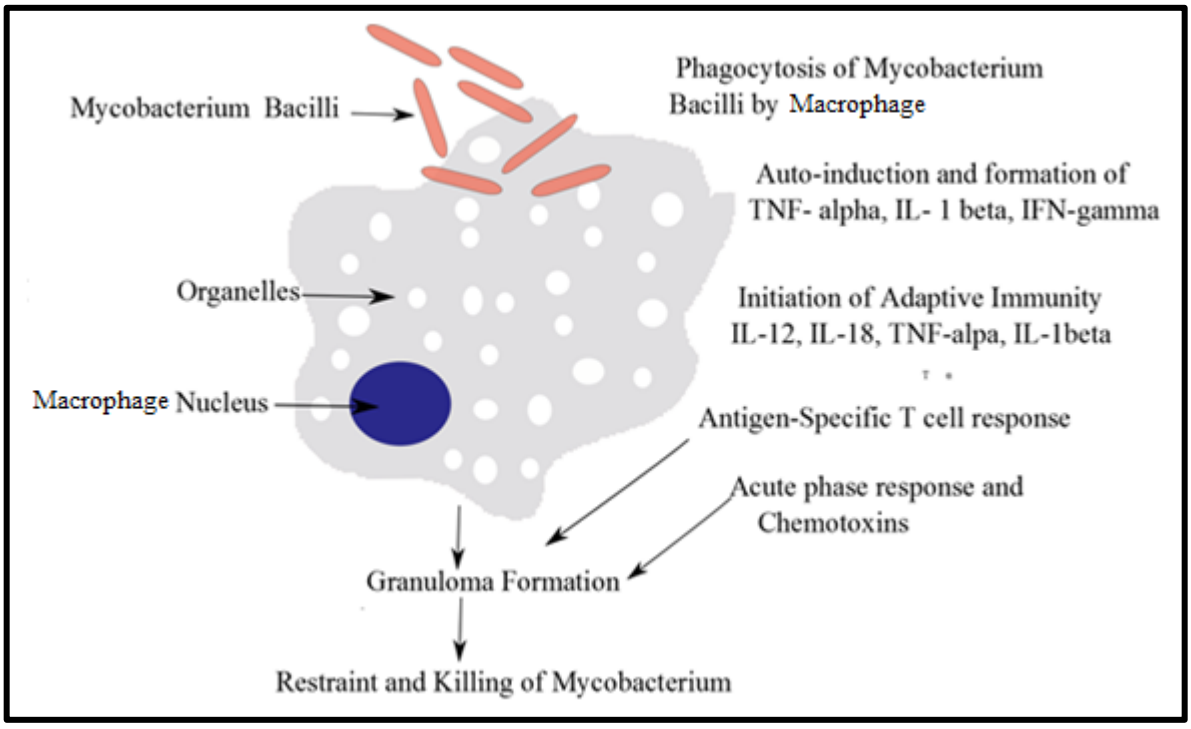

Figure 4.2: The cascade of activity in a macrophage after *M. tuberculosis* infection. Adapted from ref [125].

TNF-α plays a crucial role in protection against TB infection and in the development of clinically active TB. It promotes phagocytosis and killing of mycobacteria by macrophages by programmed apoptosis [150], recruitment and accumulation of immune cells at the site of infection and granuloma formation in latent *M. tuberculosis* infection. It is also important in controlling persistent infection and in containing organisms within granulomas [151]. The significance of TNF-α in controlling human *M. tuberculosis* was realized when anti-TNF-α therapy in rheumatoid patients led to reactivation of latent TB infections [152].

Studies have shown that NPs exposure can prompt IL-1β production in macrophages. IL-1β is a fundamental component to establishing innate resistance against *M. tuberculosis*. IL-1β plays a significant role in pathways and production of proinflammatory cytokines required to control *M. tuberculosis* infections [112].

The IL-10 cytokine also plays a major role in immune regulation during *M. tuberculosis* infection [114]. Its anti-inflammatory response to *M. tuberculosis* infections helps the progression of mycobacterium by down-regulating the production of proinflammatory cytokines [115]. IL-10 inhibits the production of proinflammatory interferon-gamma IFN-γ from T-cells [116] and inhibits phagosome maturation in mycobacterium-infected macrophages, one of the main antimicrobial mechanisms expressed by macrophages [148]. Phagosome maturation includes acidification of the phagosome, production of antimicrobial peptides, and activation of NADPH oxidase and inducible nitric oxide synthase (iNOS) which leads to the production of reactive nitrogen species and degradative enzymes such as cathepsins [153-155].

Both innate and adaptive immunity play crucial roles in the clearance, retention, and reactivation of *M. tuberculosis* in the body. Innate immunity is characterized by a Th1-like immune response and adaptive immunity is characterized by T-cell involvement in *M. tuberculosis* infections. The delicate balance between these contradictory immune responses can either foster or inhibit *M. tuberculosis* infections. Fig. 4.3 outlines the role of immunity in *M. tuberculosis* infection. High innate immunity leads to clearance of mycobacterium with no TB. An innate response with abnormal cellular responses allows *M. tuberculosis* to proliferate in less than 10% of infected people. However, normal innate and adaptive response cause latent infection with reactivation and containment in 10% and 90% of individuals, respectively [156].

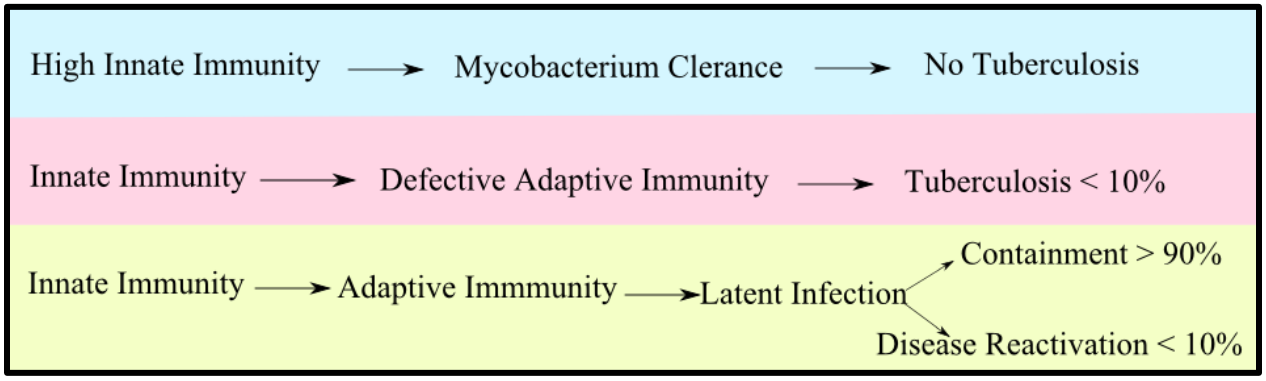

Figure 4.3: The role of immunity in mycobacterium tuberculosis infection and its possible outcomes. Adapted from ref [156].

Thus, any trigger that can activate or potentiate macrophage signaling and induce Th1 cytokines could be used to improve *M. tuberculosis* treatment. Several NPs types have been reported to induce cytokine related Th_1 release and to help treat infections [157]. A better understanding of different factors and components that may affect the immune response of macrophages can lead to the development of better *M. tuberculosis* treatments in macrophages.

The current study explores the interaction of NPs with macrophages, the ability of NPs to initiate the signaling mechanism by releasing proinflammatory TNF-α and IL-1β, or anti-inflammatory cytokines (IL-10), and the impact of NPs size on these cell responses. The interactions of macrophages with two different biodegradable polymers (Gelatin and PIBCA (PolyIsobutyl-cyanoacrylate)) and two separate anti-tuberculosis drugs (Rifampicin and Moxifloxacin (1^{st} and 2^{nd} line anti-tuberculosis drugs) were tested. These two polymeric nanoparticle were selected due to their different cytotoxic potential of the polymer and ease of obtaining different particle sizes by modifying the synthesis process.

4.2 Materials and Methods

4.2.1 Material

Gelatin type B from bovine skin (225 Bloom), glutaraldehyde grades I (25% aqueous solution), Dextran, DMSO (Dimethyl Sulfoxide), MTT (3-(4,5-dimethylthiazol-2-yl)-2,5-diphenyltetrazolium bromide), LPS (Lipopolysaccharides), Mannitol and trypan blue were purchased from Sigma (Ontario, Canada). Acetone were purchased from Caledon (Georgetown, ON, Canada). RPMI-1640 medium, 1.25% Trypsin-EDTA, fetal bovine serum (FBS), Phosphate Buffer Solution (PBS) and other cell culture supplements were supplied from Invitrogen (Ontario, Canada). All chemicals were of analytical grade and used as received.

PolyIsobutyl-cyanoacrylate monomer (Lot. 02GD9236) was a gift from Loctite Ltd. (Dublin, Ireland. Rifampicin (RIF) was obtained from PCCA (Ontario, Canada) and Moxifloxacin (MOX) from Wanquan Pharmaceuticals (Beijing, China). Dialysis membranes were from Spectrum Laboratories Inc. (RanchoDomi, guez, CA, USA). 0.45 μm polyvinylidene fluoride filter (Millipore, Billerica, MA, USA), and 0.8 μm nucleopore® membrane filter, Whatman (Ontario, Canada) Murine alveolar macrophages (MH-S) cell lines were obtained from American Type

Culture Collection (ATCC, Rockville, USA). 75ml cell culture flask, 12 well plates supply from Invitrogen (Ontario, Canada). ELISA kits by Thermo-scientific (Canada, Ontario).

4.2.2 Methodology

4.2.2.1 Gelatin nanoparticles

Gelatin NPs were prepared by a two-step desolvation process previously described by Coester et al. [158]. Briefly, 2.5 g of gelatin B was dissolved in distilled water under constant stirring (500 rpm) and heating (40 °C). The high molecular weight fraction of gelatin was precipitated in the first desolvation step using acetone. The supernatant was used to determine the lower molecular weight fraction of gelatin by removing the acetone and freeze-drying the remaining gelatin. The amount was deducted from the starting material and utilized for the drug loading calculations. The higher molecular weight gelatin was dissolved using distilled water. After redissolving the HMW gelatin with water and adjusting the pH to 2.5 using 0.1 M hydrochloric acid the acetone was added initially at a faster rate and then dropwise until the NPs were formed. The 100 µL of an 8% aqueous solution of glutaraldehyde was added as a cross-linker to stabilize the *in situ* formed NPs. Acetone remaining in the gelatin NPs dispersion was removed by evaporation under vacuum using a rotary evaporator (IKA, Staufen, Germany). The resulting NPs were purified by centrifugation at 8000 rpm for 30 min (Beckman L8-M ultracentrifuge, CA, USA) and washed three times with distilled, deionized water (ddH_2O). The NPs were collected and filtered through a hydrophilic 0.45 μm polyvinylidene fluoride filter (Millipore, Billerica, MA, USA), followed by lyophilisation for 24 h at -80 °C and 45 Pa. Two different sizes of NPs were achieved by modifying the process variable in the two step desolvation process as discussed by Azarmi et al [159].

4.2.2.2 Preparation of rifampicin and moxifloxacin loaded gelatin nanoparticles

Approximately 10 mg of moxifloxacin hydrochloride (MOX) or 5 mg rifampicin (RIF) was dissolved in acetone at a concentration of 2 mg/mL. The solutions were added in the second desolvation step in the NPs preparation after pH adjustment. The remaining procedures were the same as described for gelatin NPs.

4.2.2.3 Drug loading of gelatin nanoparticles

Drug loading was calculated as the difference between the added amount of drug and the unbound fraction of the drug found in the supernatant of the unwashed NPs suspension. 250 µL of the unwashed NPs dispersion was centrifuged at 100,000 g for 30 min using an Airfuge (Beckman) centrifuge. The supernatant was separated and analyzed for free drug using UV spectrophotometry (UV1700 Shimadzu, Japan).

4.2.2.4 Drug release from gelatin nanoparticles

The drug release kinetics of drug loaded gelatin NPs were evaluated using equilibrium dialysis to quantify drug transport across the dialysis membrane. In brief, 5 mg of drug loaded NPs were mixed in 2 mL of phosphate-buffered saline (PBS) and placed in a dialysis bag (MWCO: 12–14 kDa, surface area of 22.5 cm^2). The dialysis bag was submerged in 500 ml PBS, pH 7.4, and stirred with a magnetic stirrer at 50 rpm at 37 °C. At designated time intervals, 500 µL aliquots were collected and replaced with fresh media. The release study was carried out in triplicate for 48 hours. Drug concentrations in the samples were determined by HPLC method.

4.2.3 Polyisobutyl-cyanoacrylate nanoparticles

Polyisobutyl-cyanoacrylate (PIBCA) was used as a polymer for NP preparation. PIBCA NPs were prepared by a controlled polymerization using an emulsion polymerization method reported in the literature [160]. In brief, 100 mg of dextran was added to 10 mL of 0.01 M

hydrochloric acid, then 100 μL of polyisobutyl-cyanoacrylate monomer was added under continuous stirring at 600 rpm for another 4 hours. The NP suspension was filtered through a 0.8 μm nucleopore® membrane filter, Whatman (Ontario, Canada) under vacuum. The particles were then lyophilized with 3% (w/v) mannitol as a cryoprotectant at -80 °C and 45 Pa. Two different sizes of NPs were prepared by the emulsion polymerization process by changing the pH, the monomer and the dextran concentration as reported [161].

4.2.3.1 Preparation of moxifloxacin loaded PIBCA nanoparticles

Moxifloxacin loaded PIBCA NPs were prepared by an emulsion polymerization method [162]. In brief, an aqueous solution of HCl (pH 2–3) was mixed with 1% dextran (w/w) and stirred at 600 rpm for a few minutes. Moxifloxacin was added to the mixture at a concentration of 2 mg/mL and a 1% v/v solution of n-butyl-2-cyanoacrylate added dropwise with continuous stirring. The synthesis was continued for another 4 hours, after which the reaction was neutralized with 0.1 N NaOH. The NPs suspension was purified by centrifugation at 100,000 g for 30 min and washed three times with ddH_2O. The NPs suspension was filtered through a 0.8 μm nucleopore® membrane filter from Whatman (Ontario, Canada) under vacuum and lyophilized as described previously. Two different sizes of moxifloxacin loaded PIBCA NPs were prepared by changing the pH from 2.0 to 3.0 [161].

4.2.3.2 Drug loading of PIBCA nanoparticles

Drug loading was calculated as the difference between the added amount of drug and the unbound fraction of the drug found in the supernatant of an unwashed NPs suspension, as described above. The supernatant was separated and analyzed for the free drug by UV spectrophotometry.

4.2.3.3 Drug release from PIBCA nanoparticles

The *in vitro* release kinetics of moxifloxacin from PIBCA NPs were determined using a centrifugal ultrafiltration technique [163]. In brief, 19.5 mg lyophilized mixed with 1 mL phosphate buffered saline (PBS) at pH 7.4. The resultant mixture was further diluted 1:25 with PBS to attain sink condition at 37 °C. At predefined time points, a 0.25 ml aliquot of the solution was transferred to a centrifugal filter unit and the amount of moxifloxacin was measured in the filtrate using HPLC method. The first sample was collected immediately, and additional samples were collected after 0.5, 1, 2, 6, 8, 12, 16, 20, 24, and 48 h. The volume of medium remained constant as each withdrawn sample was replaced with an equal quantity of freshly released medium. The dilution was corrected in the drug release calculations. A moxifloxacin solution prepared under the same conditions was used as the control. Each experiment was performed in triplicate.

4.2.4 Quantitative analysis by UV spectrophotometry

A UV spectrophotometer was used for quantitative analyses of drug loading NPs. Rifampicin concentrations were measured at 337 nm (rifampicin absorbance maximum). The method was validated over the range of 0 to 15 µg/mL [164]. Moxifloxacin concentrations were measured at 295 nm (moxifloxacin absorbance maximum). The method was validated over the range of 2 to 8 µg/mL [165].

4.2.5 Quantitative analysis by HPLC method

The concentration of MOX and RIF was determined by a reversed-phase HPLC, which was previously published [98]. In Brief the column was a LiChrocart-LiCrospher 100 RP-18, 5 µm stationary phase (Merck, Darmstadt, Germany), the mobile phase consisted of a mixture of methanol and 0.3% v/v triethylamine-0.02 M PBS (pH 3.0) (40: 60 v/v) for the analysis of MOX

and a 20 µL sample was injected at a flow rate of 0.9 mL/min with UV detection at 295 nm. The mobile phase used for the analysis of RIF comprised of a mixture of methanol and 10 mM ammonium acetate (60: 40 v/v), at a flow rate of 0.9 mL/min with UV detection at 337 nm.

4.2.6 Characterization of nanoparticles

The particle size distribution was measured by dynamic light scattering (DLS) using a photon correlation spectrometer (Zetasizer HAS 3000) from Malvern (Worcestershire, UK). 100µL of the NPs suspension was dispersed in 4 ml deionized water. All of the DLS measurements were performed at 25 °C and a scattering angle of 90°. A polydispersity index was used to indicate the width of the distribution. The morphology and size distribution was confirmed by transmission electron microscopy (TEM, H-600, Hitachi, Japan).

4.3 Cell culture

MH-S cells, a continuous cell line of murine alveolar macrophages, were cultivated in 75 mL ventilated flasks (Corning, USA) using RPMI-1640 medium supplemented with 100 IU/mL penicillin, 10 µg/mL streptomycin, and 10% (v/v) fetal bovine serum. Macrophages were grown at 37 °C in a 5% CO_2 humidified incubator. For subculturing, the cells were maintained by transferring floating cells to a centrifuge tube. Adherent cells were rinsed with a 0.25% trypsin, 0.53 mM EDTA solution. The solution was removed and 1 to 2 mL of trypsin-EDTA solution was added. The flask was allowed to sit at room temperature (or at 37 °C) until the cells were detached. The detached cells were added to the floating cells collected above, and the cell suspension was centrifuged at 1000 rpm for 10 minutes. The pellet was re-suspended in fresh medium, aspirated and dispensed into clean flasks.

4.3.1 Cell viability assay

The cytotoxicity of drug loaded NPs was measured using an MTT assay, which is based on

the conversion of MTT (3-(4,5-dimethylthiazol-2-yl)-2,5-diphenyltetrazolium bromide) into formazan crystals by living cells. In brief, cells grown in flasks were washed with phosphate-buffered saline (PBS) and trypsinized using a 0.25% trypsin–EDTA solution. The cells were centrifuged, the supernatant was discarded, and the cells were resuspended in RPMI-1640 complete medium. Approximately 5000 cells were counted using a hemocytometer, seeded in each well of a 96-well plate and incubated for 24 h in a humidified atmosphere of 5% CO_2 at 37 °C. After 24 h, the wells were rinsed with PBS.

Free drug, blank NPs, rifampicin-loaded and moxifloxacin loaded NPs of two different sizes were added at desired different concentrations in a 96-well culture plate. Cells without any treatment served as negative controls. After 24 h incubation, the medium was replaced with 180 µL fresh complete medium and 20 µL MTT solution (5 mg/mL). Cells were incubated for an additional 4 h. The medium was carefully removed, and 200 µL DMSO was added to dissolve the formazan. Absorbance was measured at 570 nm using a microplate reader (VMax® Kinetic, Molecular Devices, CA) at 25 °C. Cell viability was calculated as a percentage of absorbance compared with that of untreated cells. The experiment was replicated six times for each time point.

Cell viability was expressed in the form of IC_{50} (concentration required for 50% inhibition) which reflects the cytotoxicity of NPs to the cells. The higher the toxicity of the NPs suspension, the lower the IC_{50} value.

4.3.2 Cytokine screening

For cytokine profiling, MH-S cells were seeded at a density of 1.0×10^5 cells/well in a 12 well plate and incubated for 24 h in a humidified atmosphere of 5% CO_2 at 37 °C. After 24 h, the medium was replaced with fresh medium and approximately 30 µL of the previously listed treatments were added to each well. Lipopolysaccharide (LPS) (100 ng/mL) was used as positive

control. Control wells consisted of cells incubated with medium only (untreated cells). After 24 and 48 h, the supernatants were collected from all treatments and centrifuged at 8000 rpm for 5 min to remove cellular debris and stored at -80 °C for quantitative determination of cytokine content by ELISA kits.

4.3.3 Enzyme-linked immunosorbent assay (ELISA)

ELISA kits were used to quantify the cytokine release from the collected samples. In brief, 50 µL of buffer was added to each well of a 96 well plate, then 50 µL of standard and sample treatment were added to each well in duplicate and the plate was covered and incubated for 3 hours at room temperature. The plates were washed with washing buffer 3 times. 50 µL of premixed biotinylated antibody reagent was added to each well; the plates were covered and incubated for 1 h at room temperature. The plates were washed 3 times with washing buffer and 100 µL of streptavidin-horseradish peroxidase (HRP) concentrate in dilute buffer was added to each well, the plates were covered and incubated for 30 min at room temperature. The plates were washed with washing buffer 3 times and 100 µL of tetramethyl-benzidine (TMB) substrate was added to each well. The plates were developed for 30 minutes at room temperature. The reaction was stopped by adding 100 µL of stop reaction reagent to each well.

The sample absorbance was measured with a plate reader at 450 nm and 550 nm and the result was calculated for each plate. The experiments were repeated three times with two technical duplicates in each experiment. To confirm that the cytokines detected in this experiment were excreted from macrophages and were not artifacts of the cell-culturing medium, a cytokine-free RPMI-1640-conditioned medium was used. The cytokine measurements performed by ELISA kits included TNF-α, IL-1β and IL-10.

4.3.4 Kinetic analysis of drug release profiles

The drug release data were computed using DDsolver, an Excel plug-in module [166,167] and the resultant data were fitted to the Korsmeyer-Peppas exponential equation and the Weibull exponential equation to establish the mechanism of drug release. The diffusional exponent n is an important indicator of the mechanism of drug transport from the dosage form. A value of $n \leq 0.43$ indicates that drug release is controlled by Fickian diffusion, whereas a value of $n \geq 0.85$ suggests that drug release is dominated by an erosion mechanism. For values $0.43 < n < 0.85$, the release is described as anomalous, implying that a combination of diffusion and erosion contributes to the control of drug release.

4.3.5 Statistical analysis

Results are shown as the mean ± S.D. Differences were considered statistically significant at $p < 0.05$. Statistical analysis was performed using one-way ANOVA.

4.4. Results and Discussion

4.4.1. Size, morphology and drug loading

Gelatin nanoparticles: Gelatin is a biodegradable material from natural sources and has been extensively used for NP drug delivery systems for the last three decades [168]. It has been tested in drug delivery [169], gene delivery [169] and cell targeting using antibody modified NPs [170]. The ability to obtain different gelatin NPs sizes by process modification makes them an ideal polymer for the current study.

TEM images of blank gelatin NPs are shown in Fig. 4.4. Blank gelatin NPs were prepared in sizes of 122 ± 18 nm (G1) and 266 ± 29 nm (G2) as shown in Table 4.1. Table 1 also shows polydispersity indexes (PDI) of 0.12 ± 0.003 and 0.07 ± 0.002 for G1 and G2 NPs, respectively, showing a narrow particle size distribution.

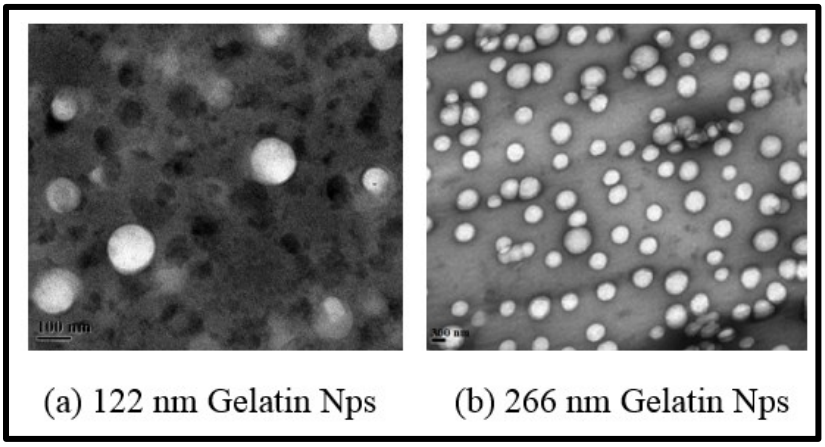

Figure 4.4: TEM images of gelatin nanoparticles (H-600, magnification 56,000×, voltage 80 kV). G1 samller NP (122nm), G2 larger NP (266nm).

Moxifloxacin and rifampicin-loaded NPs of two sizes each are also listed in Table 1. The moxifloxacin NPs are 135 ± 21 nm (GM1) and 272 ± 33 nm (GM2) (before lyophilization) and rifampicin NPs are 145 ± 22 nm (GR1) and 305 ± 35 nm (GR2) (before lyophilization). The PDI

for these NPs showed a narrow particle size distribution as shown in Table 4.1. The sizes of moxifloxacin and rifampicin NPs increased slightly after lyophilization which is consistent with reported studies due to aggregation of some particles [171].

Table 4.1: Particle size distribution, polydispersity index and drug loading for gelatin nanoparticles.

Gelatin NP	Size (nm)[a]	PDI	Size (nm)[b]	PDI	Drug loading (μg/mg)
G1	122.7 ± 18	0.12 ± 0.003	127.2 ± 23	0.11 ± 0.003	----
G2	266.3 ± 29	0.07 ± 0.002	271.4 ± 34	0.06 ± 0,002	----
GM1	134.8 ± 21	0.16 ± 0.004	142.2 ± 23	0.12 ± 0.003	5.59 ± 0.09
GM2	271.7 ± 33	0.12 ± 0.002	296.5 ± 34	0.13 ± 0.005	8.13 ± 0.11
GR1	145.2 ± 22	0.1 ± 0.002	155.0 ± 25	0.14 ± 0.002	10.05 ± 0.18
GR2	305.0 ± 35	0.06 ± 0.003	318.2 ± 33	0.03 ± 0.003	12.78 ± 0.25

[a]Before lyophilization. [b]After lyophilization.

PIBCA nanoparticles: TEM images of blank PIBCA NPs are shown in Fig. 4.5. Two different sizes of blank PIBCA NPs were prepared with a particle size of 117 ± 9.6 nm (B1) and 284 nm ± 29.7 nm (B2) respectively as shown in Table 4.2. Table 4.2 also shows PDI of 0.111 ± 0.02 and 0.08 ± 0.02 for B1 and B2, respectively, indicating that the particles have a narrow size distribution. Moxifloxacin loaded NPs with sizes of 154 ± 11.5 nm (BM1) and 270 ± 22.5 nm (BM2) are shown in Table 4.2. The PDIs for NPs BM1 and BM2 were 0.17 ± 0.05 and 0.06 ± 0.02, respectively, confirming a uniform and narrow particle size distribution.

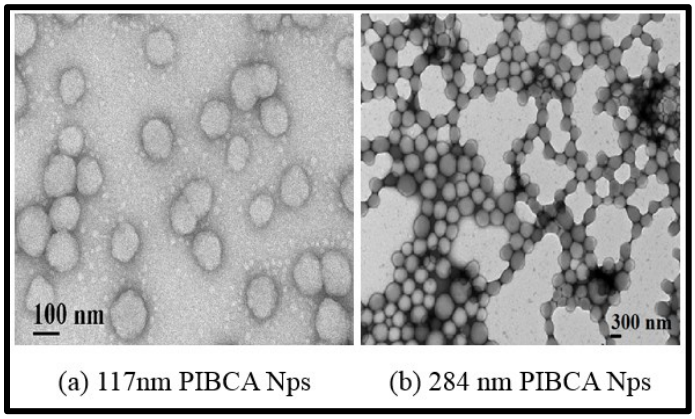

Figure 4.5: TEM images of PIBCA nanoparticles(H-600,magnification 56,000×, voltage 80 kV).

Table 4.2: Particle size distribution polydispersity index and drug loading for PIBCA nanoparticles.

PIBCA NP	Size (nm)	PDI	Drug loading (µg/mg)
B1	117.1 ± 9.6	0.11 ± 0.02	--------
B2	284.4 ± 29.7	0.08 ± 0.03	--------
BM1	153.7 ± 11.5	0.17 ±0.05	51.06 ± 0.37
BM2	270.3 ± 22.5	0.06 ± 0.02	88.84 ±0.74

4.4.2 Drug loading

The drug loading efficiencies of moxifloxacin and rifampicin gelatin NPs are shown in Table 4.1 and calculated as per procedure outline in section 4.2.2.3 and 4.2.3.2 respectively. The loading efficiency of moxifloxacin was 5.59 ± 0.09 µg/mg to 8.13 ± 0.11 µg/mg and the loading efficiency of rifampicin was 10.05 ± 0.18 µg/mg to 12.78 ± 0.25 µg/mg; in both cases the higher drug loading values reflected by an increase in NPs size. The drug loading efficiency of

moxifloxacin in PIBCA NPs (BM1, BM2) increased from 51.06 ± 0.37 µg/mg to 88.84 ± 0.74 µg/mg as the particle size increased from 153 nm to 270 nm, as shown in Table 4.2.

4.4.3 In vitro drug release

RIF release from various NPs is shown in Fig. 4. 6. The amount of RIF released from GR1 and GR2 was 80.34 ± 1.2 % and 74.68 ± 1.4 %, respectively, in 48 hours. Initially, 14% to 26% of RIF was released from GR1 and GR2, respectively, in first 30 min. The higher drug loading in GR2 in comparison to GR1 led to a slower drug release in PBS at pH 7.4, which is consistent with data reported by Gao et al. [98]. The drug release kinetics fitted well to a Weibull function with regression coefficients (r) of 0.9220 and 0.9883, and diffusional exponents (n) of 0.427 and 0.320 showing drug release controlled by fickian diffusion respectively.

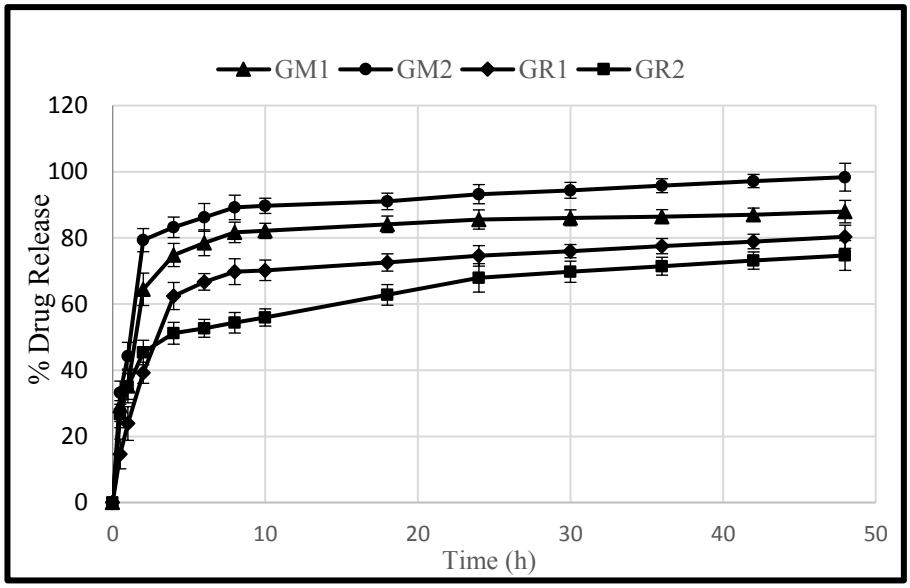

Figure 4.6: In vitro release kinetics profile of rifampicin and moxifloxacin loaded gelatin nanoparticles in PBS, pH 7.4. Data shown are the mean ± S.D. (n=3).

Fig. 4.6 shows the in vitro release kinetics of MOX loaded gelatin NPs in PBS at pH 7.4. The amount of MOX released from GM1 and GM2 was 87.14 ± 1.8 % and 98.35 ± 2.2 % in 48 hours. A burst release of 35% to 44% of the loaded MOX was observed for GM1 and GM2, which is consistent with another study [98]. The drug release kinetics fitted well to a Weibull function. The regression coefficients (r) were 0.9077 and 0.9332, respectively, with diffusion exponents (n) of 0.450 and 0.413, showing anomalous and fickian diffusion respectively.

The in vitro release kinetics profile of moxifloxacin loaded PIBCA NPs in PBS, pH 7.4 are shown in Fig. 4.7. The amount of MOX released from BM1 and BM2 was 89 ± 1.9% and 92 ± 2.3%, respectively, in 48 hours. BM1 and BM2 released 35% and 37% moxifloxacin within 30 minutes, and 46% and 47% moxifloxacin within one hour. The initial burst drug release can be

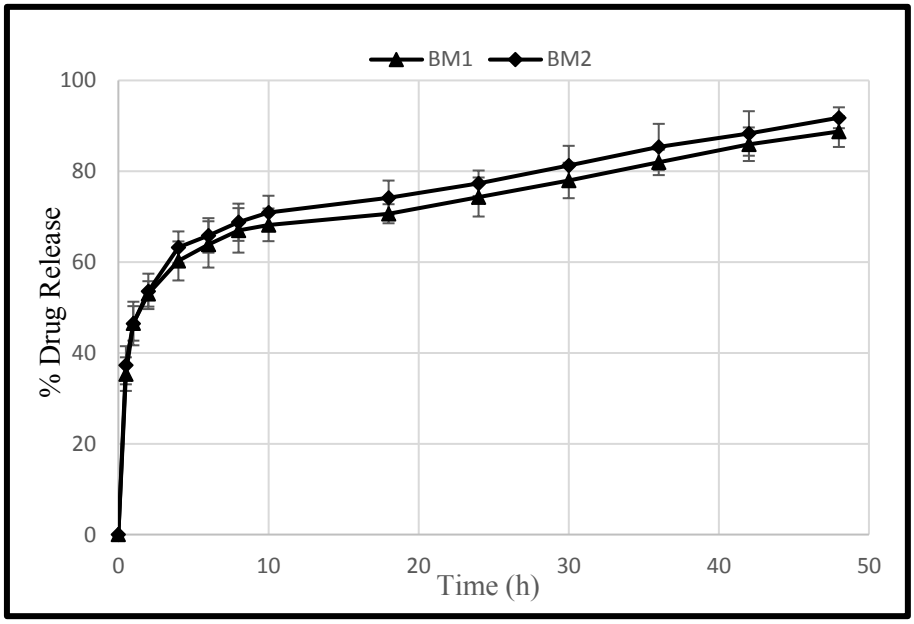

Figure 4.7: In vitro release kinetics profile of moxifloxacin loaded PIBCA nanoparticles in PBS, pH 7.4. Data shown are the mean ± S.D. (n=3).

explained by the presence of unbound drug within the NPs core. The slower drug release after 2 hours showed a zero order release which is consistent with results reported by Zhao et al. [172]. The drug release kinetics were fitted to Weibull and Korsmeyer-Peppas models [166].

The moxifloxacin release profile of both BM1 and BM2 fitted well with the Weibull model during the first 10 hours and with the Korsmeyer-Peppas model after 10 hours till 48 hours of the experiment. The regression coefficients (r) generated from fitting the BM1 drug release data to the Weibull and Korsmeyer-Peppas models were 0.9688 and 0.9686, respectively, with diffusional exponents (n) of 0.196 and 0.165, showing fickian diffusion respectively. Similarly, (r) generated from fitting the BM2 drug release data to the Weibull and Korsmeyer-Peppas models were 0.9761 and 0.9763, respectively, with diffusional exponents (n) of 0.073 and 0.168 showing fickian diffusion respectively.

4.4.4 Cell viability

A cell viability assay to determine the IC_{50} of GM1 and GM2 moxifloxacin loaded gelatin

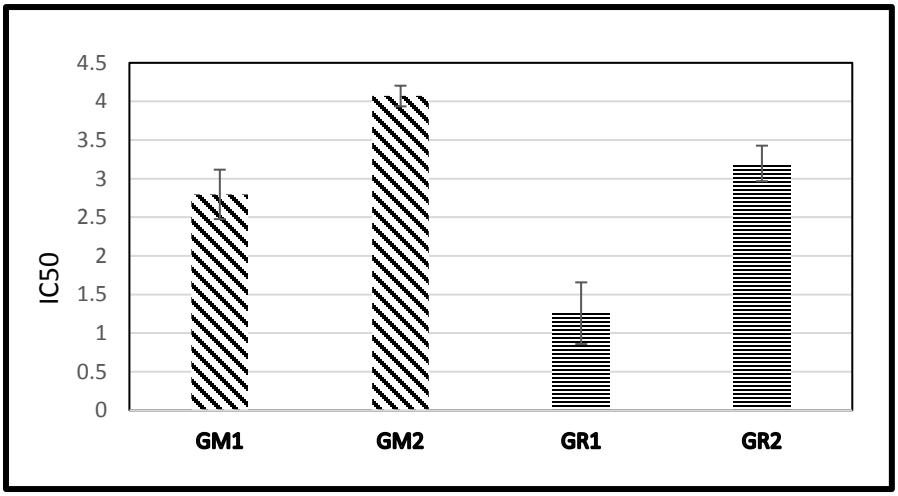

Figure 4.8: IC_{50} values of GM1 and GM2 moxifloxacin loaded gelatin nanoparticles and GR1 and GR2 rifampicin-loaded gelatin nanoparticles. Data shown are the mean ± S.D. (n=6).

NPs showed that 2.79 µg/mg and 4.07 µg/mg, were required to inhibit 50% of macrophage's viability (Fig 4.8). The lower IC_{50} of GM1 compared to that of GM2 might be due to the smaller size of GM1. Smaller NPs can have a higher uptake by macrophages as reported by Clift et al. where 20 nm NPs were more rapidly taken up by macrophages than 200 nm Nps [173]. It can increase the cytotoxic potential of NPs.

Fig. 4.8 shows the IC_{50} values of rifampicin-loaded NPs. The IC_{50} values of GR1 and GR2 are 1.257 µg/mg and 3.197µg/mg, respectively. GR1 shows a higher cytotoxicity toward cell viability than GR2; this is consistent with the above-reported results.

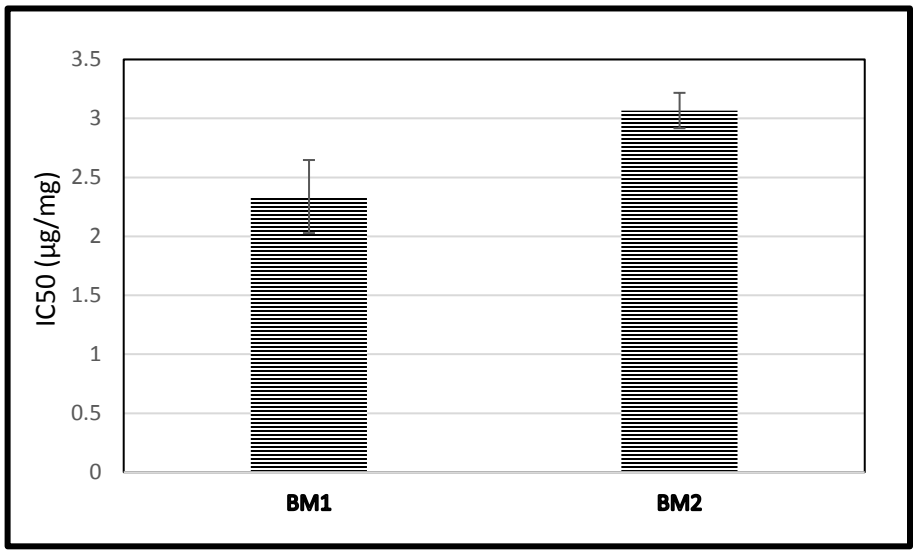

Figure 4.9: IC_{50} values of moxifloxacin loaded PIBCA nanoparticles. Data shown are the mean± S.D. (n=6).

The IC_{50} values of BM1 and BM2 were 2.337 µg/mg and 3.067 µg/mg, respectively (Fig. 4.9). BM1 showed more cytotoxicity toward cell viability than BM2, probably because of the smaller particle size and rapid cellular uptake [173] of BM1 compared to BM2.

4.4.5 Cytokine screening (ELISA)

Proinflammatory and anti-inflammatory cytokines, including TNF-α, IL-1β and IL-10, were quantitatively measured using ELISA kits.

Fig. 4.10 shows the release of TNF-α from murine macrophages after no treatment (UT) or treatment for 24 h or 48 h with blank gelatin NPs (G1, G2), drug loaded gelatin NPs (GM1, GM2, GR1, GR2), or drug (MOX, RIF) alone. The results show significant difference in TNF-α release after NPs treatment in comparison to TNF-α release from untreated cells. There was a slight increase in TNF-α with time (from 24 h to 48 h). The effect of NPs size on the release profile of TNF-α was insignificant (G1 vs. G2, GM1 vs. GM2, and GR1 vs. GR2). LPS as a potent immune stimulator and showed the maximum release of TNF-α. MOX and RIF treatments also showed some cytokine release.

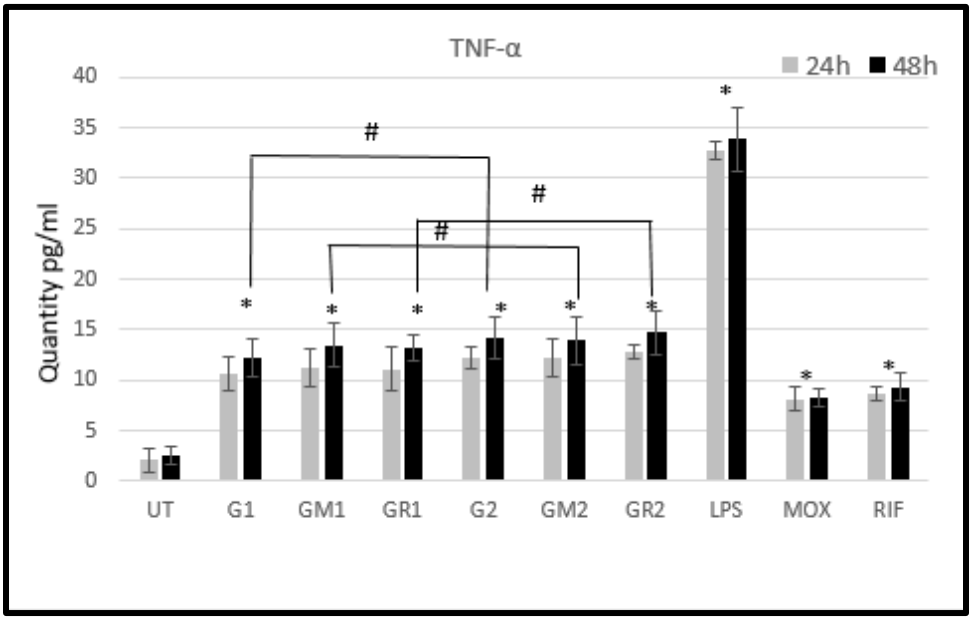

Figure 4.10: TNF-α release from murine macrophages following no treatment (UT) or exposure for 24 h or 48 h to blank nanoparticles (G1, G2), drug-loaded nanoparticles (GM1, GM2, GR1, GR2), or drug (MOX, RIF) alone. E.coli lipopolysaccharide (LPS) was

used as positive control. Data shown are the mean ± S.D. (n=3). * denotes that the treatment results were significant (*$p < 0.01$, **$p < 0.05$); # indicates that the treatment results were insignificant (#$p > 0.05$).

Fig. 4.11 shows the release of TNF-α from murine macrophages after no treatment or different treatments with PIBCA NPs. The results showed a significant difference in release of TNF-α after NPs treatment in comparison to the control (untreated cells). There was a slight increase in TNF-α release when the treatment time was increased from 24 hours to 48 hours. The effect of NPs size on the release profile of TNF-α is insignificant (BM1 vs. BM2). The release of TNF-α after BM1 and BM2 NPs treatments was greater than the release of TNF-α after GM1 and GM2 NPs treatments; this might be due to the greater cytotoxicity of the PIBCA polymer compared to gelatin as reported by Lherm et al. [174].

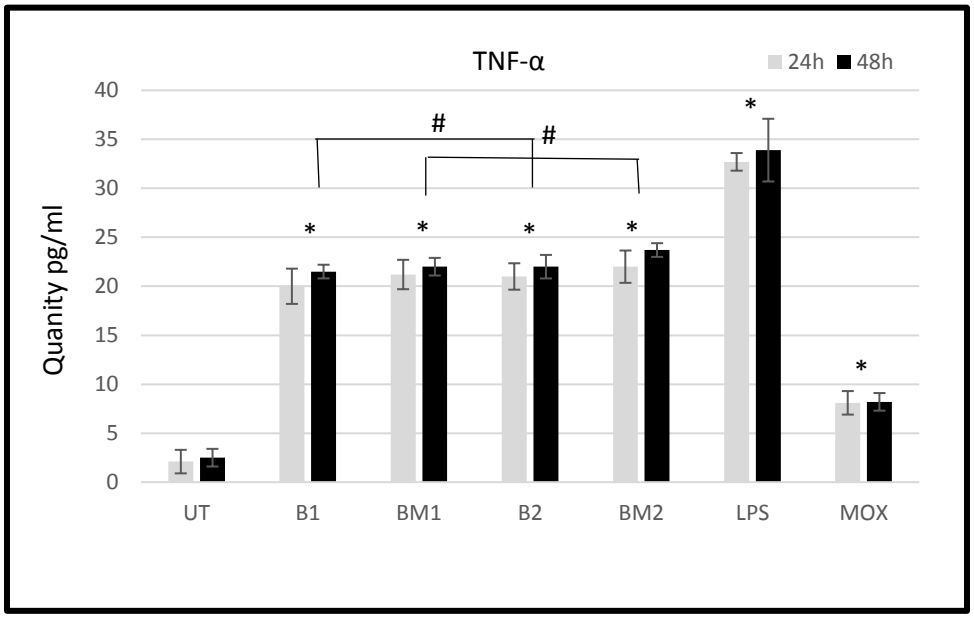

Figure 4.11: TNF-α release from murine macrophages after no treatment (UT) or exposure for 24 h or 48 h to blank nanoparticles (B1, B2), drug-loaded nanoparticles (BM1,BM2),

or drug (MOX) alone. E.coli lipopolysaccharide (LPS) was used as positive control. Data shown are the mean ± S.D. (n=3). *denotes that the treatment results were significant (*$p < 0.01$, **$p < 0.05$); # indicates that the treatment results were insignificant (# $p > 0.05$).

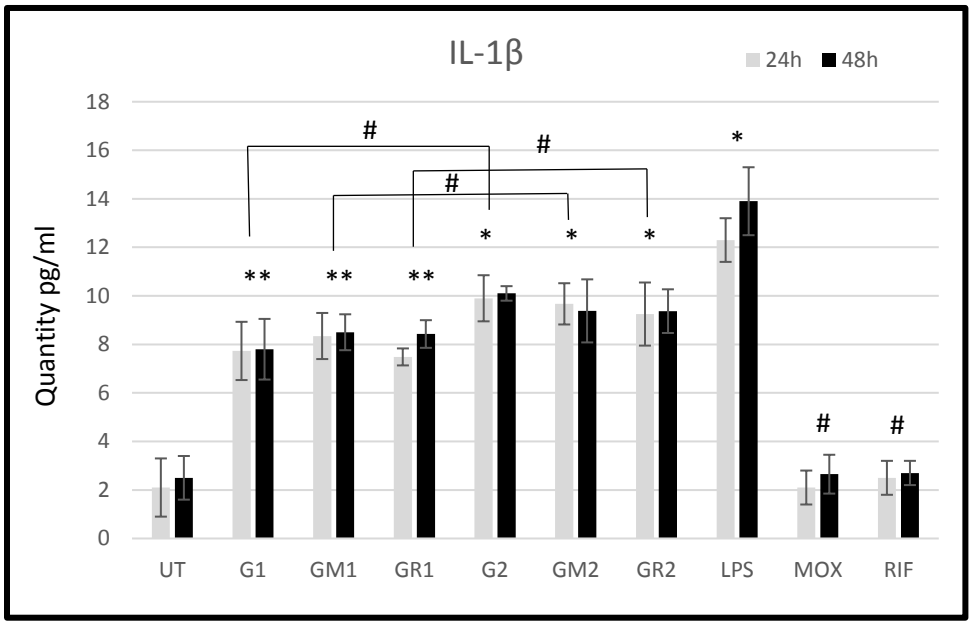

Figure 4.12: IL-1β release from murine macrophages after no treatment (UT) or exposure for 24 h or 48 h to blank nanoparticles (G1, G2), drug-loaded nanoparticles (GM1, GM2, GR1, GR2), or drug (MOX, RIF) alone. E.coli lipopolysaccharide (LPS) was used as positive control. Data shown are the mean ± S.D. (n=3). * denotes that the treatment results were significant (*$p < 0.05$, **$p < 0.01$); # indicates that the treatment results were insignificant (#$p > 0.05$).

The IL-1β production of proinflammatory cytokines is required to control M. tuberculosis infections. Fig. 4.12 shows the release of IL-1β from murine macrophages after different treatments. The results indicated a significant diffrence in IL-1β release after NPs treatment in comparison to the control (untreated cells). There was an insignificant difference in IL-1β release between cells treated with blank gelatin NPs (G1, G2) or drug loaded gelatin NPs (GM1, GM2, GR1, GR2). The effect of NPs size on the release profile of IL-1β was insignificant (GM1 vs. GM2 and GR1 vs. GR2). Treatment with LPS showed the maximum release of IL-1β.

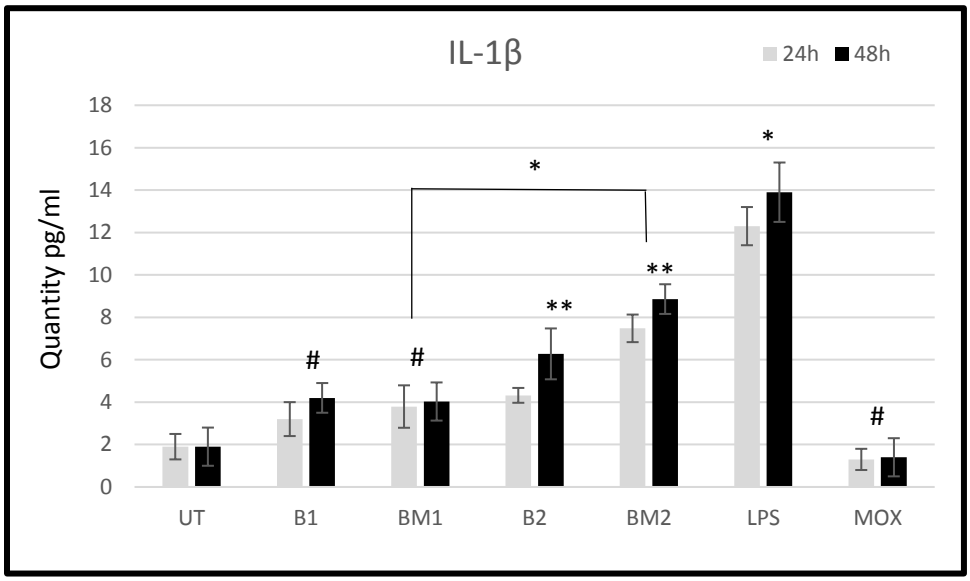

Figure 4.13: IL-1β release from murine macrophages after no treatment (UT) or exposure for 24 h or 48 h to blank nanoparticles (B1, B2), drug loaded nanoparticles (BM1, BM2), or drug (MOX) alone. E.coli lipopolysaccharide (LPS) was used as positive control. Data shown are the mean ± S.D. (n=3). * denotes that the treatment results were significant (*$p < 0.05$, **$p < 0.01$); # indicates that the treatment results were insignificant (#$p > 0.05$).

Fig. 4.13 shows the release of IL-1β from murine macrophages after different treatments. The results showed an insignificant difference in release of IL-1β after PIBCA NPs (B1, BM1) treatment in comparison to the control (untreated cells). However, a significant difference in cytokine release was observed with B2, BM2 NPs. There was a slight increase in the IL-1β release as the treatment time was increased from 24 h to 48 h for all treatments. The effect of NPs size on the release profile of IL-1β was significant different (BM1 vs. BM2). The difference between BM1 and BM2 may be due to the NPs size difference. LPS showed the maximum release of IL-1β.

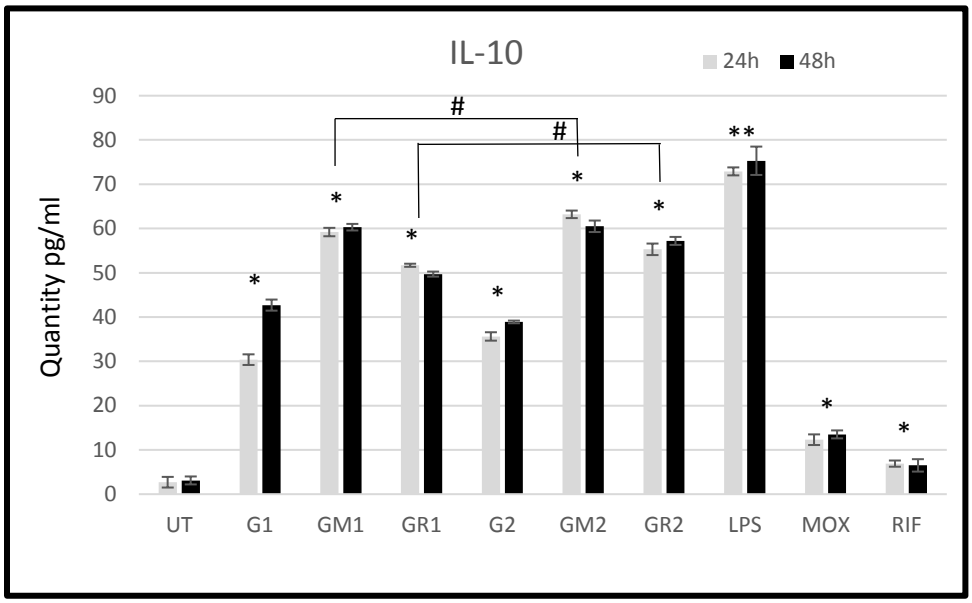

Figure 4.14: IL-10 release from murine macrophages after no treatment (UT) or exposure for 24 h or 48 h to blank nanoparticles (G1, G2), drug-loaded nanoparticles (GM1, GM2, GR1, GR2), or drug (MOX, RIF) alone. E.coli lipopolysaccharide (LPS) was used as positive control. Data shown are the mean ± S.D. (n=3). * denotes that the treatment results were significant (*$p < 0.04$, **$p < 0.01$); # indicates that the treatment results were insignificant (#$p > 0.04$).

Fig. 4.14 shows the release of IL-10 from murine macrophages after different treatments. The results show a significant difference in release of IL-10 after NPs treatment in comparison to the (untreated cells). There was a significant diffrence in IL-10 release from drug loaded NPs (GM1, GR1, GM2, GR2) in comparison to blank NPs (G1, G2). However, the IL-10 release from GM1 and GM2 was greater than that of GR1 and GR2. This difference might be due to nature of drug under study. The effect of NPs size on the release profile of IL-10 was insignificant (GM1 vs. GM2 and GR1 vs. GR2). LPS as a positive control showed the maximum release of IL-10.

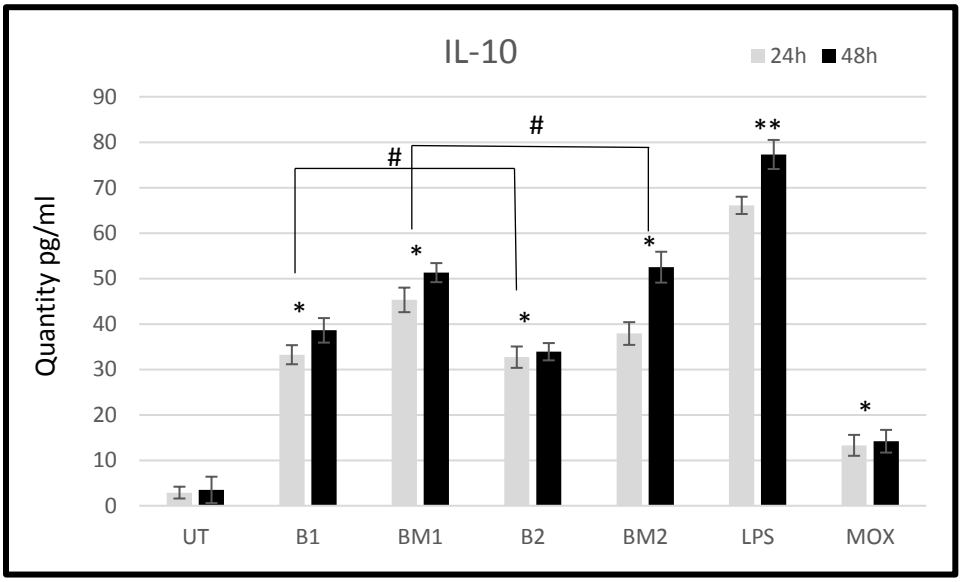

Figure 4.15: IL-10 release from murine macrophages after no treatment (UT) or exposure for 24 h or 48 h to blank nanoparticles (B1, B2), drug-loaded nanoparticles (BM1, BM2), or drug (MOX) alone. E.coli lipopolysaccharide (LPS) was used as positive control. Data shown are the mean ± S.D. (n=3). * denotes that the treatment results were significant (*$p < 0.05$), **$p < 0.01$); # indicates that the treatment results were insignificant (#$p > 0.05$).

Fig. 4.15 shows the release of IL-10 from murine macrophages after different treatments. The results indicate a significant difference in IL-10 release after NPs treatment in comparison to

the control (untreated cells). There was a slight increase in the IL-10 release as the treatment time was increased from 24 h to 48 h for all treatments. There was a significant diffrence in IL-10 release from drug loaded NPs (BM1, BM2) in comparison to blank NPs (B1, B2). The effect of NPs size on the release profile of IL-10 is insignificant (B1 vs. B2 or BM1 vs. BM2). LPS as a positive control showed the maximum release of IL-10.

4.5 Discussion

Targeting macrophages in *M .tuberculosis* infections using NPs as a drug carrier can play a major role in initiating an innate immune response in macrophages. During a *M. tuberculosis* infection, macrophages release cytokines such as tumor necrosis factor (TNF-α), interlukin-10 (IL-10), and interlukin-1β (IL-1β) [112,114,144-149]

TNF-α is an early proinflammatory cytokine whose role in the clearance of mycobacteria from the host is well established [144,145]. The ELISA quantitative analysis of cells treated with different NPs, with or without drug loading, showed a significant diffrence in TNF-α release in comparison to untreated control cells. Insignificant difference in TNF-α release between RIF and MOX loaded and unloaded gelatin and PIBCA NPs was observed. The cells treated with RIF and MOX showed significant diffrence in TNF-α release in comparison to untreated control cells. A small increase in the TNF-α release was noted in all treatments applied for 24 or 48 hours. Cells treated with NPs within the range of 120–300 nm showed insignificant diffrence in TNF-α release. Cells treated with PIBCA NPs showed more TNF-α release than cells treated with gelatin NPs. This behavior was due to the higher cytotoxicity of PIBCA compared to gelatin [174]. As an increase of TNF-α release indicates an increase in TNF-α cell concentration, it is concluded that NPs treatment helped to potentiate the host innate immune response and this might help to clear the mycobacterium at an early stage in an infection and avoid that the infection reaches a chronic stage.

Other proinflammatory cytokines like IL-1β, play a fundamental role in host resistance against the *M .tuberculosis* [149]. The ELISA of different NPs treatments of cells, with or without drug loading, showed significant diffrence in IL-1β release compared to that of untreated cells, except for the smaller NPs (B1, BMI) which showed an insignificant diffrence in IL-1β release in

comparison to that of untreated cells. RIF and MOX treatments showed insignificant difference in IL-1β as compared to untreated control cells. LPS showed a significant diffrence and maximum IL-1β release and was used as a positive control in the study. Thus NPs application can help to improve the host's initial innate immune response and might be able to control the *M .tuberculosis* infection via an increase of IL-1β concentrations in the cells.

Macrophages also secrete anti-inflammatory IL-10 cytokines in response to *M. tuberculosis* infection. IL-10 helps the progression of mycobacterium by down-regulating the production of proinflammatory cytokines and by inhibiting the proliferation of IFN-γ [114] and phagosome maturation in mycobacterium-infected macrophages [148]. Overall, IL-10 induced by mycobacteria suppresses the generation of anti-tuberculosis immunity. The ELISA of NPs treated cells, with or without drug loading, showed significant diffrence in IL-10 concentrations in comparison with untreated cells. A maximum release of IL-10 was observed after cells were treated with LPS (positive control). Cells treated with RIF and MOX also showed significant diffrence in IL-10 release in comparison to untreated cells.

The use of antituberculosis drug loaded NPs showed some promise to potentiate the innate immune response by increasing the cell concentrations of proinflammatory cytokines like TNF-α and IL-1β. It has the potential to control the *M .tuberculosis* via immune responses in addition to chemotherapeutic effects by the drug alone. However, an increase in anti-inflammatory cytokine IL-10 was also observed. If this will affect the resistance of macrophages against the mycobacterium is not known. The study showed that an enhancement of innate immune responses by targeting macrophages opens a new avenue for treating tuberculosis via chemotherapy and immune stimulation.

4.6. Conclusion

The treatment of alveolar macrophages with anti-tuberculosis drug loaded NPs stimulated the cellular immune response by secreting proinflammatory and anti-inflammatory cytokines (secondary toxicity effect). Proinflammatory cytokines can strengthen the host's immune response and help to clear mycobacteria early in the infection cycle and avoid that the infection reaches a chronic immune response. NPs together with chemotherapeutic drugs might be able to treat *M. tuberculosis* infections in macrophages via an immune response and drug action. A targeted and more efficient anti-TB treatment might be possible when drug loaded NPs are used to treat TB infections.

4.7. Future prospective:

The study shows that NPs can trigger inflammatory immune responses, which are important in the early infection cycle to fight the *M .tuberculosis*. There must be a delicate balance between such effects and chemotherapeutic drug effects to achieve therapeutic effectiveness without triggering systemic side effects. At this time point, we do not know where this balance has to be. This study used different polymers, particle sizes, and entrapped drugs. The current study is only a first step in this direction and further studies need to investigate the interplay between immune responses of NPs and chemotherapeutic approaches.

4.8. Executive summary:

- The targeting of alveolar macrophage using Anti-TB loaded NPs has been studied in this study.
- The focus of the research was the investigation of the balance between proinflammatory and anti-inflammatory cytokine release of the macrophages after interaction with NPs.

- NPs with two different polymers (Gelatin and Polyisobutyl-cyanoacrylate) and two different sizes were evaluated in the study.
- Rifampicin and Moxifloxacin were taken as model drugs.
- Drug release kinetics shows faster drug release from Moxifloxacin loaded NPs than for Rifampicin loaded NPs.
- Cell Viability indicates that the IC50 values of Rifampicin loaded gelatin NPs is lower than the one of the Moxifloxacin loaded gelatin NPs.
- The IC50 values of Moxifloxacin loaded Polyisobutyl-cyanoacrylate NPs was lower than the one for rifampicin-loaded Polyisobutyl-cyanoacrylate NPs.
- Proinflammatory and anti-inflammatory cytokine (secondary toxicity effect) analysis were performed using ELISA kits.
- Two proinflammatory cytokines, TNF-α and IL-1β, showed a significant diffrence compared to untreated control cells.
- IL-10, an anti-inflammatory cytokine also show significant diffrence in comparison to untreated cells.
- NPs together with chemotherapeutic drugs might be able to trigger an immune response in macrophages.
- The combined effect of NPs and drug might be able to overcome mycobacteria infections.

Chapter 5

Inflammation caused by nano-sized delivery systems: Is there a benefit?

This study has already been published as Muhammad Sarfraz, Nadia Bou-Chacra, Wilson Roa, & Raimar Löbenberg with the title *of Inflammation caused by nano-sized delivery systems: Is there a benefit? in Journal of Molecular Pharmaceutics August* 2016, *13* :9: :3270–3278.

Abstract

Background: Secondary macrophage cytotoxicity induced by nanoparticles was described before. The study aim was to investigate the role of secondary cytotoxic effect in a macrophage-lung cancer co-culture model after nanoparticle treatment in the presence and absence of anti-inflammatory drugs.

Methodology: An in vitro co-culture model composed of confluent alveolar macrophage MH-S and A-549 lung cancer cells separated by a 0.4 μm porous membrane was used in the study. Macrophages were treated with two sizes of gelatin nanoparticles and two sizes of Poly (Isobutyl Cyanoacrylate) (PIBCA) nanoparticles, with and without doxorubicin as a chemotherapeutic drug. The treatment effect with and without the presence of anti-inflammatory drug was studied using an MTT (3-(4,5-dimethylthiazol-2-yl)-2,5-diphenyltetrazolium bromide) assay. The model drugs were Ibuprofen, celecoxib, prednisolone, dexamethasone, and methotrexate.

Results: Different nanoparticles in different sizes were synthesized with a range of physicochemical characteristics. Doxorubicin loaded nanoparticles were prepared with an entrapment efficiency of 82–83% for PIBCA and 39–42% for gelatin. Nanoparticle treatment of macrophages showed a secondary cytotoxic effect on A-549 cancer cells at 24 h and 36 h, with a drop in cell viability of 40–62%. However, this effect was significantly reduced to 10–48% if the macrophages were exposed to anti-inflammatory drugs. When Ibuprofen and celecoxib were used the cell viability rebounded between 24 and 36 h. For prednisolone, dexamethasone and methotrexate the cell viability dropped further between 24 and 36 h.

Conclusion: Macrophages exposed to nanoparticles show secondary cytotoxicity, which has a significant anti-tumour effect in the microclimate of the co-culture model. The beneficial nanoparticle treatment effect was significantly reduced if nonsteroidal anti-inflammatory drugs (NSAIDs), glucocorticoids, or methotrexate was given at the same time. The data suggest that anti-inflammatory treatments can decrease the carrier-induced macrophage cytotoxicity and its anti-tumor effectiveness with chemotherapy.

Keywords: Macrophage, Inflammation, Nanoparticles, Gelatin, Poly (Isobutyl Cyanoacrylate)

5.1 Introduction

Rudolf Virchow first reported a correlation between inflammation and cancer in the 1800s, postulating that chronic irritation and previous injury are preconditions for tumorigenesis [175]. More than a century later, there is sufficient evidence to confirm an interplay between cancer and chronic inflammation, and scientists have discovered molecular and cellular pathways that play crucial roles in tumorigenesis [176,177]. Our immune system can respond innate and adaptively to external stimuli [178]. In a healthy individual, external stimuli first engender an innate response, characterised by a protective inflammation [179,180] then mounts an adaptive immunity defence if the stimuli persist [181]. Stimuli that escape the host's innate and adaptive defences can cause tumor progression.[181,182] Macrophages are the only known immune cells that infiltrate tumor cells [183] and can represent 50% of the tumor mass [24]. Immune-surveillance and tumor association have enabled researchers to classify macrophages as tumor killing or tumor promoting, depending on whether the macrophage helps to resolve or promote inflammation (and tumorigenesis), respectively [184,185]. In a cancer microenvironment, chronic inflammation is characterised by the antibody mediated humoral immune response in combination with Th2 cytokine release to promote tumorigenesis [186]. In contrast, cytokines of the Th1 type promote inflammation (acute) and cell mediated response to kill tumor cells [187]. Hence, inflammation is a found in tumor microenvironments. It is a possible pharmacological target for interventions [188]. Many attempts have been made to block the macrophage promotion of inflammation and to enhance its antitumor activities. This has been achieved by receptor neutralizing antibodies and drug interventions [189-191]. The nonsteroidal anti-inflammatory drugs (NSAIDs) ibuprofen and celecoxib are usually administered in cancer chemotherapy to reduce inflammation [192-194]. The glucocorticoids (GCs) dexamethasone [195,196] and prednisolone [197] also possess anti-

inflammatory and immune-regulatory properties that enhance tumor immunity, thus, they are used in tumor immunotherapy. Methotrexate is a nonsteroidal antifolate cancer chemotherapeutic drug which can modify inflammatory activities [198].

In the last decade, researchers have studied the immunomodulatory (immunostimulatory and immunosuppression) effects of colloidal drug delivery systems [199-201]. In particular, numerous nanoparticles have been investigated about their chemical nature, surface charge, particle size, solubility, and degree of accumulation in human tissues and other biological systems [202,203]. Nanoparticles show immunomodulatory effects and lower immunotoxicology; their stability, favourable biodistribution and controlled drug release kinetics make them ideal candidates for targeted drug delivery [201]. Most researchers have targeted adaptive immunity [204] in contrast to innate immunity to treat cancers [205]. The current study focuses on the innate immune response that is triggered in macrophages by nanoparticles. The goal was to investigate the behaviour of macrophages after exposing them to doxorubicin loaded nanoparticles in a cancer microenvironment. A-549 cancer cells were cocultured by the procedure reported by Al-Hallak [81]. Our study investigated two different polymers (gelatin and Poly (Isobutyl Cyanoacrylate) (PIBCA) nanoparticles) with different particle sizes. The in vitro model was tested with or without NSAIDs (ibuprofen, celecoxib), GCs (prednisolone and dexamethasone) and methotrexate.

5.2. Materials and Methods

5.2.1 Materials

Grade I Glutaraldehyde (25% aqueous solution), 3-(4,5-dimethylthiazol-2- yl)-2,5-diphenyltetrazolium bromide (MTT) cell viability reagent, Type B Gelatin (Bloom 225) from bovine skin, mannitol, dimethyl sulfoxide (DMSO), trypan blue (CAS # 72-57-1), sodium

hydroxide, dexamethasone powder (CAS # 50-02-02) methotrexate hydrate powder (CAS # 133073-73-1), and prednisolone (CAS # 50-24-8) were obtained from Sigma-Aldrich, Oakville ON, Canada.

1.25% trypsin-EDTA, phosphate buffered saline (PBS), 75 ml cell culture flasks, RPMI 1640 medium, 6 well transwell plates (#3412), fetal bovine serum (FBS) and all other cell culture related materials were purchased from Invitrogen (Ontario, Canada). Caledon (Georgetown, ON, Canada) provided us with acetone. All chemicals used in the study were of analytical grade. Lung cancer cell line A-549 (CCL-185) and murine alveolar macrophage (CRL-2019) were purchased from American Type Culture Collection (ATCC).

Doxorubicin was received from Novopharm Ltd. (Ontario, Canada) and PIBCA monomer (Lot. 02GD9236) was from Loctite Ltd (Dublin, Ireland) respectively. Celecoxib powder was a gift from Searle (Harbor Beach MI, USA), ibuprofen powder was purchased from PCCA (London, ON, Canada), 0.45 μm polyvinylidene fluoride filters were purchased from Millipore (Billerica, MA, USA), and 0.8 μm nucleopore® membrane filters were from Whatman (Ontario, Canada).

5.2.2. Methodology

5.2.2.1 Gelatin nanoparticles synthesis

A two step desolvation method was employed for the preparation of gelatin nanoparticles as previously reported by Azarmi et al [159]. In brief: 2.5 g gelatin was added to distilled water at 40ºC under constant stirring of 500 rpm until dissolved. Acetone was added to trigger the first desolvation step, the high molecular weight (HMW) gelatin fraction separated out from lower molecular weight (LMW) gelatin fraction which stayed in solution. The LMW gelatin fraction in the supernatant was removed from the HMW fraction and the acetone was removed using a rotary evaporator under vacuum (IKA, Staufen, Germany). After freeze drying the remaining LMW

fraction was used to determine the amount of HMW gelatin by subtracting the LMW fraction from the total gelatin used. The HMW gelatin was further processed by dissolving it in distilled water with continuous stirring and adjusting the pH to 2.5 to provide acidic environment using 0.1 M hydrochloric acid. In a second desolvation step, acetone was fast added until the first precipitation was observed, then it was added dropped wise until the nanoparticles synthesis was completed. To stabilise the in-situ formed nanoparticles, 100 mL glutaraldehyde solution (8%) was added to cross-link the synthesised nanoparticles and was stirred for 24 h.

To remove the acetone from the synthesised nanoparticles dispersion, the dispersion was further processed using a rotary evaporator under vacuum. The nanoparticles obtained after evaporation were centrifuged at 8000 rpm for 30 min using Beckman L8-M Ultracentrifuge. The centrifuged nanoparticles were washed thrice with deionized distilled water and centrifuged again. The purified nanoparticles collected after the last centrifugation cycle were filtered using 0.45µm hydrophilic polyvinylidene fluoride filter provided (Millipore, Billerica, MA, USA). The filtered nanoparticles were lyophilisation under vacuum of 45 Pa at -80 °C for 24 h. As reported by Azarmi et al [159] slight modification in the process variables will result in different particles sizes. For this study two nanoparticles sizes of about 170-183 nm and 303-316 nm were synthesized.

Doxorubicin (antitumor drug) was loaded with gelatin nanoparticles at a concentration of 2 mg/ml upto 6mg before the second desolvation step with acetone was performed. The remaining synthesis was identical.

5.2.2.2 Determination of the entrapment efficiency of doxorubicin loaded gelatin nanoparticles

A standard procedure published before [82] was used to calculate the entrapment efficiency. The total drug amount found in the supernatant was subtracted from the initial amount

used for the nanoparticle synthesis. In brief: approximately 250 µL of unwashed nanoparticles dispersion was centrifuged using an Airfuge (Beckman) for 30 min at 100,000 g. After centrifugation, a clear supernatant was obtained, which was analysed for the presence of a free drug with UV spectrophotometry at 480 nm (UV1700 Shimadzu, Japan).

5.2.2.3 Poly (Isobutyl Cyanoacrylate) nanoparticles

The PIBCA polymer was used for nanoparticle preparation. A well established emulsion polymerization method was used for the synthesis of PIBCA nanoparticles [82]. In brief: 10 ml of either 0.01 M, or 0.02 M hydrochloric acid was used to synthesize different particle sizes. 100 mg of dextran 70 were dissolved under continuous stirring at 600 rpm. 100 µL PIBCA monomer was added drop-wise to the solution. After 4 h the resultant nanoparticles dispersion was neutralized with 0.1 N sodium hydroxide solution. The nanoparticles were filtered under vacuum using 0.8 µm nucleopore® membrane filter (Whatman, Ontario, Canada). The nanoparticles were lyophilized as described before using a cryoprotectant of 3% (w/v) mannitol.

5.2.2.4 Preparation of doxorubicin loaded PIBCA nanoparticles

Loaded doxorubicin PIBCA nanoparticles were synthesised as described for PIBCA nanoparticles doxorubicin solution was added to the PIBCA synthesis process 30 min after the addition of the polymer. The final concentration of DOX was 0.25%

5.2.2.5 Determination of the entrapment efficiency of doxorubicin loaded PIBCA nanoparticles

The same procedure as described for the gelatin nanoparticles was used [82]. The free drug in the supernatant was analysed by using the Ultra Violet spectrophotometry at (λ) 235 nm [162] .

5.2.2.6 Characterization of nanoparticles

The surface charge (zeta potential), particle size distribution and polydispersity index (PI) of the nanoparticle dispersions were measured by Zetasizer Nano-DTS 1060 from Malvern (Worcestershire, UK) at an angle of 90^{o}. Briefly, NPs were suspended in an aqueous medium (100 µl in 1ml of deionized water) and placed in a cuvette at 25 °C, and particle size and PI of the nanoparticles (NPs) were determined by light scattering at a scattering angle of 90°. The continuous phase refractive index and viscosity of water was used for the measurement. At the same time, the polydispersity index (PDI) was determined to evaluate the nanoparticle size distribution [82]. The zeta potential was measured in a clear zeta dip cell using the above mentioned Zetasizer. The dilution of all samples was done by double distilled water before the measurement. Each sample was measured 10 times, after which the average value was used for further calculations.

5.3 Cell Culture

MH-S cells were cultured in 75ml ventilated flasks (Corning, USA) in complete growth media (RPMI-1640 medium with standard additives: 100 IU/mL penicillin, 10 µg/mL streptomycin, and 10% (v/v) fetal bovine serum (FBS). The MH-S were incubated at 37°C in 5% CO_2 atmosphere. Subculturing of cells was performed as follows: The culture medium was removed and transferred to 50 ml centrifuge for the collection of floating cells. 0.25% (w/v) trypsin and 0.53 mM EDTA solution were used to detach the MH-S cell from ventilated flask. The detachment was observed using an inverted microscope. The detached cells were transferred to a 50 ml centrifuge tube and then centrifuged for ten minutes at 1000rpm. After centrifugation, the pellet was collected from the bottom of the tube and the cells were re-suspended in complete

growth medium with gentle pipetting. An appropriate number of cells was added to clean flask with complete growth medium [81].

A549 cells were cultivated similarly as described before only the growth medium was (F-12K (30-2004™) with the addition of standard antibiotics and FBS as described before.

5.4 Coculture experiments

5.4.1 Nanoparticle treatment of macrophages

MH-S cells were grown to confluency in 75 ml culture flasks. At confluency, the media was changed with serum free media and treated with aliquots of different concentrations of blank nanoparticles, DOX-loaded nanoparticles of two different sizes, and DOX solution (n = 3). Equal amounts of blank nanoparticles and DOX-loaded NPs were added. The concentration of free DOX solution was equivalent to the corresponding DOX-NP concentration. Untreated cells were used as a control. All treatments were incubated for 2 h in a humidified atmosphere of 5% CO_2 at 37 °C. After the 2 h incubation, the MH-S cells were treated as described under subculturing before. Approximately 2×10^5 MH-S cells were counted using a hemocytometer, seeded in the upper compartment (insert) of a 24 mm transwell coculture system that contained 6 inserts (upper compartment) separated by a 0.4 μm porous membrane from the lower compartment, and incubated for 24 h in a humidified atmosphere of 5% CO_2 at 37 °C.

Similarly, A-549 cells were cultivated in 75 ml ventilated flask, after reaching the confluency, the cell were washed thrice using PBS. Cells were treated as discussed earlier under subcluturing. Approximately 2 $x10^{-5}$ cells were counted and seeded to lower compartment of a transwell plate and kept in an incubator at 37 °C with 5% CO_2 for another 24 h to attain confluency.

A-549 cell viability was measured at 24h and 36h in each well of the lower compartment as described before [82]. In brief: 100 μl of MTT reagent freshly prepared at a concentration of

0.5mg/ml was added to each well. Plates were incubated and kept for another 4h in an incubator. After incubation, the MTT was removed from each well and treated with 200 µl of isopropanol. Now the plates were placed on a shaker for another 1 hour to dissolve the formazan crystals. The plates were read using bio-Tek EL 312e microplate reader and the color intensity was measured at 550nm.

5.4.2 Post-treatment of macrophages with NSAIDs, glucocorticoids (GCs), and methotrexate

After MH-S and A-549 cells reached confluency in upper and lower compartments, respectively, of transwell plates, the MH-S cells were removed from the incubator and treated as follows.

(i) *Nonsteroidal anti-inflammatory drugs.* Ibuprofen (a nonselective COX inhibitor) [192] and celecoxib (a selective COX-2 inhibitor) [193,194] solutions were prepared by dissolving the drugs in DMSO and diluting the resulting solution with cell culture medium. 100 µl of (121 µM) ibuprofen [206] and 100 µl of 65.53 µM celecoxib [207] were directly added to the upper compartment containing confluent MH-S cells.

(ii) *Glucocorticoids.* Dexamethasone [195,196] and prednisolone [197] were tested in separate experiments. 100 µl of 10 µM dexamethasone [208] and 100 µl of 10 µM prednisone[209] solubilized in DMSO and subsequently diluted in cell culture medium were directly added to the upper compartment of confluent MH-S cells**.**

(iii) *Methotrexate.* 100 µl of 10 µM methotrexate [210] solubilized in DMSO and subsequently diluted in cell culture medium were directly added to the upper compartment of confluent MH-S cells.

The cells were incubated in a humidified atmosphere of 5% CO_2 at 37 °C for 1 h with an empty lower compartment. Then the upper compartments were removed from the incubator and washed three times with PBS. Then these upper compartments were placed over the lower compartments containing A-549 cells for 24 h and 36 h. MTT cell viability assay was conducted at predefined time points to determine the A-549 cancer cell viability in each well of the lower compartment.

5.4.3 Statistical analysis

Systat software (Sigma Stat for Windows) was used to determine the statistical significance difference among the treatment group and its corresponding control. Student Newman Keul's test, a 1- way analysis of variance (ANOVA) was performed to calculate the statistical significance between all treatment groups; the details are given in the results section as appropriate. Differences were considered significant when $p < 0.05$ with $\alpha=0.05$.

5.5 Result and Discussion

5.5.1 Size, polydispersity, and zeta potential of nanoparticles

Gelatin nanoparticles

Nanoparticles made from gelatin are based on a natural, biodegradable proteins. Such nanoparticles have shown long-term stability and low antigenicity properties. This has made them to an ideal suitable drug delivery system [168,170]. Moreover, the ease of achieving desired particle sizes by modifying the process variables has been used in this study [159]. Table 5.1 shows the bank nanoparticles sizes of 170 ± 21 nm and 316 ± 26 nm for (G1) and (G2) respectively. The narrow nanoparticle size distribution was also reported by PDI values of 0. 0481 ± 0. 029 and 0. 0785 ± 0. 021 for G1 and G2 respectively. The zeta potential values for G1 and G2 nanoparticles were 13.7± 0.25 and 14.1± 0.32, respectively.

Doxorubicin loaded gelatin nanoparticles of 183 ± 16 nm (G1D) and 303 ± 33 nm (G2D) were prepared. G1D and G2D nanoparticles showed a narrow particle size distribution with PDI values of 0.0821 ± 0.035 and 0.0687± 0.051, respectively. Zeta potential values were + 12.2± 0.37 and + 12.7± 0.29 for G1D and G2D nanoparticles, respectively (Table 5.1).

Table 5.1: Particle size, zeta potential (ξ), polydispersity index (PDI) and entrapment efficiency for gelatin nanoparticles.

Gelatin NP	Size (nm)	PDI	ξ (mV)	%Entrapment Efficiency*
G1	170 ± 21	0.0481 ± 0.029	+ 13.7± 0.25	----
G2	316 ± 26	0.0785 ± 0.021	+ 14.1± 0.32	----
G1D	183 ± 16	0.0821 ± 0.035	+ 12.2± 0.37	39 ± 2.7
G2D	303 ± 33	0.0687± 0.051	+ 12.7± 0.29	42 ± 3.2

G1 and G2 = gelatin NPs of different size; G1D and G2D = DOX loaded gelatin NPs of different size. *[mg DOX adsorbed/mg total DOX in the colloidal suspension] ×100.

PIBCA nanoparticles

Blank PIBCA nanoparticles of 137.2 ± 8.57 nm (B1) and 285.7 ± 11.3 nm (B2) and doxorubicin loaded PIBCA nanoparticles with sizes of 142.2 ± 5.32 nm (B1D) and 292.4 ± 6.72 nm (B2D) were prepared, as shown in Table 5.2. Table 5.2 shows PDI and zeta potential values of 0.12 ± 0.03 and −23.5 ± 0.41, respectively, for B1 nanoparticles, 0.19 ± 0.04 and −19.5 ± 0.41, respectively, for B2 nanoparticles, 0.17 ±0.05 and -11.5 ± 0.73, respectively, for B1D nanoparticles, and 0.21 ± 0.02 and -10.2 ± 0.51, respectively, for B2D nanoparticles. Zeta potential values of BID and B2D were significantly different than those of blank nanoparticles; this might be due to drug absorption on the nanoparticle surface, consistent with other studies [211] where drug absorption reduced the zeta potential of nanoparticles prepared by a similar method.

Table 5.2: Particle size, zeta potential (ξ), polydispersity index (PDI) and entrapment efficiency for PIBCA nanoparticles.

PIBCA NP	Size (nm)	PDI	ξ (mV)	%Entrapment Efficiency*
B1	137.2 ± 8.57	0.12 ± 0.03	-23.5 ± 0.41	-----
B2	285.7 ± 11.3	0.19 ± 0.04	-19.5 ± 0.41	-----
B1D	142.2 ± 5.32	0.17 ±0.05	-11.5 ± 0.73	80 ± 3.7
B2D	292.4 ± 6.72	0.21 ± 0.02	-10.2 ± 0.51	83 ± 4.2

B1 and B2 = PIBCA NPs of different size; B1D and B2D = DOX loaded PIBCA NPs of different size. *[mg DOX adsorbed/mg total DOX in the colloidal suspension] ×100.

5.5.2 Drug entrapment efficiency

Drug entrapment efficiencies of 39 ± 2.7% and 42 ± 3.2%, respectively, were observed for doxorubicin loaded gelatin nanoparticles G1D and G2D (Table 5.1), and 80 ± 3.7% and 83 ± 4.2%, respectively, for doxorubicin loaded PIBCA nanoparticles B1D and B2D (Table 5.2). Similar entrapment efficiency was reported by Al-Hallak for doxorubicin loaded PIBCA nanoparticles [81].

5.5.3 Cell Viability Assays

5.5.3.1 Nanoparticle treatment of macrophage

Figure 5.1 shows the impact of macrophages on A-549 cancer cell viability in a coculture model after exposing them to blank nanoparticles; DOX-loaded nanoparticles, and DOX alone.

Untreated cells were used as a control. The decrease in A-549 cancer cell viability was considered to be equivalent to the treatment effectiveness. The DOX alone showed a treatment effectiveness of 11–13% compared to the control cells at 24 h and 36 h; this is consistent with a study by Azarmi et al. This study showed that A549 cells are resistant to doxorubicin, however, drug-loaded nanoparticles could overcome the resistance [162]. Lipopolysaccharide (LPS) was used as a positive control and showed a treatment effectiveness of 75–74%. Figure 5.1 shows a treatment effectiveness increased to 35–45% when MH-S macrophages were treated with blank nanoparticles (G1, G2, B1, B2) and to 40–62% when MH-S macrophages were treated with doxorubicin loaded nanoparticles (G1D, G2D, B1D, B2D). Poly (Isobutyl Cyanoacrylate) nanoparticles (B1D, B2D) were 20% more treatment effective than doxorubicin loaded gelatin nanoparticles. There was a statistically significant difference between all blank nanoparticle formulations and their corresponding drug loaded formulation. Furthermore, gelatin nanoparticles were statistically different from PIBCA nanoparticles at 24 and 36 h (except G2 vs. B2).

The increase treatment effectiveness might be due to higher cytotoxicity of the PIBCA polymer [174] compared to the lower cytotoxic properties of gelatin nanoparticles [212]. Significant differences in treatment effectiveness were also observed after treating macrophages with nanoparticles of various size (G1 vs. G2, B1 vs. B2, G1D vs. G2D, B1D vs. B2D). Smaller nanoparticles were taken up by cells more easily than larger nanoparticles. These findings were in accordance with a study in which cellular uptake was greater for macrophages treated with 20 nm nanoparticles than for macrophages treated with 200 nm nanoparticles [173].

Macrophages treated with nanoparticles attained an inflammatory state over 24 hours. The significant difference between the DOX and nanoparticle treatment can be explained by secondary toxicity. Macrophages produce a secondary toxicity by releasing Th-1 type cytokines (tumor

necrosis factor alpha (TNF-α), interferon gamma (IFN-γ), monocytes chemoattractant protein-1 (MCP-1), and macrophage inflammatory protein (MIP-1). These cytokines and chemokines lower the cancer cell viability [81].

Macrophage activation by LPS had been reported to enhance the release of proinflammatory mediators. This includes TNF-α, interleukin-1β as primary mediators and prostaglandins and leukotrienes as secondary mediators[213]. LPS is also responsible for the release of cyclooxygenase 2 (COX-2) [214] Cyclooxygenase 2 (COX-2) is responsible for the production of inflammation mediators.

The treatment effectiveness was slightly reduced over time (24 h to 36 h) for most nanoparticle treatments but not for the DOX, LPS and larger drug loaded nanoparticles. This partial decrease in treatment effectiveness at 36 h was presumably due to a decreasing activation of the macrophage due to digestion of the nanoparticles along with A-549 cell multiplication.

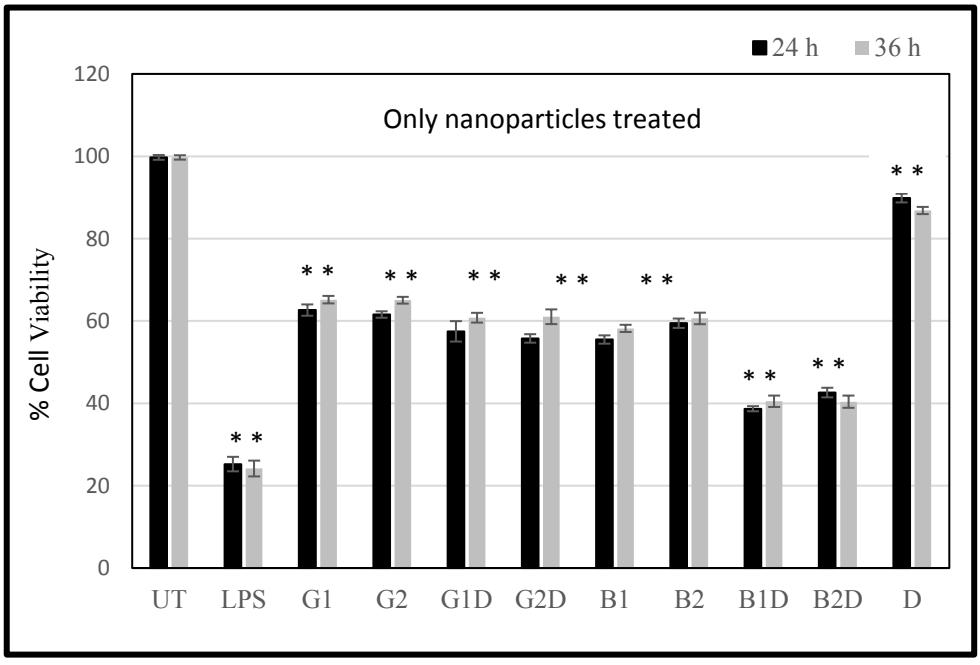

Figure 5.1: A-549 cancer cell viability after 24 h or 36 h after seeding macrophages in the upper compartment of a transwell coculture system: (UT) no treatment (control cells),

Lipopolysaccharide (LPS) was used as positive control, (G1 and G2 = gelatin NPs of different size, G1D and G2D = DOX loaded gelatin NPs of different size. B1 and B2 = PIBCA NPs of different size, B1D and B2D = DOX loaded PIBCA NPs of different size. D = doxorubicin (DOX) alone. Data shown were the mean ± S.D. (n = 3); *denotes that the treatment results were significantly different (* $p < 0.05$).

5.5.3.2 Anti-inflammatory treatment of macrophage

5.5.3.2.1 Nonsteroidal Anti-inflammatory Drugs (ibuprofen and celecoxib)

The treatments described in the previous section (nanoparticle treatment of macrophage) were used with the addition of ibuprofen [206]. Figure 5.2 shows the impact of ibuprofen on A-549 cancer cell viability. Cells without ibuprofen treatment were used as a control. The decrease in A-549 cancer cell viability was considered to be equivalent to the treatment effectiveness. Figure 5.2 shows that treatment effectiveness was reduced to 15–32% from 35–45% when MH-S macrophages were treated with blank nanoparticles (G1IB, G2IB, B1IB, B2IB) and reduced to 10–28% from 40–62% when MH-S macrophages were treated with doxorubicin loaded nanoparticles (G1DIB, G2DIB, B1DIB, B2DIB). There was a statistically significant difference between all blank and their corresponding drug loaded gelatin and PIBCA nanoparticle formulations at 24 and 36 h (except G1IB vs. G1DIB at 36h; B2IB vs. B2DIB at 24 h). Additional comparison to highlight the treatment and nanoparticle size effect was shown as appendix-II.

In a similar experiment, treatments described in the previous section (nanoparticle treatment of macrophage) were used with the addition of celecoxib [207]. Cells without celecoxib treatment were used as a control. Figure 5.3 shows that treatment effectiveness was reduced to 18–38% from 35–45% when MH-S macrophages were treated with blank nanoparticles (G1C, G2C,

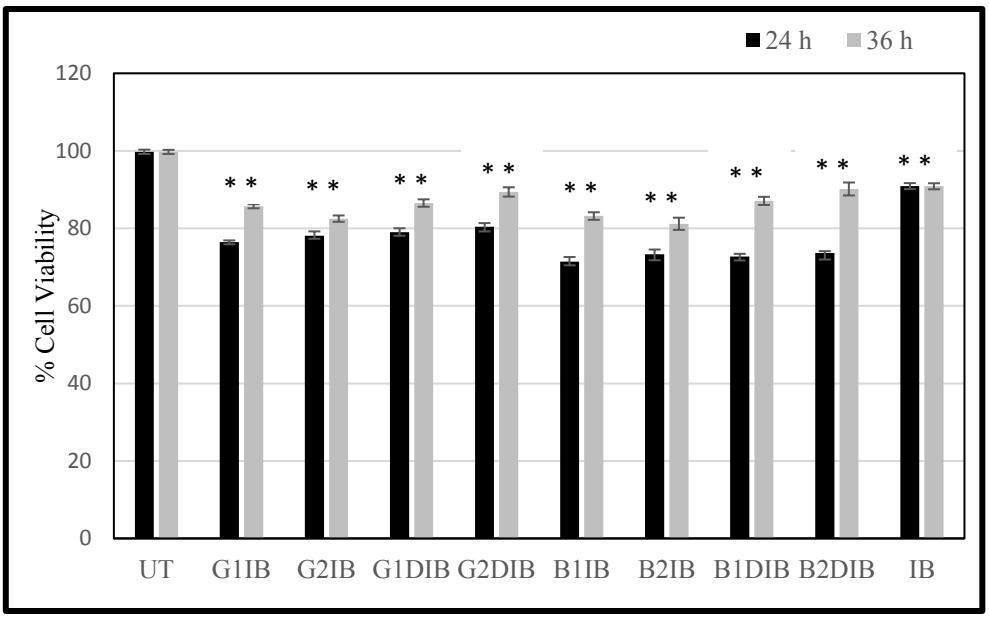

Figure 5.2: A-549 cancer cells viability after 24 h or 36 h in a co-culture model after ibuprofen treatment of macrophages seeding in the upper compartment. UT= Control cells. G1IB and G2IB= Ibuprofen treated gelatin NPs of different sizes, G1DIB and G2DIB= Ibuprofen treated Dox loaded gelatin NPs of different sizes. B1IB and B2IB= Ibuprofen treated PIBCA NPs of different sizes, B1DIB and B2DIB= Ibuprofen treated Dox loaded PIBCA NPs of different sizes, IB=Ibuprofen alone. Data shown were the mean ± S.D. (n=3) * denotes that the treatment results were significantly different (* $p < 0.05$).

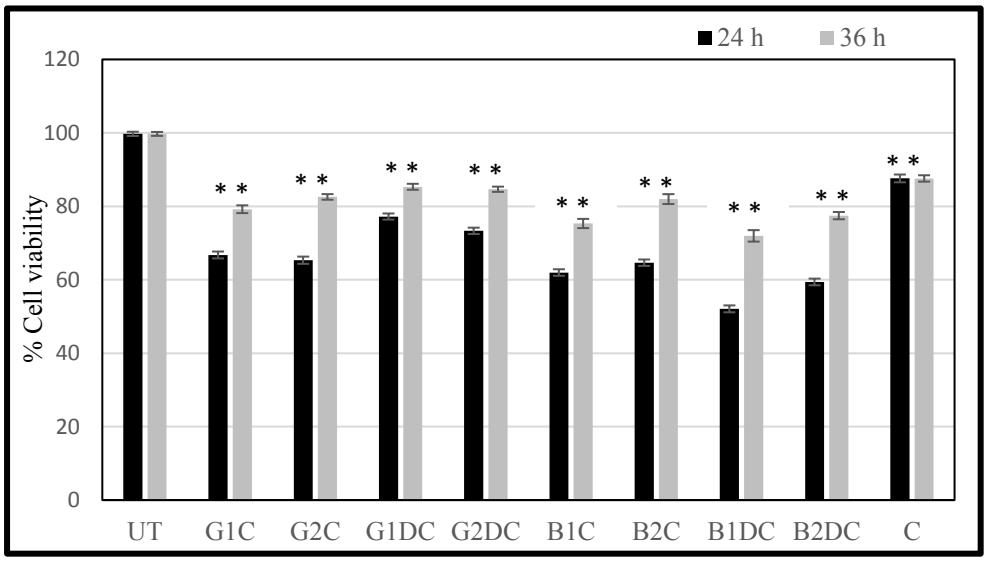

Figure 5.3: A-549 cancer cells viability after 24 h or 36 h in co-culture model after celecoxib treatment of macrophages seeding in the upper compartment. UT= Control cells. G1C and G2C= Celecoxib treated gelatin NPs of different sizes, G1DIB and G2DIB= Celecoxib treated Dox-loaded gelatin NPs of different sizes. B1C and B2C= Celecoxib treated PIBCA NPs of different sizes, B1DC and B2DC= Celecoxib treated Dox loaded PIBCA NPs of different sizes, C=Celecoxib alone. Data shown were the mean ± S.D. (n=3) * denotes that the treatment results were significantly different (* $p < 0.05$).

B1C, B2C) and reduced to 15–48% from 40–62% when MH-S macrophages were treated with doxorubicin loaded nanoparticles (G1DC, G2DC, B1DC, B2DC). There was a statistically significant difference between all blank and their corresponding drug loaded gelatin and PIBCA nanoparticle formulations at 24 and 36 h.

Figures 5.2 and 5.3 show that the gelatin treatment effectiveness and the PIBCA treatment effectiveness were significantly different. However, the NSAIDs (ibuprofen and celecoxib)

reduced the treatment effectiveness of all nanoparticle treatments. This drop in treatment effectiveness might be due to the anti-inflammatory activity of NSAIDs through inhibition of COX-2 enzyme activity which produces prostaglandin from the arachidonic acid pathway (precursor of inflammatory responses), as reported by Vane et al [215].

These findings are in accordance with reported studies in which celecoxib reduced inflammation by modulating prostaglandin production in alveolar macrophages of active human smokers[216]. Similarly, a reduced pulmonary inflammation was reported in mice [217].

There was a significant difference in the treatment effectiveness of the NSAIDs ibuprofen and celecoxib. The treatment effectiveness of celecoxib (selective COX-2 inhibitor) was lower than that of ibuprofen (a nonselective COX inhibitor). This might be due to an apoptotic effect of celecoxib on cancer cells. Liu et al reported that celecoxib directly induced apoptosis in A-549 cells [218]. The treatment effectiveness decreased significantly over time (24 h to 36 h) for all nanoparticle treatments. This might be due to a decrease in macrophage activation as the nanoparticles biodegraded over time and to the multiplication of A-549 cells.

5.5.3.2.2 Glucocorticoids (prednisolone and dexamethasone)

The treatments described in the previous section (nanoparticle treatment of macrophage) were used with the addition of prednisolone[209] . Cells without prednisolone treatment were used as a control. Figure 5.4 shows a treatment effectiveness reduced to 12–22% from 35–45% when MH-S macrophages were treated with blank nanoparticles (G1P, G2P, B1P, B2P) and reduced to 11–29% from 40–62% when MH-S macrophages were treated with doxorubicin-loaded nanoparticles (G1DP, G2DP, B1DP, B2DP). There was a statistically significant difference between all blank and their corresponding drug loaded gelatin and PIBCA nanoparticle

formulations at 24 and 36 h (except G2P vs. G2DP at 24 h).

The treatments described in the previous section (nanoparticle treatment of macrophage) were used with the addition of dexamethasone [208]. Cells without dexamethasone treatment were used as a control. The treatment effectiveness was reduced to 13–24% from 35–45% when MH-S macrophages were treated with blank nanoparticles (G1Dex, G2Dex, B1Dex, B2Dex) and reduced to 12–30% from 40–62% when MH-S macrophages were treated with doxorubicin-loaded nanoparticles (G1DDex, G2DDex, B1DDex, B2DDex) (Figure 5.5). There was a statistically significant difference between all blank and their corresponding drug loaded gelatin and PIBCA nanoparticle formulations at 36 h. No differences were observed at 24 h for both gelatin and PIBCA nanoparticle formulations (except for B1Dex vs. B1DDex).

The initial decrease in treatment effectiveness might be due to several glucocorticoids (GC) mechanisms. First, GC inhibition of phospholipase A2 enzyme activity could decrease the production of inflammatory markers due to a resultant decrease in the synthesis of arachidonic acid from phospholipids in the cell membrane [215]. Second, the decrease in treatment effectiveness might be due to the production of IL-10, an anti-inflammatory cytokine produced by the macrophage after exposure to GCs, as reported in Erchen et al [219]. Third, the observed decrease in treatment effectiveness might be due to a decrease in the metabolic activity of the macrophages when exposed to GCs, as reported in Werb et al [220].

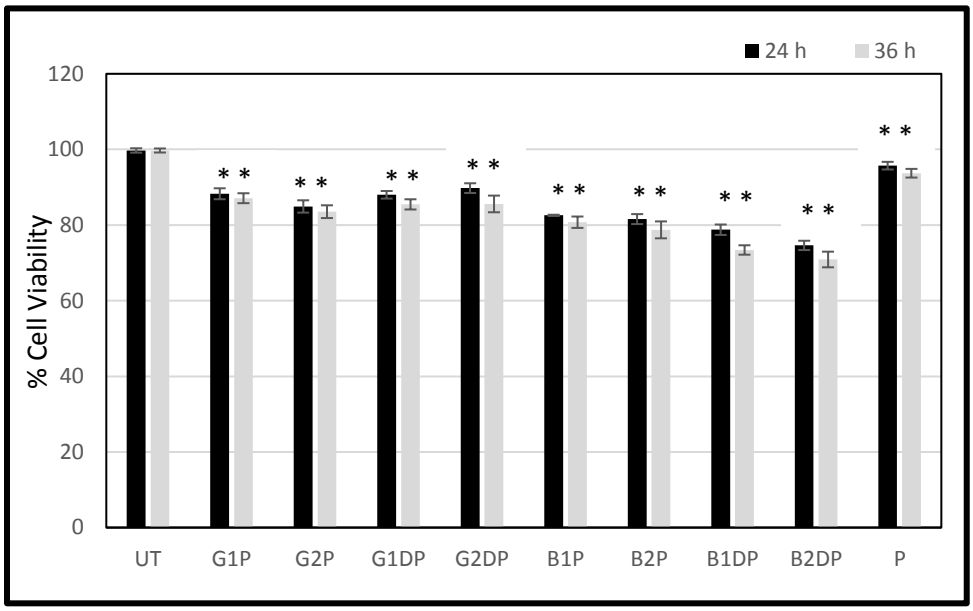

Figure 5.4: A-549 cancer cells viability after 24 h or 36 h in a co-culture model after prednisolone treatment of macrophages seeding in the upper compartment. UT= Control cells. G1P and G2P= Prednisolone treated gelatin NPs of different sizes, G1DP and G2DP=Prednisolone treated Dox loaded gelatin NPs of different sizes. B1P and B2P= Prednisolone treated PIBCA NPs of different sizes, B1DP and B2DP= Prednisolone treated Dox loaded PIBCA NPs of different sizes, P= Prednisolone alone. Data shown were the mean ± S.D. (n=3) * denotes that the treatment results were significantly different (* $p < 0.05$).

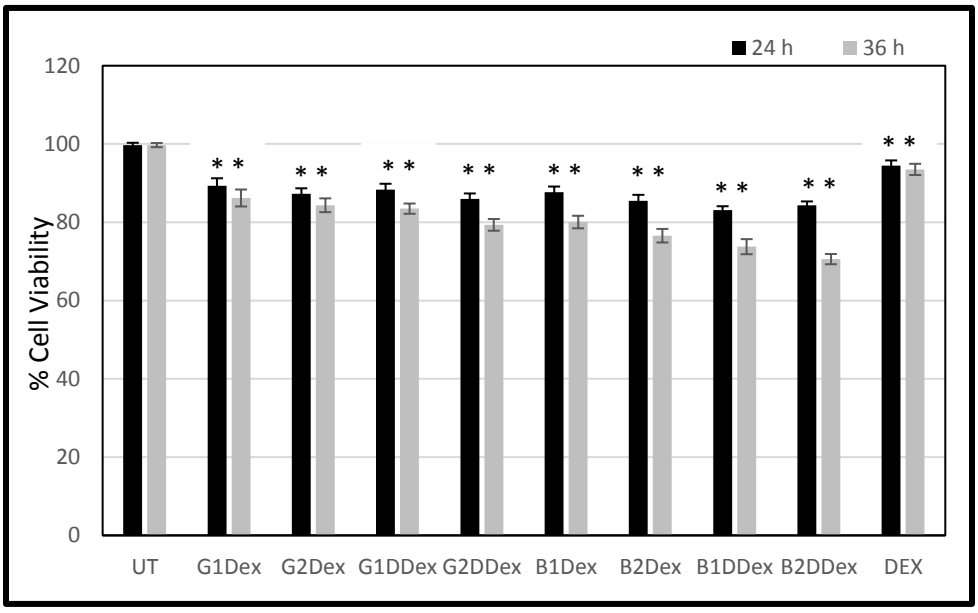

Figure 5.5: A-549 cancer cells viability after 24 h or 36 h in co-culture model after dexamethasone treatment of macrophages seeding in the upper compartment. UT= Control cells. G1Dex and G2Dex= Dexamethasone treated gelatin NPs of different sizes, G1DDex and G2DDex= Dexamethasone treated Dox loaded gelatin NPs of different sizes. B1Dex and B2Dex= Dexamethasone treated PIBCA NPs of different sizes, B1DDex and B2DDex= Dexamethasone treated Dox loaded PIBCA NPs of different sizes, Dex= Dexamethasone alone. Data shown were the mean ± S.D. (n=3) * denotes that the treatment results were significantly different (* $p < 0.05$).

The treatment effectiveness significantly increased over time (24 h to 36 h) because there were enough nanoparticles present at 36 h to activate the macrophage. The increase in treatment effectiveness was more pronounced for dexamethasone than for prednisolone. This might be due to the greater potency of dexamethasone compared to prednisolone (7:1) [221,222], and to inhibition of metabolism early on. After 24 h, an increase in macrophage metabolic activity occurred, similar to the behaviour reported by Werb et al [220]. The increase in macrophage

metabolic activity including nanoparticle degradation led to an increase in cytokine and chemokine release by macrophages and subsequently increased the treatment effectiveness.

5.5.3.2.3 Methotrexate

Methotrexate is an antifolate chemotherapeutic agent that inhibits dihydrofolate reductase, which leads to the inhibition of DNA synthesis and eventually blocks cell replication. Methotrexate is used to reduce inflammation in rheumatoid arthritis [198].

The treatments described in the previous section (nanoparticle treatment of macrophage) were used with the addition of methotrexate [210]. Control cells were not treated with methotrexate. Figure 6 shows that the treatment effectiveness was reduced to 15–20% from 35–38% when MH-S macrophages were treated with blank gelatin nanoparticles (G1M, G2M) and reduced to 22–26% from 39–45% when MH-S macrophages were treated with doxorubicin loaded gelatin nanoparticles (G1DM, G2DM). Similarly, the treatment effectiveness was reduced to 10–25% from 40–45% when MH-S macrophages were treated with blank PIBCA nanoparticles (B1M, B2M) and reduced to 14–37% from 38–42% when MH-S macrophages were treated with doxorubicin loaded PIBCA nanoparticles (B1DM, B2DM). There was a statistically significant difference between all blank and their corresponding drug loaded gelatin and PIBCA nanoparticle formulations at 24 and 36 h (except B1M vs. B1DM at 24h).

The initial decrease in treatment effectiveness might be explained if methotrexate operated through a mechanism different from the inhibition of dihydrofolate reductase [198]. Methotrexate has been reported to reduce inflammation through the release of adenosine which inhibits the secretion of TNF-α, IL-6, and IL-8 (proinflammatory) cytokines and increases the secretion of IL-10 (anti-inflammatory) cytokines [223]. Methotrexate also increases IL-4 and IL-10 (anti-

inflammatory) production and decreases IL-2 and IFN-γ (proinflammatory) concentrations in peripheral blood monocytes [224]. The reduction in cytokines and release of chemokines from the macrophages could have decreased treatment effectiveness in the first 24 hours.

From 24 h to 36 h the treatment effectiveness significantly increased for all treatments, including the methotrexate only treatment. The overproduction of adenosine induced by methotrexate could suppress cell proliferation and could cause cell death. Cell death may lead to a further release of proinflammatory cytokines from dead macrophages and thus decrease cancer cell viability [223].

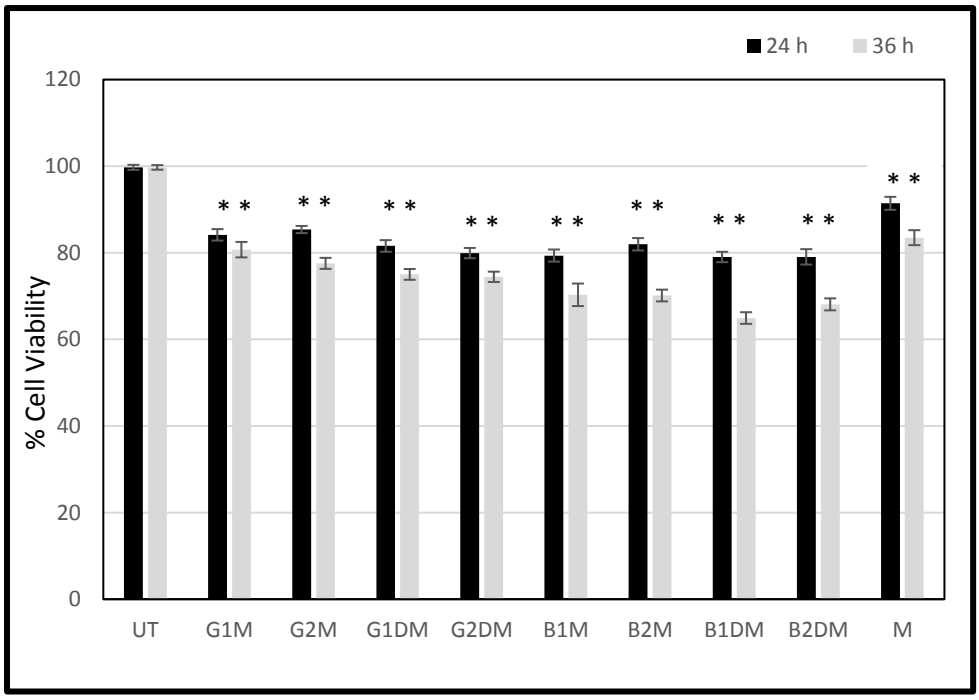

Figure 5.6: A-549 cancer cells viability after 24 h or 36 h in co-culture model after methotrexate treated macrophages seeding to upper compartment. UT= Control cells. G1M and G2M= Methotrexate treated gelatin NPs of different sizes, G1DM and G2DM= Methotrexate treated Dox loaded gelatin NPs of different sizes. B1M and B2M= Methotrexate treated PIBCA NPs of

different sizes, B1DM and B2DM= Methotrexate treated Dox loaded PIBCA NPs of different sizes, M= Methotrexate alone. Data shown were the mean ± S.D. (n=3) * denotes that the treatment results were significant (* $p < 0.05$).

5.6 Discussion

Macrophages infiltrating a tumor, so called tumor-associated macrophages (TAM), These macrophages can represent up to 50% of the tumor mass [24]. TAMs play a important role in regulating the immune response within a tumor by releasing different soluble mediators [225]. The nanoparticle of appropriate size is easily phagocytised by macrophages, [226] and the decade old belief that nanosized drug delivery systems need to be protected from phagocytosis needs to be reassessed [67]. Researchers have developed polymeric and lipid nanoparticles for transferring drugs to macrophages [139,227]. However, the impact of nanoparticles and their interaction with the host immune response has not been thoroughly investigated. A recent study highlighted the gaps in understanding the mechanisms responsible for the interactions of tumor cells with the immune cell in cancer microenvironments [228].

After nanoparticle engulfment by macrophages, [229] the cells undergo an acute stage of inflammation and release Th-1 type antitumor cytokines that decrease H-460 cancer cell viability. Another study showed the significance of acute inflammation of the macrophage and its cytokine release profile after nanoparticle engulfment [81]. Our current study shows a decrease from 40–62% in A-549 cancer cell viability after treating macrophages with different drug loaded nanoparticles. These results agree with our previous study that used drug loaded nanoparticles to kill H-460 cells [81]. However, after treating macrophages with ibuprofen and celecoxib, the A-549 cancer cell viability enhanced up to 34% and 24% respectively, indicating that ibuprofen and celecoxib affect the inflamed macrophage and suppress the release of its cytokines and chemokines. Treatment of macrophages with ibuprofen and celecoxib loaded nanoparticles led to less inhibition of tumor cell growth as compared to the treatment without anti-inflammatory drugs. This is in accordance with a study which reported a 60% reduction in prostaglandin production in

celecoxib fed mice. However, the mice had larger lung tumors than mice that did not receive celecoxib [217].

For prednisolone, dexamethasone and methotrexate the treatment enhanced cancer cell viability up to 30%. However, these treatments showed after 36 hours a lower cancer cell viability compared to 24 h. This might be due to their anti-cancer properties.

Current cancer treatments administer nonsteroidal anti-inflammatory drugs (NSAIDs) along with cancer chemotherapeutics to reduce inflammation and to augment the efficacy of anticancer treatment [230,231]. However, the promising preclinical data are not seen in clinical outcomes [231]. Our data show that NSAIDs were counterproductive when used along with nanosized delivery systems in cancer chemotherapy. The glucocorticoids dexamethasone and prednisolone frequently used in cancer immunotherapy showed similar unproductive outcomes. The anti-inflammatory effect of these drugs initially inhibited tumor suppression. Our findings indicate that an acutely inflamed state of the macrophage is achieved after nanoparticle exposure and leads to secondary toxicity and an increase in treatment effectiveness. We believe the anti-inflammatory drugs affected the inflamed state of the macrophages (lowering it) and reduced secondary toxicity. The reduction in secondary toxicity led to a decrease in the treatment effectiveness of nanoparticle therapy.

5.7 Conclusion

Macrophages exposed to nanoparticles show secondary toxicity, which has a significant antitumor effect in the microclimate of a coculture cancer cell model. However, the treatment effectiveness was significantly reduced if NSAIDs, glucocorticoids, or methotrexate were given at the same time. The data suggest that anti-inflammatory treatments reduce the effectiveness of chemotherapy when nanosized carriers are used. Macrophage targeting with nanoparticles in cancer treatment is a promising way to augment chemotherapy with a cellular immune reaction of macrophages. The use of anti-inflammatory treatments together with nanosized delivery systems needs to be carefully considered due to the decrease in treatment efficacy.

Chapter 6

General Conclusion and Future Prospective

6.1 General Conclusion

Two different diseases, tuberculosis and lung cancer, were selected as a model for the current study. Tuberculosis is an infectious disease caused by mycobacterium tubercle and lung cancer, is characterized by the uncontrolled proliferation of cells in lungs tissue. The mode of spread, pathogenies, diagnosis, prognosis and management of both diseases is quite different. However, the role of the macrophage in both of these diseases is the major area of interest. In tuberculosis, the life cycle of mycobacterium tubercle starts by harboring and multiplying inside the host immune cells (macrophage) followed by the latent and chronic stages of tuberculosis. Similarly, in lung cancer, the macrophages are the only immune which infiltrates the tumor tissue. The behavior of macrophage inside the tumor microenvironment either contributes toward the tumor progression by angiogenesis, resistance to apoptosis, decrease host immunity and tumor growth or tumor suppression by immunostimulation, tumor suppression and cytotoxicity.

The interaction between colloidal drug delivery systems (i.e. nanocarriers) and macrophages needs to be investigated regarding secondary toxicity effects. Different aspects of this nanocarriers macrophage interaction need to be understood for the development of any optimal colloidal drug delivery system to target these two diseases. The significance of macrophages in these two diseases, as well as target drug delivery by nanocarriers and potential of secondary toxicity effects, are the main factors investigated in the current study. The present investigation includes (i) To inquire into secondary toxicity effects triggered by two colloidal drug carriers (micelles and nanoparticles) (ii) To analyze the secondary toxicity effects in a microclimate of a lung cancer model. (iii) To study the effect of different drugs on secondary toxicity.

Initially, secondary toxicity effect was explored using newly synthesize micelles as nanocarriers after interaction with alveolar macrophages. We successfully synthesized and

characterized nanocarrier (HA-TS micelles). The micelles were self-assembled in aqueous solution with mean particle size of 212–294.6 nm possess good colloidal stability and biocompatibility. The hydrophobic drug RIF was efficiently encapsulated with drug loadings of 70.7–79.1%. Both of the *in vitro* release curves showed that the incorporated RIF was sustained released from RIF loaded HA-TS micelles. The RIF-HA-TS micelles were taken up more efficiently by the alveolar macrophages (MH-S) as compared to the free RIF. The greater cellular uptake of RIF-HA-TS micelles was due to the targeting of CD44 receptors on macrophage surface by HA component of RIF-HA-TS micelles. The RIF-HA-TS micelles were primarily localized in the cytoplasm. The cellular uptake of RIF-HA-TS was time-dependent as well as dose-dependent and carried out by phagocytosis and receptor-mediated endocytosis. The cellular uptake of RIF-HA-TS micelles induced the secondary toxicity effect (Th-1 type cytokines release) from macrophages which were qualitatively and quantitatively measured by cytokines membrane array kits. Secondary toxicity in alveolar macrophages might contribute towards the overall effectiveness of a tuberculosis treatment.

Our second study focused on the secondary toxicity effect using nanoparticle as nanocarrier instead of micelles after interaction with alveolar macrophages. We prepared and physicochemically characterized RIF and MOX loaded gelatin and PIBCA nanoparticles. The nanoparticles of two different mean sizes in the range of 120 nm to 155 nm and 265 nm to 305 nm size were prepared respectively. The RIF and MOX showed poor drug loadings in gelatin nanoparticles as compared to the PIBCA polymer. Both of the *in vitro* release curves revealed that the incorporated RIF and MOX were sustained released from their nanoparticles and follow fickian diffusion drug transport. The cell viability values of MOX-PIBCA nanoparticles were lower than the one for RIF-PIBCA nanoparticles. The cellular uptake of nanoparticles induced the pro-

inflammatory and anti-inflammatory secondary toxicity in macrophages. The proinflammatory cytokines, TNF-α and IL-1β showed a significant difference in treated cells as compared to the untreated control cells. In contrast, an anti-inflammatory cytokine IL-10 was also significantly different in comparison to untreated cells. Nanoparticles along with chemotherapeutic drugs might be able to trigger a secondary toxicity effect in macrophages via an immune response and drug action. A targeted and more efficient anti-tuberculosis treatment, directly to macrophages, might be possible when drug loaded nanoparticles will be used to treat tuberculosis infections. The combined effect might be able to overcome mycobacteria infections.

In our third study, the objective was to explore the nanoparticle fed macrophage secondary toxicity behavior in a cancer microenvironment using a co-culture model. The study also investigated the effect of different drugs affecting the secondary toxicity. We prepared and physicochemically characterized the DOX-loaded gelatin and PIBCA nanoparticles of two different sizes. The DOX showed 80-83% drug entrapment efficiency in PIBCA nanoparticles as compared to the gelatin nanoparticles with 39-42% entrapment efficiency. The nanoparticles fed macrophages induced a secondary toxicity effect with the release of Th-1 type cytokines. These cytokines dropped the A-549 cancer cell viability. However, the effectiveness of nanoparticle treatment was significantly different from the two polymers.

The data also showed the effect of the various drugs on secondary toxicity. The use of NSAIDs (Ibuprofen and Celecoxib) with nanoparticles fed macrophages had significantly dropped the treatment effectiveness due to a decrease in secondary toxicity effects. Similar findings were observed after GCs (Prednisolone and Dexamethasone) and methotrexate treatment. Both GCs and methotrexate treatment with nanoparticle fed macrophages had dropped the treatment effectiveness significantly due to a decrease in secondary toxicity effect.

All of the above studies concluded that this nano-carrier (micelles and nanoparticles) had the potential to activate the macrophages and to induce secondary toxicity. Among the nanocarriers, these effects were much more significant with nanoparticles as compared to micelles. The level of activation by these nanocarriers depends on the particle sizes, surface charges and chemical nature of the polymer. It also depends on the nanocarriers cellular uptake by macrophages and microclimate in the case of tumor model. So the decades-old belief of inert characteristics of colloidal drug delivery system should have to be reevaluated in the light of beneficial secondary toxicity effects.

Secondary toxicity was induced when alveolar macrophages were treated with anti-tuberculosis drug loaded nanocarriers. A significant increase of TNF-α was observed after nanocarrier treatment. It was already reported that TNF-α produced nitric oxide synthase 2 (NOS2) to generate nitric oxide (NO) which can kill the intracellular harboring *M.tb* inside the macrophage [41,42].So TNF-α production helps in eradication of intracellular harboring *M.tb* Nanocarriers also induced a significant production of IL-1β. The importance of IL-1β in *M.tb* infection was already established in knockout mice studies. Animals in which both IL-1β and IL-1α had been deleted, from larger granulomas after infection and were unable to clear the mycobacteria as efficiently as the wildtype mice [47]. Thus, IL-1β production will help in controlling the spread of *M.tb* at an earlier stage without going into the latent stage of granuloma formation. Nanocarriers also induced the significance production of IFN-γ. It has also been proved that IFN-γ activates macrophages, enhances their production of proinflammatory cytokines and up-regulates their surface expression of cytokine and chemokine receptors and enhances its antigen presentation [48]. In another study, mice deficient in IFN-γ failed to produce nitric oxide due to low iNOS expression and exhibited unrestricted *M.tb* growth and tissue necrosis with mice

suffering from *M.tb* infection faster [50]. The patients with clinically active tuberculosis have been reported with a low level of IFN-γ when compared with latent tuberculosis [51]. Thus, IFN-γ production will help to enhance eradication of *M.tb.* In contrast to proinflammtory response, nanocarriers also induced significant production of IL-10, an anti-inflammatory cytokine. It has also been proved that IL-10 down-regulates the production of proinflammatory cytokines [115]. It also inhibits the proliferation of interferon-gamma IFN-γ [116]. So the targeted and more efficient anti-tuberculosis treatment might be possible by controlling the release of cytokines.

Shifting the macrophage balance towards the anti-tumor phenotype was a strategy to circumvent the pro-tumoral features of TAMs as discussed earlier (sec 1.3.4). It was achieved by secondary toxicity when macrophages were exposed to nanoparticles. This secondary toxicity has significant anti-tumor effects in a tumor microclimate. Similar secondary toxicity was reported by Al-Hallak due to the release of Th-1 type cytokines (TNF-α), (IFN-γ), (MCP-1) and (MIP-1) against H-460 cells in a tumor microclimate [81]. Moreover, these anti-tumor effects were significantly reduced with the concomitant use of NSAIDs, glucocorticoids and methotrexate. The findings were in accordance with a study in which there was a 60% reduction in prostaglandin production in celecoxib fed mice. However, the mice had larger lung tumors as compared to the mice without celecoxib treatment [217]. The data suggested that anti-inflammatory treatments reduced the effectiveness of chemotherapy when nano-sized carriers were used. The insight gained by these studies can be utilized for new treatments approaches toward these chronic diseases.

6.2 Future perspectives

The current study highlighted the importance of secondary toxicity in murine alveolar macrophages and a lung cancer model. It also showed the benefits of targeting drug delivery (nano-carriers) to macrophages in macrophage oriented diseases. However, the effects can be further validated using animal models. Based on the results of this thesis the following are my suggestions for future studies to verify and extend these findings.

Animal Studies

Cancer Model

I. Carry out the animal studies using the tumor-bearing BALB/c nude mice model. Two different lung cancer model with H-460 (doxorubicin non-resistance model) and (A-549 (doxorubicin resistance model) should be considered for future studies.

II. Investigate the effect of co-treatment of these cancer-bearing mice model with NSAIDs (ibuprofen) along with doxorubicin-loaded nanoparticles (chemotherapy treatment).

Mycobacterium Model

III. Mice mycobacterium tuberculosis model should be evaluated by using anti-tuberculosis drug loaded nanoparticles.

Acute and Chronic Inflamed Model

IV. Both, acute and chronically inflamed state in a mouse model (Cancer and Mycobacterium model), should be investigated using the above nanoparticles and their co-treatments.

Bibliography

1. Janeway CA,Jr: The immune system evolved to discriminate infectious nonself from noninfectious self. *Immunol. Today* 13(1), 11-16 (1992).

2. Mogensen TH: Pathogen recognition and inflammatory signaling in innate immune defenses. *Clin. Microbiol. Rev.* 22(2), 240-73, Table of Contents (2009).

3. Fujiwara N, Kobayashi K: Macrophages in inflammation. *Curr. Drug Targets Inflamm. Allergy* 4(3), 281-286 (2005).

4. Murphy K, Travers P, Walport M: Immunobiology: Part II The Recognition of Antigen, Chapter 3: Antigen recognition by B-Cll and T-cell receptors. 7th ed. In: , Garland Science, New York, 111-118 (2007).

5. LeBien TW, Tedder TF: B lymphocytes: how they develop and function. *Blood* 112(5), 1570-1580 (2008).

6. Ehrlich P: Collected papers of Paul Ehrlich. Pergamon, New York (1957).

7. Burnet M: Cancer - a biological approach: I. The procceses of control. II.The significance of somatic mutation. *Br Med J.* 1 (5022), 779-786 (1957).

8. Swann JB, Smyth MJ: Immune surveillance of tumors. *J. Clin. Invest.* 117(5), 1137-1146 (2007).

9. Dunn GP, Bruce AT, Ikeda H, Old LJ, Schreiber RD: Cancer immunoediting: from immunosurveillance to tumor escape. *Nat. Immunol.* 3(11), 991-998 (2002).

10. Hanahan D, Weinberg RA: The Hallmarks of Cancer. *Cell* 100(1), 57-70 (2000).

11. Garrido F, Cabrera T, Concha A, Glew S, Ruiz-Cabello F, Stern PL: Natural history of HLA expression during tumour development. *Immunol. Today* 14(10), 491-499 (1993).

12. Dunn GP, Old LJ, Schreiber RD: The Immunobiology of Cancer Immunosurveillance and Immunoediting. *Immunity* 21(2), 137-148 (2004).

13. Smyth MJ, Dunn GP, Schreiber RD: Cancer Immunosurveillance and Immunoediting: The Roles of Immunity in Suppressing Tumor Development and Shaping Tumor Immunogenicity. *Adv. Immunol.* 90, 1-50 (2006).

14. Teng M, Swann J, Koebel C, Schreiber R, Smyth M: Immune-mediated dormancy: an equilibrium with cancer. J Leukoc Biol 2008;84:988–93. *J Leukos Biol* 84, 988-993 (2008).

15. Zitvogel L, Tesniere A, Kroemer G: Cancer despite immunosurveillance: immunoselection and immunosubversion. *Nat. Rev. Immunol.* 6(10), 715-727 (2006).

16. Seliger B, Maeurer MJ, Ferrone S: Antigen-processing machinery breakdown and tumor growth. *Immunol. Today* 21(9), 455-464 (2000).

17. Spiotto MT, Rowley DA, Schreiber H: Bystander elimination of antigen loss variants in established tumors. *Nat. Med.* 10(3), 294-298 (2004).

18. Groh V, Wu J, Yee C, Spies T: Tumour-derived soluble MIC ligands impair expression of NKG2D and T-cell activation. *Nature* 419(6908), 734-738 (2002).

19. Gordon S, Taylor PR: Monocyte and macrophage heterogeneity. *Nat. Rev. Immunol.* 5(12), 953-964 (2005).

20. Murray PJ, Wynn TA: Protective and pathogenic functions of macrophage subsets. *Nat. Rev. Immunol.* 11(11), 723-737 (2011).

21. Gordon S: Alternative activation of macrophages. *Nat. Rev. Immunol.* 3(1), 23-35 (2003).

22. Sica A, Allavena P, Mantovani A: Cancer related inflammation: The macrophage connection. *Cancer Lett.* 267(2), 204-215 (2008).

23. Mantovani A, Allavena P, Sica A, Balkwill F: Cancer-related inflammation. *Nature* 454(7203), 436-444 (2008).

24. Solinas G, Germano G, Mantovani A, Allavena P: Tumor-associated macrophages (TAM) as major players of the cancer-related inflammation. *J. Leukoc. Biol.* 86(5), 1065-1073 (2009).

25. Allavena P, Signorelli M, Chieppa M *et al.*: Anti-inflammatory properties of the novel antitumor agent yondelis (trabectedin): inhibition of macrophage differentiation and cytokine production. *Cancer Res.* 65(7), 2964-2971 (2005).

26. Dineen SP, Lynn KD, Holloway SE *et al.*: Vascular endothelial growth factor receptor 2 mediates macrophage infiltration into orthotopic pancreatic tumors in mice. *Cancer Res.* 68(11), 4340-4346 (2008).

27. Ferrara N, Hillan KJ, Novotny W: Bevacizumab (Avastin), a humanized anti-VEGF monoclonal antibody for cancer therapy. *Biochem. Biophys. Res. Commun.* 333(2), 328-335 (2005).

28. Krieg AM: Therapeutic potential of Toll-like receptor 9 activation. *Nat. Rev. Drug Discov.* 5(6), 471-484 (2006).

29. Guiducci C, Vicari AP, Sangaletti S, Trinchieri G, Colombo MP: Redirecting in vivo elicited tumor infiltrating macrophages and dendritic cells towards tumor rejection. *Cancer Res.* 65(8), 3437-3446 (2005).

30. Flynn JL: Immunology of tuberculosis and implications in vaccine development. *Tuberculosis (Edinb)* 84(1-2), 93-101 (2004).

31. Davis AS, Vergne I, Master SS, Kyei GB, Chua J, Deretic V: Mechanism of inducible nitric oxide synthase exclusion from mycobacterial phagosomes. *PLoS Pathog.* 3(12), e186 (2007).

32. Crowle AJ, Dahl R, Ross E, May MH: Evidence that vesicles containing living, virulent Mycobacterium tuberculosis or Mycobacterium avium in cultured human macrophages are not acidic. *Infect. Immun.* 59(5), 1823-1831 (1991).

33. Cooper AM: Cell-mediated immune responses in tuberculosis. *Annu. Rev. Immunol.* 27, 393-422 (2009).

34. Ulrichs T, Kaufmann SH: New insights into the function of granulomas in human tuberculosis. *J. Pathol.* 208(2), 261-269 (2006).

35. Kaplan G, Post FA, Moreira AL *et al.*: Mycobacterium tuberculosis growth at the cavity surface: a microenvironment with failed immunity. *Infect. Immun.* 71(12), 7099-7108 (2003).

36. Dheda K, Booth H, Huggett JF, Johnson MA, Zumla A, Rook GA: Lung remodeling

in pulmonary tuberculosis. *J. Infect. Dis.* 192(7), 1201-1209 (2005).

37. Dheda K, Barry CE,3rd, Maartens G: Tuberculosis. *Lancet* 387(10024), 1211-1226 (2016).

38. Russell DG: Who puts the tubercle in tuberculosis? *Nat. Rev. Microbiol.* 5(1), 39-47 (2007).

39. Janeway, C.T., Paul,M., Walport M, Shlomchik M: Immunobiology: The Immune System in Health and Disease. Garland Science Publishing, New York (2005).

40. Keane J, Gershon S, Wise RP *et al.*: Tuberculosis associated with infliximab, a tumor necrosis factor alpha-neutralizing agent. *N. Engl. J. Med.* 345(15), 1098-1104 (2001).

41. Ding AH, Nathan CF, Stuehr DJ: Release of reactive nitrogen intermediates and reactive oxygen intermediates from mouse peritoneal macrophages. Comparison of activating cytokines and evidence for independent production. *J. Immunol.* 141(7), 2407-2412 (1988).

42. Flesch IE, Hess JH, Oswald IP, Kaufmann SH: Growth inhibition of Mycobacterium bovis by IFN-gamma stimulated macrophages: regulation by endogenous tumor necrosis factor-alpha and by IL-10. *Int. Immunol.* 6(5), 693-700 (1994).

43. Bean AG, Roach DR, Briscoe H *et al.*: Structural deficiencies in granuloma formation in TNF gene-targeted mice underlie the heightened susceptibility to aerosol Mycobacterium tuberculosis infection, which is not compensated for by lymphotoxin. *J. Immunol.* 162(6), 3504-3511 (1999).

44. Flynn JL, Goldstein MM, Chan J *et al.*: Tumor necrosis factor-alpha is required in the protective immune response against Mycobacterium tuberculosis in mice. *Immunity* 2(6), 561-572 (1995).

45. Jacobs M, Brown N, Allie N, Ryffel B: Fatal Mycobacterium bovis BCG infection in TNF-LT-alpha-deficient mice. *Clin. Immunol.* 94(3), 192-199 (2000).

46. Dinarello CA: Biologic basis for interleukin-1 in disease. *Blood* 87(6), 2095-2147 (1996).

47. Yamada H, Mizumo S, Horai R, Iwakura Y, Sugawara I: Protective role of interleukin-1 in mycobacterial infection in IL-1 alpha/beta double-knockout mice. *Lab. Invest.* 80(5), 759-767 (2000).

48. Boehm U, Klamp T, Groot M, Howard JC: Cellular responses to interferon-gamma. *Annu. Rev. Immunol.* 15, 749-795 (1997).

49. Cooper AM, Dalton DK, Stewart TA, Griffin JP, Russell DG, Orme IM: Disseminated tuberculosis in interferon gamma gene-disrupted mice. *J. Exp. Med.* 178(6), 2243-2247 (1993).

50. Flynn JL, Chan J, Triebold KJ, Dalton DK, Stewart TA, Bloom BR: An essential role for interferon gamma in resistance to Mycobacterium tuberculosis infection. *J. Exp. Med.* 178(6), 2249-2254 (1993).

51. Zhang M, Lin Y, Iyer DV, Gong J, Abrams JS, Barnes PF: T-cell cytokine responses in human infection with Mycobacterium tuberculosis. *Infect. Immun.* 63(8), 3231-3234 (1995).

52. Sabat R: IL-10 family of cytokines. *Cytokine Growth Factor Rev.* 21(5), 315-324 (2010).

53. Mege JL, Meghari S, Honstettre A, Capo C, Raoult D: The two faces of interleukin 10 in human infectious diseases. *Lancet Infect. Dis.* 6(9), 557-569 (2006).

54. Mohan VP, Scanga CA, Yu K *et al.*: Effects of tumor necrosis factor alpha on host immune response in chronic persistent tuberculosis: possible role for limiting pathology. *Infect. Immun.* 69(3), 1847-1855 (2001).

55. Awomoyi AA, Charurat M, Marchant A *et al.*: Polymorphism in IL1B: IL1B-511 association with tuberculosis and decreased lipopolysaccharide-induced IL-1beta in IFN-gamma primed ex-vivo whole blood assay. *J. Endotoxin Res.* 11(5), 281-286 (2005).

56. Beamer GL, Flaherty DK, Assogba BD *et al.*: Interleukin-10 promotes Mycobacterium tuberculosis disease progression in CBA/J mice. *J. Immunol.* 181(8), 5545-5550 (2008).

57. O'Leary S, O'Sullivan MP, Keane J: IL-10 blocks phagosome maturation in mycobacterium tuberculosis-infected human macrophages. *Am. J. Respir. Cell Mol. Biol.* 45(1), 172-180 (2011).

58. Raja A: Immunology of tuberculosis. *Indian J. Med. Res.* 120(4), 213-232 (2004).

59. Mayer-Barber KD, Andrade BB, Barber DL *et al.*: Innate and adaptive interferons suppress IL-1alpha and IL-1beta production by distinct pulmonary myeloid subsets during Mycobacterium tuberculosis infection. *Immunity* 35(6), 1023-1034 (2011).

60. Benoit M, Desnues B, Mege JL: Macrophage polarization in bacterial infections. *J. Immunol.* 181(6), 3733-3739 (2008).

61. Flynn JL, Chan J: Immunology of tuberculosis. *Annu. Rev. Immunol.* 19, 93-129 (2001).

62. Howard AD, Zwilling BS: Reactivation of tuberculosis is associated with a shift from type 1 to type 2 cytokines. *Clin. Exp. Immunol.* 115(3), 428-434 (1999).

63. Kahnert A, Seiler P, Stein M *et al.*: Alternative activation deprives macrophages of a coordinated defense program to Mycobacterium tuberculosis. *Eur. J. Immunol.* 36(3), 631-647 (2006).

64. Beija M, Salvayre R, Lauth-de Viguerie N, Marty JD: Colloidal systems for drug delivery: from design to therapy. *Trends Biotechnol.* 30(9), 485-496 (2012).

65. Illum L, Davis SS: The organ uptake of intravenously administered colloidal particles can be altered using a non-ionic surfactant (Poloxamer 338). *FEBS Lett.* 167(1), 79-82 (1984).

66. Lenaerts V, Nagelkerke JF, Van Berkel TJ *et al.*: In vivo uptake of polyisobutyl cyanoacrylate nanoparticles by rat liver Kupffer, endothelial, and parenchymal cells. *J. Pharm. Sci.* 73(7), 980-982 (1984).

67. Moghimi SM, Hunter AC, Murray JC: Long-circulating and target-specific nanoparticles: theory to practice. *Pharmacol. Rev.* 53(2), 283-318 (2001).

68. Moghimi SM, Szebeni J: Stealth liposomes and long circulating nanoparticles: critical issues in pharmacokinetics, opsonization and protein-binding properties. *Prog. Lipid Res.* 42(6), 463-478 (2003).

69. Nahar M, Dubey V, Mishra D, Mishra PK, Dube A, Jain NK: In vitro evaluation of surface functionalized gelatin nanoparticles for macrophage targeting in the therapy of visceral

leishmaniasis. *J. Drug Target.* 18(2), 93-105 (2010).

70. Al-Hallak MH, Sarfraz MK, Azarmi S, Kohan MH, Roa WH, Lobenberg R: Microcalorimetric method to assess phagocytosis: macrophage-nanoparticle interactions. *AAPS J.* 13(1), 20-29 (2011).

71. Nimje N, Agarwal A, Saraogi GK *et al.*: Mannosylated nanoparticulate carriers of rifabutin for alveolar targeting. *J. Drug Target.* 17(10), 777-787 (2009).

72. Nahar M, Jain NK: Preparation, characterization and evaluation of targeting potential of amphotericin B-loaded engineered PLGA nanoparticles. *Pharm. Res.* 26(12), 2588-2598 (2009).

73. Byrne JD, Betancourt T, Brannon-Peppas L: Active targeting schemes for nanoparticle systems in cancer therapeutics. *Adv. Drug Deliv. Rev.* 60(15), 1615-1626 (2008).

74. Hobbs SK, Monsky WL, Yuan F *et al.*: Regulation of transport pathways in tumor vessels: role of tumor type and microenvironment. *Proc. Natl. Acad. Sci. U. S. A.* 95(8), 4607-4612 (1998).

75. Haley B, Frenkel E: Nanoparticles for drug delivery in cancer treatment. *Urol. Oncol.* 26(1), 57-64 (2008).

76. Brannon-Peppas L, Blanchette JO: Nanoparticle and targeted systems for cancer therapy. *Adv. Drug Deliv. Rev.* 56(11), 1649-1659 (2004).

77. Bhardwaj V, Ankola DD, Gupta SC, Schneider M, Lehr CM, Kumar MN: PLGA nanoparticles stabilized with cationic surfactant: safety studies and application in oral delivery of paclitaxel to treat chemical-induced breast cancer in rat. *Pharm. Res.* 26(11), 2495-2503 (2009).

78. Danhier F, Vroman B, Lecouturier N *et al.*: Targeting of tumor endothelium by RGD-grafted PLGA-nanoparticles loaded with paclitaxel. *J. Control. Release* 140(2), 166-173 (2009).

79. Kawata K, Osawa M, Okabe S: In vitro toxicity of silver nanoparticles at noncytotoxic doses to HepG2 human hepatoma cells. *Environ. Sci. Technol.* 43(15), 6046-6051 (2009).

80. Lin W, Huang Y, Zhou X, Ma Y: In vitro toxicity of silica nanoparticles in human lung cancer cells. *Toxicol. Appl. Pharmacol.* 217(3), 252-259 (2006).

81. Al-Hallak KM, Azarmi S, Anwar-Mohamed A, Roa WH, Lobenberg R: Secondary cytotoxicity mediated by alveolar macrophages: a contribution to the total efficacy of nanoparticles in lung cancer therapy? *Eur. J. Pharm. Biopharm.* 76(1), 112-119 (2010).

82. Sarfraz M, Shi W, Gao Y *et al.*: Immune response to antituberculosis drug-loaded gelatin and polyisobutyl-cyanoacrylate nanoparticles in macrophages. *Therapeutic Delivery* 7(4), 213-228 (2016).

83. Mantovani A, Sozzani S, Locati M, Allavena P, Sica A: Macrophage polarization: Tumor-associated macrophages as a paradigm for polarized M2 mononuclear phagocytes. *Trends Immunol.* 23(11), 549-555 (2002).

84. Balkwill F, Mantovani A: Inflammation and cancer: Back to Virchow? *Lancet* 357(9255), 539-545 (2001).

85. Gordon S: Alternative activation of macrophages. *Nature Reviews Immunology* 3(1), 23-35 (2003).

86. Griffiths G, Nystrom B, Sable SB, Khuller GK: Nanobead-based interventions for the treatment and prevention of tuberculosis. *Nat. Rev. Microbiol.* 8(11), 827-834 (2010).

87. Hirota K, Hasegawa T, Nakajima T *et al.*: Delivery of rifampicin-PLGA microspheres into alveolar macrophages is promising for treatment of tuberculosis. *J. Control. Release* 142(3), 339-346 (2010).

88. Ahmad Z, Sharma S, Khuller GK: Chemotherapeutic evaluation of alginate nanoparticle-encapsulated azole antifungal and antitubercular drugs against murine tuberculosis. *Nanomedicine* 3(3), 239-243 (2007).

89. Oganesian EA, Bud'ko AP, Stukalov I *et al.*: Development and estimation of nanosomal rifampicin. *Antibiot. Khimioter.* 50(8-9), 15-19 (2005).

90. Saraogi GK, Gupta P, Gupta UD, Jain NK, Agrawal GP: Gelatin nanocarriers as potential vectors for effective management of tuberculosis. *Int. J. Pharm.* 385(1-2), 143-149 (2010).

91. Nimje N, Agarwal A, Saraogi GK *et al.*: Mannosylated nanoparticulate carriers of rifabutin for alveolar targeting. *J. Drug Target.* 17(10), 777-787 (2009).

92. McKee CM, Penno MB, Cowman M *et al.*: Hyaluronan (HA) fragments induce chemokine gene expression in alveolar macrophages. The role of HA size and CD44. *J. Clin. Invest.* 98(10), 2403-2413 (1996).

93. Katoh S, Miyagi T, Taniguchi H *et al.*: Cutting edge: an inducible sialidase regulates the hyaluronic acid binding ability of CD44-bearing human monocytes. *J. Immunol.* 162(9), 5058-5061 (1999).

94. Leemans JC, Florquin S, Heikens M, Pals ST, van der Neut R, Van Der Poll T: CD44 is a macrophage binding site for Mycobacterium tuberculosis that mediates macrophage recruitment and protective immunity against tuberculosis. *J. Clin. Invest.* 111(5), 681-689 (2003).

95. Won,Young-Wook, Yoon,Sun-Mi, Sonn C,Hee, Lee,Kyung-Mi, Kim,Yong-Hee: Nano Self-Assembly of Recombinant Human Gelatin Conjugated with α-Tocopheryl Succinate for Hsp90 Inhibitor, 17-AAG, Delivery. *ACS Nano* 5(5), 3839-3848 (2011).

96. Yang C, Tan JPK, Cheng W *et al.*: Supramolecular nanostructures designed for high cargo loading capacity and kinetic stability. *Nano Today* 5(6), 515-523 (2010).

97. Onoshita T, Shimizu Y, Yamaya N *et al.*: The behavior of PLGA microspheres containing rifampicin in alveolar macrophages. *Colloids Surf. B Biointerfaces* 76(1), 151-157 (2010).

98. Gao Y, Zuo J, Bou-Chacra N *et al.*: In vitro release kinetics of antituberculosis drugs from nanoparticles assessed using a modified dissolution apparatus. *Biomed. Res. Int.* 1, 1-9 (2013).

99. Esmaeili F, Hosseini-Nasr M, Rad-Malekshahi M, Samadi N, Atyabi F, Dinarvand R: Preparation and antibacterial activity evaluation of rifampicin-loaded poly lactide-co-glycolide nanoparticles. *Nanomedicine: Nanotechnology, Biology and Medicine* 3(2), 161-167 (2007).

100. Schneider A, Picart C, Senger B, Schaaf P, Voegel JC, Frisch B: Layer-by-layer films from hyaluronan and amine-modified hyaluronan. *Langmuir* 23(5), 2655-2662 (2007).

101. Noh SM, Han SE, Shim G *et al.*: Tocopheryl oligochitosan-based self assembling oligomersomes for siRNA delivery. *Biomaterials* 32(3), 849-857 (2011).

102. Choi KY, Min KH, Yoon HY *et al.*: PEGylation of hyaluronic acid nanoparticles improves tumor targetability in vivo. *Biomaterials* 32(7), 1880-1889 (2011).

103. Min GK, Bevan MA, Prieve DC, Patterson GD: Light scattering characterization of polystyrene latex with and without adsorbed polymer. *Colloids Surf. Physicochem. Eng. Aspects* 202(1), 9-21 (2002).

104. Ito T, Sun L, Bevan MA, Crooks RM: Comparison of nanoparticle size and electrophoretic mobility measurements using a carbon-nanotube-based coulter counter, dynamic light scattering, transmission electron microscopy, and phase analysis light scattering. *Langmuir* 20(16), 6940-6945 (2004).

105. Nimje N, Agarwal A, Saraogi GK *et al.*: Mannosylated nanoparticulate carriers of rifabutin for alveolar targeting. *J. Drug Target.* 17(10), 777-787 (2009).

106. Kumar PV, Agashe H, Dutta T, Jain NK: PEGylated dendritic architecture for development of a prolonged drug delivery system for an antitubercular drug. *Curr. Drug Deliv.* 4(1), 11-19 (2007).

107. Agrawal S, Panchagnula R: Implication of biopharmaceutics and pharmacokinetics of rifampicin in variable bioavailability from solid oral dosage forms. *Biopharm. Drug Dispos.* 26(8), 321-334 (2005).

108. Philips JA, Ernst JD: Tuberculosis pathogenesis and immunity. *Annu. Rev. Pathol.* 7, 353-384 (2012).

109. Flynn JL, Chan J: Immunology of tuberculosis. *Annu. Rev. Immunol.* 19, 93-129 (2001).

110. Flesch IE, Hess JH, Oswald IP, Kaufmann SH: Growth inhibition of Mycobacterium bovis by IFN-gamma stimulated macrophages: regulation by endogenous tumor necrosis factor-alpha and by IL-10. *Int. Immunol.* 6(5), 693-700 (1994).

111. Fenton MJ, Vermeulen MW, Kim S, Burdick M, Strieter RM, Kornfeld H: Induction of gamma interferon production in human alveolar macrophages by Mycobacterium tuberculosis. *Infect. Immun.* 65(12), 5149-5156 (1997).

112. Mayer-Barber KD, Barber DL, Shenderov K *et al.*: Caspase-1 independent IL-1beta production is critical for host resistance to mycobacterium tuberculosis and does not require TLR signaling in vivo. *J. Immunol.* 184(7), 3326-3330 (2010).

113. Opal SM, DePalo VA: Anti-inflammatory cytokines. *Chest* 117(4), 1162-1172 (2000).

114. Fulton SA, Cross JV, Toossi ZT, Boom WH: Regulation of interleukin-12 by interleukin-10, transforming growth factor-beta, tumor necrosis factor-alpha, and interferon-gamma in human monocytes infected with Mycobacterium tuberculosis H37Ra. *J. Infect. Dis.* 178(4), 1105-1114 (1998).

115. Redford PS, Murray PJ, O'Garra A: The role of IL-10 in immune regulation during M. tuberculosis infection. *Mucosal Immunol.* 4(3), 261-270 (2011).

116. Rojas RE, Balaji KN, Subramanian A, Boom WH: Regulation of Human CD4+αβ T-Cell-Receptor-Positive (TCR+) and γδ TCR+ T-Cell Responses to*Mycobacterium tuberculosis* by Interleukin-10 and Transforming Growth Factor β. Kaufmann SHE, ed. *Infection and Immunity* 67(12), 6461-6472 (1999).

117. O'Leary S, O'Sullivan MP, Keane J: IL-10 blocks phagosome maturation in mycobacterium tuberculosis-infected human macrophages. *Am. J. Respir. Cell Mol. Biol.* 45(1), 172-180 (2011).

118. Jones B, Chen J: Inhibition of IFN-gamma transcription by site-specific methylation during T helper cell development. *EMBO J.* 25(11), 2443-2452 (2006).

119. Kapuscinski J: DAPI: a DNA-specific fluorescent probe. *Biotech. Histochem.* 70(5), 220-233 (1995).

120. Belitsos PC, Hildreth JE, August JT: Homotypic cell aggregation induced by anti-CD44(Pgp-1) monoclonal antibodies and related to CD44(Pgp-1) expression. *J. Immunol.* 144(5), 1661-1670 (1990).

121. Schrijvers DM, Martinet W, De Meyer GR, Andries L, Herman AG, Kockx MM: Flow cytometric evaluation of a model for phagocytosis of cells undergoing apoptosis. *J. Immunol. Methods* 287(1-2), 101-108 (2004).

122. Hillaireau H, Couvreur P: Nanocarriers' entry into the cell: relevance to drug delivery. *Cell Mol. Life Sci.* 66(17), 2873-2896 (2009).

123. Zaki NM, Nasti A, Tirelli N: Nanocarriers for cytoplasmic delivery: cellular uptake and intracellular fate of chitosan and hyaluronic acid-coated chitosan nanoparticles in a phagocytic cell model. *Macromol. Biosci.* 11(12), 1747-1760 (2011).

124. Mosmann TR, Cherwinski H, Bond MW, Giedlin MA, Coffman RL: Two types of murine helper T cell clone. I. Definition according to profiles of lymphokine activities and secreted proteins. *J. Immunol.* 136(7), 2348-2357 (1986).

125. van Crevel R, Ottenhoff TH, van der Meer JW: Innate immunity to Mycobacterium tuberculosis. *Clin. Microbiol. Rev.* 15(2), 294-309 (2002).

126. Qhattal HS, Liu X: Characterization of CD44-mediated cancer cell uptake and intracellular distribution of hyaluronan-grafted liposomes. *Mol. Pharm.* 8(4), 1233-1246 (2011).

127. Champion JA, Walker A, Mitragotri S: Role of particle size in phagocytosis of polymeric microspheres. *Pharm. Res.* 25(8), 1815-1821 (2008).

128. Akagi T, Shima F, Akashi M: Intracellular degradation and distribution of protein-encapsulated amphiphilic poly(amino acid) nanoparticles. *Biomaterials* 32(21), 4959-4967 (2011).

129. Kamat M, El-Boubbou K, Zhu DC *et al.*: Hyaluronic acid immobilized magnetic nanoparticles for active targeting and imaging of macrophages. *Bioconjug. Chem.* 21(11), 2128-2135 (2010).

130. Muto J, Yamasaki K, Taylor KR, Gallo RL: Engagement of CD44 by hyaluronan suppresses TLR4 signaling and the septic response to LPS. *Mol. Immunol.* 47(2-3), 449-456 (2009).

131. Craig EA, Parker P, Camenisch TD: Size-dependent regulation of Snail2 by

hyaluronan: its role in cellular invasion. *Glycobiology* 19(8), 890-898 (2009).

132. Gee K, Lim W, Ma W *et al.*: Differential regulation of CD44 expression by lipopolysaccharide (LPS) and TNF-alpha in human monocytic cells: distinct involvement of c-Jun N-terminal kinase in LPS-induced CD44 expression. *J. Immunol.* 169(10), 5660-5672 (2002).

133. Sharma R, Muttil P, Yadav AB *et al.*: Uptake of inhalable microparticles affects defence responses of macrophages infected with Mycobacterium tuberculosis H37Ra. *J. Antimicrob. Chemother.* 59(3), 499-506 (2007).

134. Elzoghby AO, Samy WM, Elgindy NA: Albumin-based nanoparticles as potential controlled release drug delivery systems. *J. Controlled Release* 157(2), 168-182 (2012).

135. Kanapathipillai M, Brock A, Ingber DE: Nanoparticle targeting of anti-cancer drugs that alter intracellular signaling or influence the tumor microenvironment. *Adv. Drug Deliv. Rev.* 79–80, 107-118 (2014).

136. Roa WH, Azarmi S, Al-Hallak MH, Finlay WH, Magliocco AM, Lobenberg R: Inhalable nanoparticles, a non-invasive approach to treat lung cancer in a mouse model. *J. Control. Release* 150(1), 49-55 (2011).

137. Illum L, Davis SS, Muller RH, Mak E, West P: The organ distribution and circulation time of intravenously injected colloidal carriers sterically stabilized with a block copolymer--poloxamine 908. *Life Sci.* 40(4), 367-374 (1987).

138. Bazile DV, Ropert C, Huve P *et al.*: Body distribution of fully biodegradable [14C]-poly(lactic acid) nanoparticles coated with albumin after parenteral administration to rats. *Biomaterials* 13(15), 1093-1102 (1992).

139. Löbenberg R, Kreuter J: Macrophage targeting of azidothymidine: a promising strategy for AIDS therapy. *AIDS Res. Hum. Retroviruses* 12(18), 1709-1715 (1996).

140. Lee WH, Loo CY, Traini D, Young PM: Nano- and micro-based inhaled drug delivery systems for targeting alveolar macrophages. *Expert Opin. Drug Deliv.* 12(6), 1009-1026 (2015).

141. Kumar A, Abbas W, Herbein G: HIV-1 latency in monocytes/macrophages. *Viruses* 6(4), 1837-1860 (2014).

142. Kaye P, Scott P: Leishmaniasis: complexity at the host-pathogen interface. *Nat. Rev. Microbiol.* 9(8), 604-615 (2011).

143. Slagle T, Ben Youssef M, Calonge G, Ben Amor Y: Lessons from Africa: developing a global human rights framework for tuberculosis control and prevention. *BMC Int. Health. Hum. Rights* 14, 34-014-0034-7 (2014).

144. Jacobs M, Samarina A, Grivennikov S *et al.*: Reactivation of tuberculosis by tumor necrosis factor neutralization. *Eur. Cytokine Netw.* 18(1), 5-13 (2007).

145. Quesniaux VF, Jacobs M, Allie N *et al.*: TNF in host resistance to tuberculosis infection. *Curr. Dir. Autoimmun.* 11, 157-179 (2010).

146. Chan J, Flynn J: The immunological aspects of latency in tuberculosis. *Clin. Immunol.* 110(1), 2-12 (2004).

147. Flynn JL, Goldstein MM, Chan J *et al.*: Tumor necrosis factor-α is required in the protective immune response against mycobacterium tuberculosis in mice. *Immunity* 2(6), 561-572

(1995).

148. O'Leary S, O'Sullivan MP, Keane J: IL-10 blocks phagosome maturation in mycobacterium tuberculosis-infected human macrophages. *Am. J. Respir. Cell Mol. Biol.* 45(1), 172-180 (2011).

149. Law K, Weiden M, Harkin T, Tchou-Wong K, Chi C, Rom WN: Increased release of interleukin-1 beta, interleukin-6, and tumor necrosis factor-alpha by bronchoalveolar cells lavaged from involved sites in pulmonary tuberculosis. *Am. J. Respir. Crit. Care Med.* 153(2), 799-804 (1996).

150. Balcewicz-Sablinska MK, Keane J, Kornfeld H, Remold HG: Pathogenic Mycobacterium tuberculosis evades apoptosis of host macrophages by release of TNF-R2, resulting in inactivation of TNF-alpha. *J. Immunol.* 161(5), 2636-2641 (1998).

151. Kaneko H, Yamada H, Mizuno S *et al.*: Role of tumor necrosis factor-alpha in Mycobacterium-induced granuloma formation in tumor necrosis factor-alpha-deficient mice. *Lab. Invest.* 79(4), 379-386 (1999).

152. Keane J, Gershon S, Wise RP *et al.*: Tuberculosis associated with infliximab, a tumor necrosis factor alpha-neutralizing agent. *N. Engl. J. Med.* 345(15), 1098-1104 (2001).

153. Miller BH, Fratti RA, Poschet JF *et al.*: Mycobacteria inhibit nitric oxide synthase recruitment to phagosomes during macrophage infection. *Infect. Immun.* 72(5), 2872-2878 (2004).

154. Liu W, Peng Y, Yin Y, Zhou Z, Zhou W, Dai Y: The involvement of NADPH oxidase-mediated ROS in cytokine secretion from macrophages induced by Mycobacterium tuberculosis ESAT-6. *Inflammation* 37(3), 880-892 (2014).

155. Zanetti M: The role of cathelicidins in the innate host defenses of mammals. *Curr. Issues Mol. Biol.* 7(2), 179-196 (2005).

156. Bhatt K, Salgame P: Host innate immune response to Mycobacterium tuberculosis. *J. Clin. Immunol.* 27(4), 347-362 (2007).

157. Moyano DF, Goldsmith M, Solfiell DJ *et al.*: Nanoparticle hydrophobicity dictates immune response. *J. Am. Chem. Soc.* 134(9), 3965-3967 (2012).

158. Coester CJ, Langer K, van Briesen H, Kreuter J: Gelatin nanoparticles by two step desolvation--a new preparation method, surface modifications and cell uptake. *J. Microencapsul.* 17(2), 187-193 (2000).

159. Azarmi S, Huang Y, Chen H *et al.*: Optimization of a two-step desolvation method for preparing gelatin nanoparticles and cell uptake studies in 143B osteosarcoma cancer cells. *J. Pharm. Pharm. Sci.* 9(1), 124-132 (2006).

160. Couvreur P: Polyalkylcyanoacrylates as colloidal drug carriers. *Crit. Rev. Ther. Drug Carrier Syst.* 5(1), 1-20 (1988).

161. Douglas SJ, Illum L, Davis SS: Particle size and size distribution of poly(butyl 2-cyanoacrylate) nanoparticles. II. Influence of stabilizers. *J. Colloid Interface Sci.* 103(1), 154-163 (1985).

162. Azarmi S, Tao X, Chen H *et al.*: Formulation and cytotoxicity of doxorubicin nanoparticles carried by dry powder aerosol particles. *Int. J. Pharm.* 319(1–2), 155-161 (2006).

163. Kisich KO, Gelperina S, Higgins MP *et al.*: Encapsulation of moxifloxacin within poly(butyl cyanoacrylate) nanoparticles enhances efficacy against intracellular Mycobacterium tuberculosis. *Int. J. Pharm.* 345(1-2), 154-162 (2007).

164. Pramod. P. Dahibhate, O.D. Chandwani, S.S. Kadam. S.R. Dhaneshwar: Simultaneous spectrophotometric estimation of rifampicin, Isoniazide and pyrazinamide from combined dosage forms. *Indian Drugs* 34(2), 95-98 (1997).

165. Motwani SK, Chopra S, Ahmad FJ, Khar RK: Validated spectrophotometric methods for the estimation of moxifloxacin in bulk and pharmaceutical formulations. *Spectrochim. Acta A Mol. Biomol. Spectrosc.* 68(2), 250-256 (2007).

166. Zuo J, Gao Y, Bou-Chacra N, Lobenberg R: Evaluation of the DDSolver software applications. *Biomed. Res. Int.* 1, 1-9 (2014).

167. Zhang Y, Huo M, Zhou J *et al.*: DDSolver: an add-in program for modeling and comparison of drug dissolution profiles. *AAPS J.* 12(3), 263-271 (2010).

168. Lai P, Daear W, Löbenberg R, Prenner EJ: Overview of the preparation of organic polymeric nanoparticles for drug delivery based on gelatine, chitosan, poly(d,l-lactide-co-glycolic acid) and polyalkylcyanoacrylate. *Colloids Surf. B Biointerfaces* 118, 154-163 (2014).

169. Elzoghby AO: Gelatin-based nanoparticles as drug and gene delivery systems: Reviewing three decades of research. *J. Controlled Release* 172(3), 1075-1091 (2013).

170. Sahoo N, Sahoo RK, Biswas N, Guha A, Kuotsu K: Recent advancement of gelatin nanoparticles in drug and vaccine delivery. *Int. J. Biol. Macromol.* 81, 317-331 (2015).

171. Sham JO-, Zhang Y, Finlay WH, Roa WH, Löbenberg R: Formulation and characterization of spray-dried powders containing nanoparticles for aerosol delivery to the lung. *Int. J. Pharm.* 269(2), 457-467 (2004).

172. Zhao N, Zhang H, Wang Y: Preparation and in vitro release of moxifloxacin polybutylcyanoacrylate nanopart icles. *Chin Hosp Pharm J* 29(10), 808-811 (2009).

173. Clift MJ, Rothen-Rutishauser B, Brown DM *et al.*: The impact of different nanoparticle surface chemistry and size on uptake and toxicity in a murine macrophage cell line. *Toxicol. Appl. Pharmacol.* 232(3), 418-427 (2008).

174. Lherm C, Müller RH, Puisieux F, Couvreur P: Alkylcyanoacrylate drug carriers: II. Cytotoxicity of cyanoacrylate nanoparticles with different alkyl chain length. *Int. J. Pharm.* 84(1), 13-22 (1992).

175. Heidland A, Klassen A, Rutkowski P, Bahner U: The contribution of Rudolf Virchow to the concept of inflammation: what is still of importance? *J. Nephrol.* 19 Suppl 10, S102-9 (2006).

176. Coussens LM, Werb Z: Inflammation and cancer. *Nature* 420(6917), 860-867 (2002).

177. Mantovani A, Allavena P, Sica A, Balkwill F: Cancer-related inflammation. *Nature* 454(7203), 436-444 (2008).

178. Medzhitov R, Janeway Jr CA: Innate immune recognition and control of adaptive immune responses. *Semin. Immunol.* 10(5), 351-353 (1998).

179. Matzinger P: Friendly and dangerous signals: is the tissue in control? *Nat. Immunol.*

8(1), 11-13 (2007).

180. Gonzalez-Mejia ME, Doseff AI: Regulation of monocytes and macrophages cell fate. *Front. Biosci. (Landmark Ed)* 14, 2413-2431 (2009).

181. Iwasaki A, Medzhitov R: Regulation of adaptive immunity by the innate immune system. *Science* 327(5963), 291-295 (2010).

182. Gajewski TF, Schreiber H, Fu YX: Innate and adaptive immune cells in the tumor microenvironment. *Nat. Immunol.* 14(10), 1014-1022 (2013).

183. Ino Y, Yamazaki-Itoh R, Shimada K *et al.*: Immune cell infiltration as an indicator of the immune microenvironment of pancreatic cancer. *Br. J. Cancer* 108(4), 914-923 (2013).

184. Mills CD, Kincaid K, Alt JM, Heilman MJ, Hill AM: M-1/M-2 macrophages and the Th1/Th2 paradigm. *J. Immunol.* 164(12), 6166-6173 (2000).

185. Sica A, Larghi P, Mancino A *et al.*: Macrophage polarization in tumour progression. *Semin. Cancer Biol.* 18(5), 349-355 (2008).

186. Lee PP, Zeng D, McCaulay AE *et al.*: T helper 2-dominant antilymphoma immune response is associated with fatal outcome. *Blood* 90(4), 1611-1617 (1997).

187. Dinarello CA: Historical insights into cytokines. *Eur. J. Immunol.* 37 Suppl 1, S34-45 (2007).

188. Mantovani A, Sica A: Macrophages, innate immunity and cancer: balance, tolerance, and diversity. *Curr. Opin. Immunol.* 22(2), 231-237 (2010).

189. Coussens LM, Zitvogel L, Palucka AK: Neutralizing tumor-promoting chronic inflammation: a magic bullet? *Science* 339(6117), 286-291 (2013).

190. Quail DF, Joyce JA: Microenvironmental regulation of tumor progression and metastasis. *Nat. Med.* 19(11), 1423-1437 (2013).

191. Strachan DC, Ruffell B, Oei Y *et al.*: CSF1R inhibition delays cervical and mammary tumor growth in murine models by attenuating the turnover of tumor-associated macrophages and enhancing infiltration by CD8 T cells. *Oncoimmunology* 2(12), 926-968 (2013).

192. Yao M, Zhou W, Sangha S *et al.*: Effects of nonselective cyclooxygenase inhibition with low-dose ibuprofen on tumor growth, angiogenesis, metastasis, and survival in a mouse model of colorectal cancer. *Clin. Cancer Res.* 11(4), 1618-1628 (2005).

193. Nakanishi Y, Nakatsuji M, Seno H *et al.*: COX-2 inhibition alters the phenotype of tumor-associated macrophages from M2 to M1 in ApcMin/+ mouse polyps. *Carcinogenesis* 32(9), 1333-1339 (2011).

194. Arun B, Goss P: The role of COX-2 inhibition in breast cancer treatment and prevention. *Semin. Oncol.* 31, Supplement 7, 22-29 (2004).

195. Kato M, Goto S, Soma G: Lymphokine-activated killer cell therapy combined with high-dose glucocorticoid showed clinical efficacy towards advanced lung carcinoma. *Anticancer Res.* 30(8), 3125-3128 (2010).

196. Naito M, Itoh K, Komatsu N *et al.*: Dexamethasone did not suppress immune boosting by personalized peptide vaccination for advanced prostate cancer patients. *Prostate* 68(16), 1753-1762 (2008).

197. Dorff TB, Crawford ED: Management and challenges of corticosteroid therapy in men with metastatic castrate-resistant prostate cancer. *Ann. Oncol.* 24(1), 31-38 (2013).

198. Cronstein B: How does methotrexate suppress inflammation? *Clin. Exp. Rheumatol.* 28(5 Suppl 61), S21-3 (2010).

199. Stevenson R, Hueber AJ, Hutton A, McInnes IB, Graham D: Nanoparticles and inflammation. *ScientificWorldJournal* 11, 1300-1312 (2011).

200. Jacobsen NR, Moller P, Jensen KA *et al.*: Lung inflammation and genotoxicity following pulmonary exposure to nanoparticles in ApoE-/- mice. *Part Fibre Toxicol.* 6, 2-8977-6-2 (2009).

201. Zolnik BS, González-Fernández Á, Sadrieh N, Dobrovolskaia MA: Minireview: Nanoparticles and the Immune System. *Endocrinology* 151(2), 458-465 (2010).

202. Syed S, Zubair A, Frieri M: Immune response to nanomaterials: implications for medicine and literature review. *Curr. Allergy Asthma Rep.* 13(1), 50-57 (2013).

203. Szeto GL, Lavik EB: Materials design at the interface of nanoparticles and innate immunity. *J. Mater. Chem. B* 4(9), 1610-1618 (2016).

204. Baselga J: The EGFR as a target for anticancer therapy focus on cetuximab. *Eur. J. Cancer* 37 Suppl 4, S16-22 (2001).

205. Saleh M, Trinchieri G: Innate immune mechanisms of colitis and colitis-associated colorectal cancer. *Nat. Rev. Immunol.* 11(1), 9-20 (2011).

206. Endo H, Yano M, Okumura Y, Kido H: Ibuprofen enhances the anticancer activity of cisplatin in lung cancer cells by inhibiting the heat shock protein 70. *Cell. Death Dis.* 5, e1027 (2014).

207. Liu DB, Hu GY, Long GX, Qiu H, Mei Q, Hu GQ: Celecoxib induces apoptosis and cell-cycle arrest in nasopharyngeal carcinoma cell lines via inhibition of STAT3 phosphorylation. *Acta Pharmacol. Sin.* 33(5), 682-690 (2012).

208. Franchimont D, Louis E, Dewe W *et al.*: Effects of dexamethasone on the profile of cytokine secretion in human whole blood cell cultures. *Regul. Pept.* 73(1), 59-65 (1998).

209. Borger P, Kauffman HF, Timmerman JA, Scholma J, van den Berg JW, Koeter GH: Cyclosporine, FK506, mycophenolate mofetil, and prednisolone differentially modulate cytokine gene expression in human airway-derived epithelial cells. *Transplantation* 69(7), 1408-1413 (2000).

210. Genestier L, Paillot R, Fournel S, Ferraro C, Miossec P, Revillard JP: Immunosuppressive properties of methotrexate: apoptosis and clonal deletion of activated peripheral T cells. *J. Clin. Invest.* 102(2), 322-328 (1998).

211. Harivardhan-Reddy L, Murthy R: Study of influence of polymerization factors on formation of poly (butyl cyanoacrylate) nanoparticles and in vitro drug release kinetics. *Ars Pharmaceutica* 45(3), 211-234 (2004).

212. Saraogi GK, Gupta P, Gupta UD, Jain NK, Agrawal GP: Gelatin nanocarriers as potential vectors for effective management of tuberculosis. *Int. J. Pharm.* 385(1–2), 143-149 (2010).

213. Eliopoulos AG, Dumitru CD, Wang CC, Cho J, Tsichlis PN: Induction of COX-2 by LPS in macrophages is regulated by Tpl2-dependent CREB activation signals. *EMBO J.* 21(18), 4831-4840 (2002).

214. Lee SH, Soyoola E, Chanmugam P *et al.*: Selective expression of mitogen-inducible cyclooxygenase in macrophages stimulated with lipopolysaccharide. *J. Biol. Chem.* 267(36), 25934-25938 (1992).

215. Vane J, Botting R: Inflammation and the mechanism of action of anti-inflammatory drugs. *FASEB J.* 1(2), 89-96 (1987).

216. Mao JT, Roth MD, Serio KJ *et al.*: Celecoxib modulates the capacity for prostaglandin E2 and interleukin-10 production in alveolar macrophages from active smokers. *Clin. Cancer Res.* 9(16 Pt 1), 5835-5841 (2003).

217. Kisley LR, Barrett BS, Dwyer-Nield LD, Bauer AK, Thompson DC, Malkinson AM: Celecoxib reduces pulmonary inflammation but not lung tumorigenesis in mice. *Carcinogenesis* 23(10), 1653-1660 (2002).

218. Liu X, Yue P, Zhou Z, Khuri FR, Sun SY: Death receptor regulation and celecoxib-induced apoptosis in human lung cancer cells. *J. Natl. Cancer Inst.* 96(23), 1769-1780 (2004).

219. Ehrchen J, Steinmuller L, Barczyk K *et al.*: Glucocorticoids induce differentiation of a specifically activated, anti-inflammatory subtype of human monocytes. *Blood* 109(3), 1265-1274 (2007).

220. Werb Z: Biochemical actions of glucocorticoids on macrophages in culture. Specific inhibition of elastase, collagenase, and plasminogen activator secretion and effects on other metabolic functions. *J. Exp. Med.* 147(6), 1695-1712 (1978).

221. Ichii S, Satoh Y, Izawa M, Iwasaki K: Stability of receptor complexes in the rat liver bound to glucocorticoids of different biopotencies. *Endocrinol. Jpn.* 31(5), 583-594 (1984).

222. Inaba H, Pui CH: Glucocorticoid use in acute lymphoblastic leukaemia. *Lancet Oncol.* 11(11), 1096-1106 (2010).

223. Cronstein BN: The mechanisim of action of methotrexate. *Rheumatic Disease Clinics of North America* 23(4), 739-755 (1997).

224. Constantin A, Loubet-Lescoulie P, Lambert N *et al.*: Antiinflammatory and immunoregulatory action of methotrexate in the treatment of rheumatoid arthritis: evidence of increased interleukin-4 and interleukin-10 gene expression demonstrated in vitro by competitive reverse transcriptase-polymerase chain reaction. *Arthritis Rheum.* 41(1), 48-57 (1998).

225. Balkwill F, Mantovani A: Inflammation and cancer: back to Virchow? *Lancet* 357(9255), 539-545 (2001).

226. Azarmi S, Roa WH, Löbenberg R: Targeted delivery of nanoparticles for the treatment of lung diseases. *Adv. Drug Deliv. Rev.* 60(8), 863-875 (2008).

227. Jain NK, Mishra V, Mehra NK: Targeted drug delivery to macrophages. *Expert Opin. Drug Deliv.* 10(3), 353-367 (2013).

228. Xu MM, Pu Y, Zhang Y, Fu YX: The Role of Adaptive Immunity in the Efficacy of Targeted Cancer Therapies. *Trends Immunol.* 37(2), 141-153 (2016).

229. Schafer V, von Briesen H, Andreesen R *et al.*: Phagocytosis of Nanoparticles by Human Immunodeficiency Virus (HlV)-Infected Macrophages: A Possibility for Antiviral Drug Targeting. *Pharm. Res.* 9(4), 541-546 (1992).

230. Chang SH, Liu CH, Conway R *et al.*: Role of prostaglandin E2-dependent angiogenic switch in cyclooxygenase 2-induced breast cancer progression. *Proc. Natl. Acad. Sci. U. S. A.* 101(2), 591-596 (2004).

231. Liu R, Xu KP, Tan GS: Cyclooxygenase-2 inhibitors in lung cancer treatment: Bench to bed. *Eur. J. Pharmacol.* 769, 127-133 (2015).

Appendix-I Cytokine and Chemokine release from MH-S cells, micelles vs LPS.

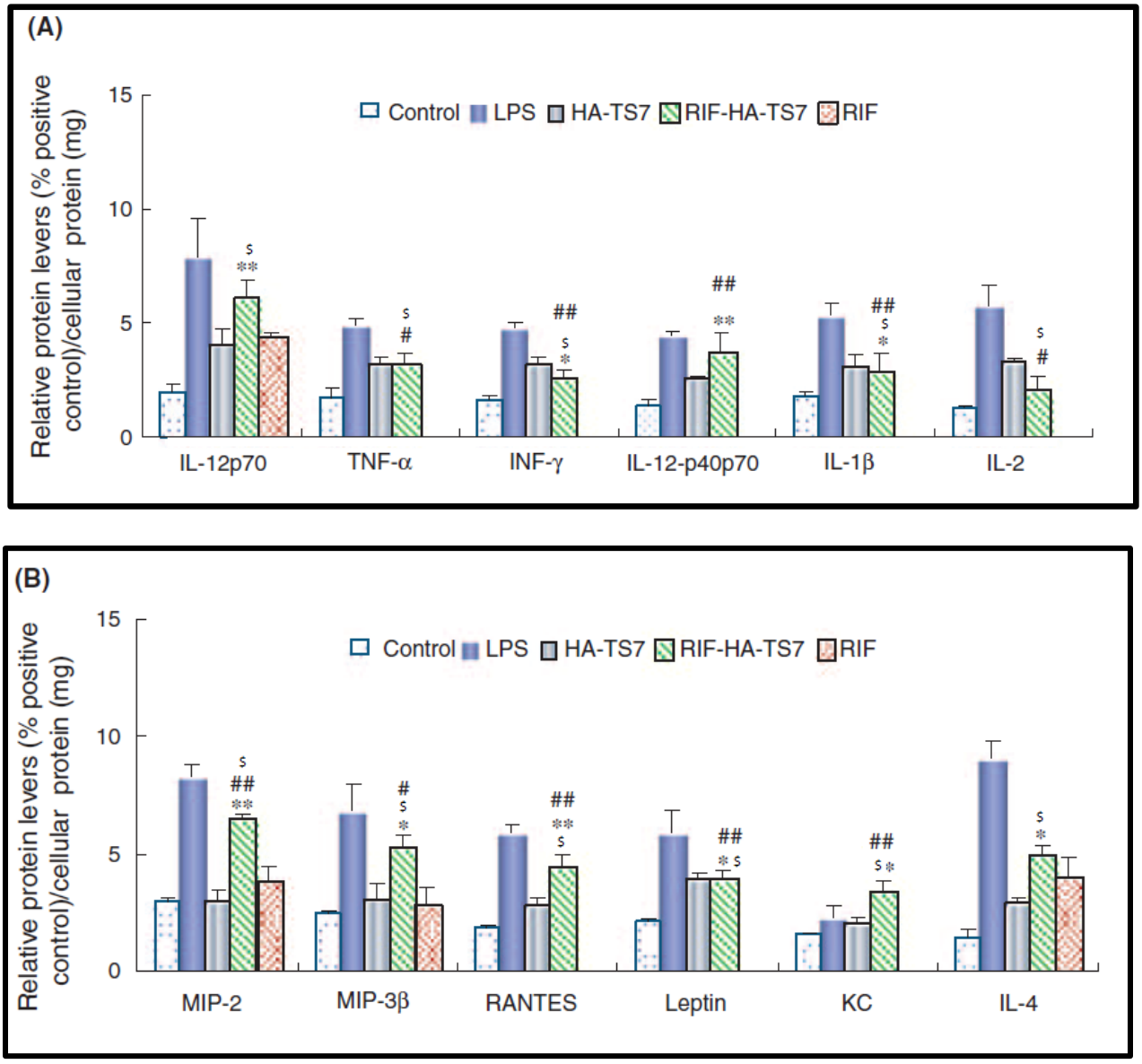

Figure (A-B): Cytokines and chemokines release from MH-S cells following exposure to LPS, blank HA-TS_7 micelles, RIF-HA-TS_7 micelles and free RIF solution, which was determined using the microarray at 6h. Untreated cells were used as a control. *Significant of RIF-HA-TS versus control, $ Significant of RIF-HA-TS versus LPS, # Significant of RIF-HA-TS vs. free RIF solution. **, ## $p < 0.01$, *, #, $ $p < 0.05$.

Appendix-II Effect on A-549 cell viability using different NPs sizes and treatments.

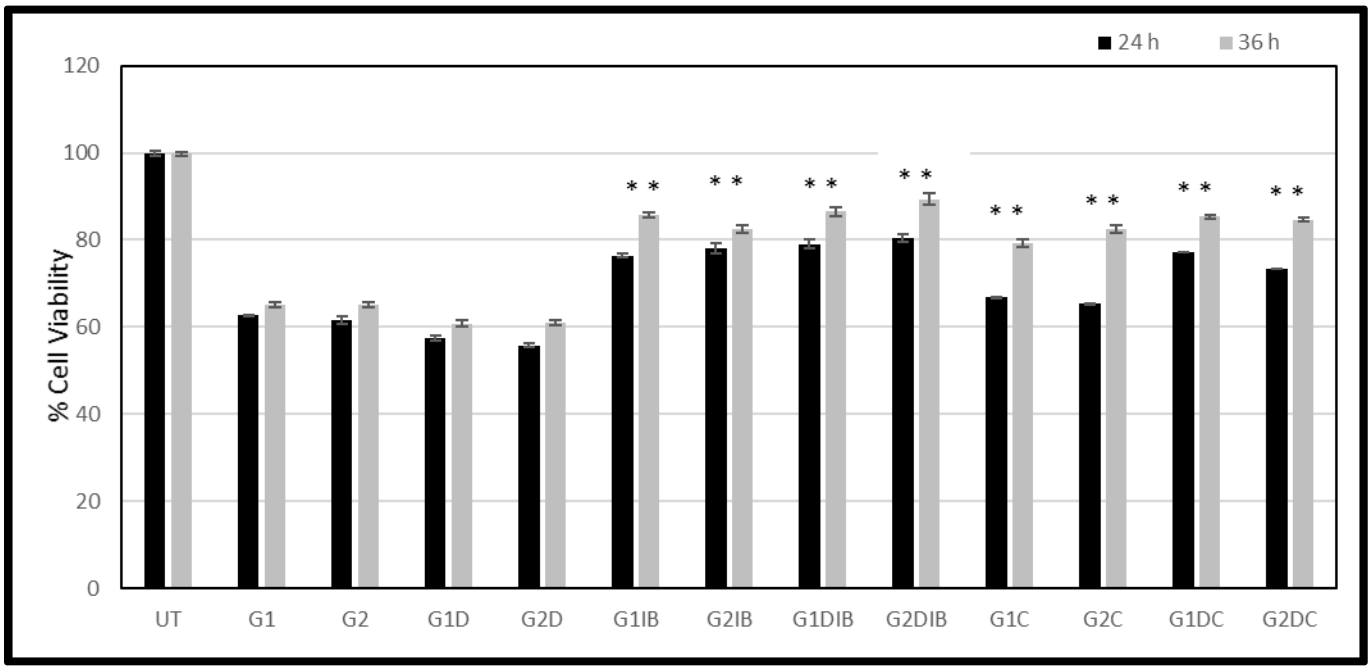

Figure 1: Comparison between the blank gelatin (G1, G2) and drug loaded gelatin nanoparticles (G1D, G2D) before and after treatment with Ibuprofen and Celecoxib and its effect on A-549 cell viability at 24 and 36 h. Data shown were the mean ± S.D. (n=3) *denotes that the treatment results were significantly different (* $p < 0.05$)

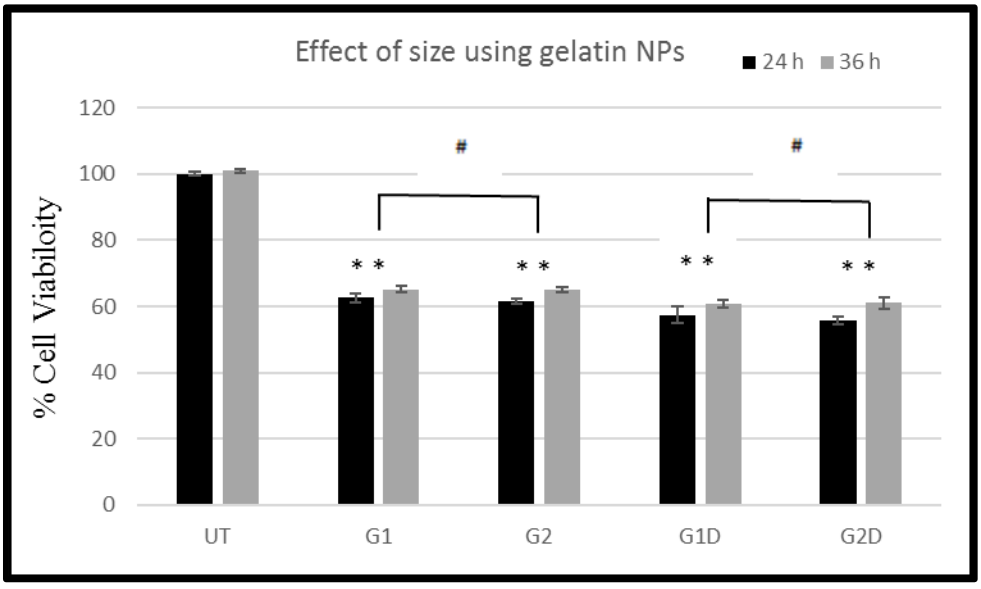

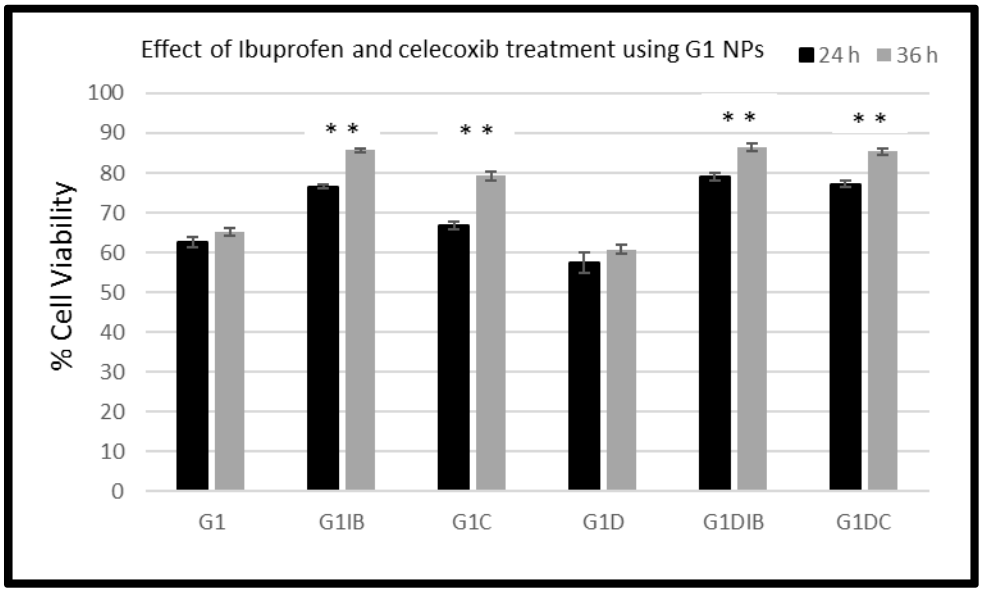
Effect of Ibuprofen and celecoxib treatment using G1 NPs
24 h
36 h
% Cell Viability
100
90
80
70
60
50
40
30
20
10
0
* *
* *
* *
* *
G1
G1IB
G1C
G1D
G1DIB
G1DC

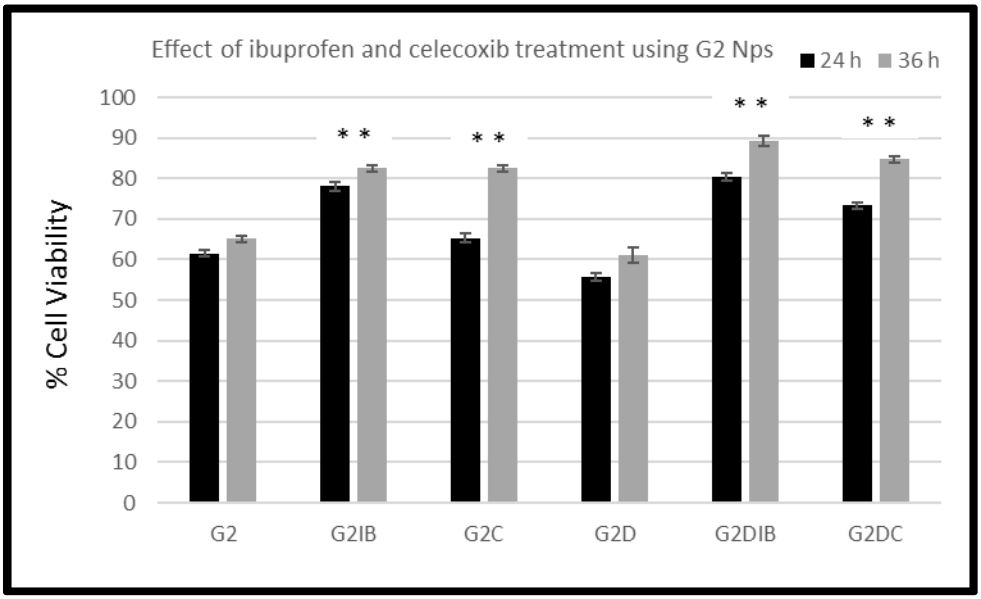
Effect of ibuprofen and celecoxib treatment using G2 Nps
24 h
36 h
% Cell Viability
100
90
80
70
60
50
40
30
20
10
0
* *
* *
* *
* *
G2
G2IB
G2C
G2D
G2DIB
G2DC

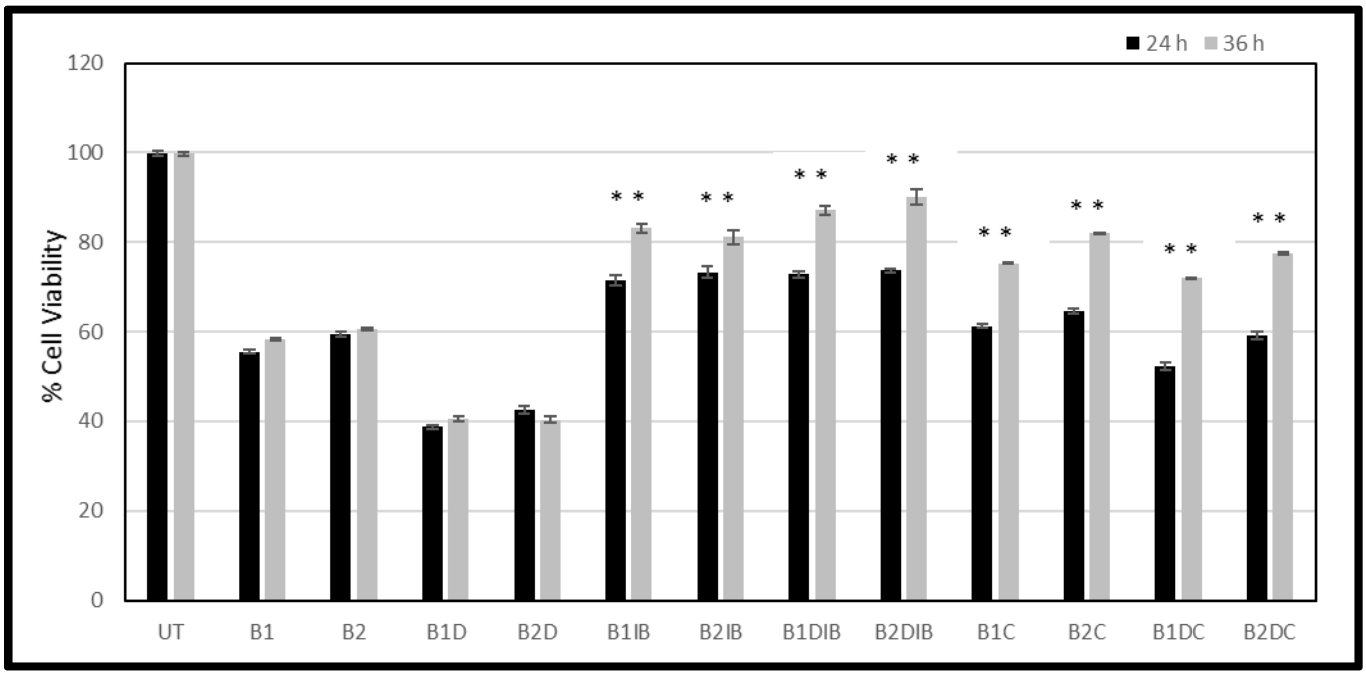

Figure 2: Comparison between the blank PIBCA (B1, B2) and drug loaded PIBCA nanoparticles (B1D, B2D) before and after treatment with Ibuprofen and Celecoxib and its effect on A-549 cell viability at 24 and 36 h. Data shown were the mean ± S.D. (n=3) *denotes that the treatment results were significantly different (* $p < 0.05$)

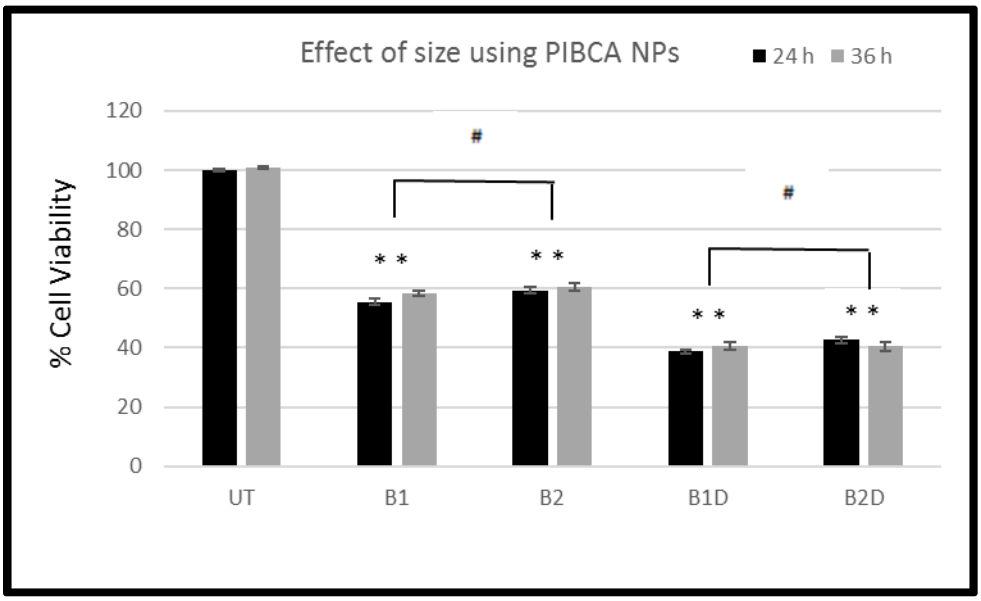

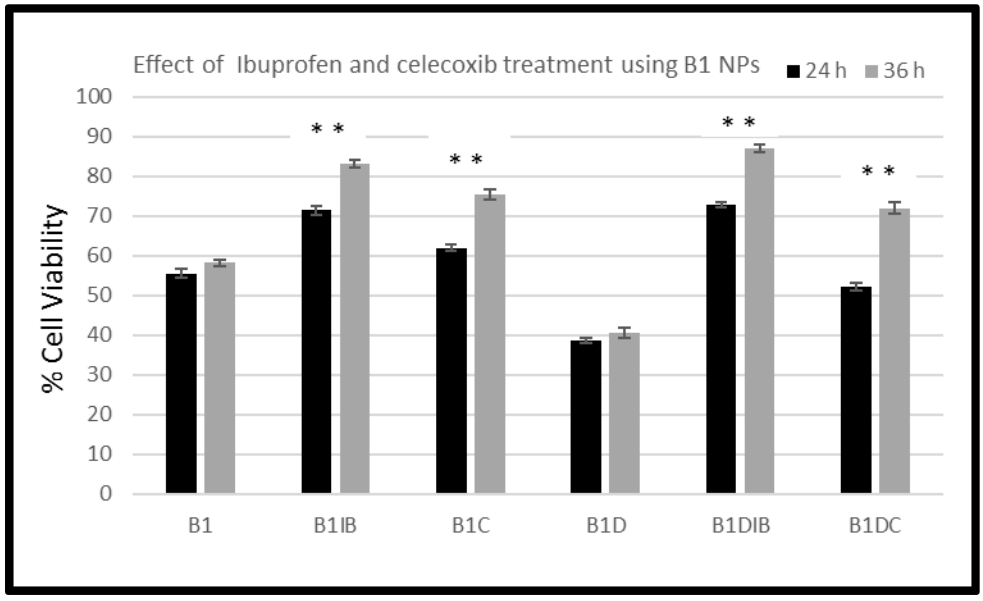
Effect of Ibuprofen and celecoxib treatment using B1 NPs
24 h
36 h
% Cell Viability
100
90
80
70
60
50
40
30
20
10
0
* *
* *
* *
* *
B1
B1IB
B1C
B1D
B1DIB
B1DC

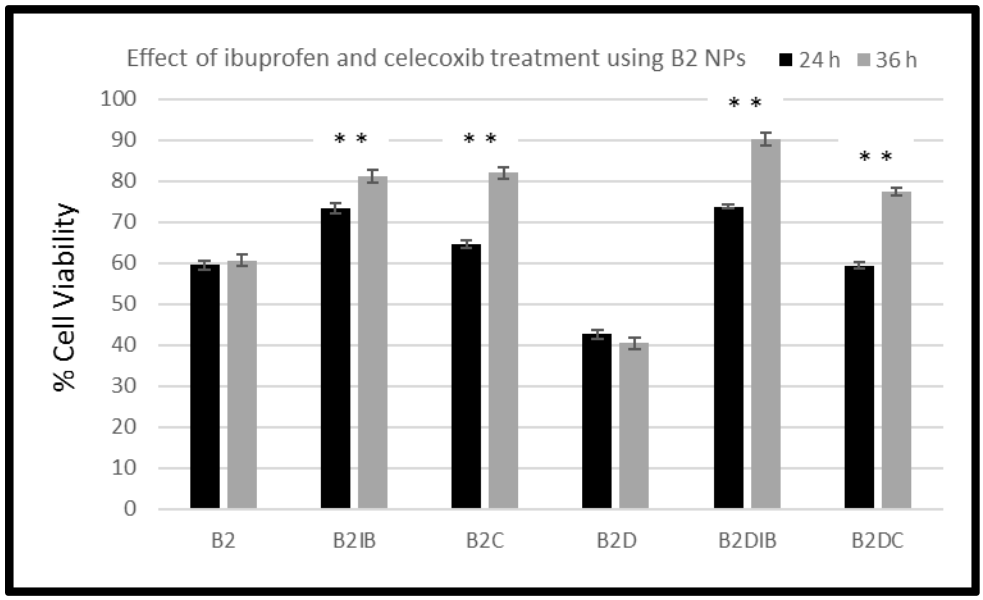
Effect of ibuprofen and celecoxib treatment using B2 NPs
24 h
36 h
% Cell Viability
100
90
80
70
60
50
40
30
20
10
0
* *
* *
* *
* *
B2
B2IB
B2C
B2D
B2DIB
B2DC

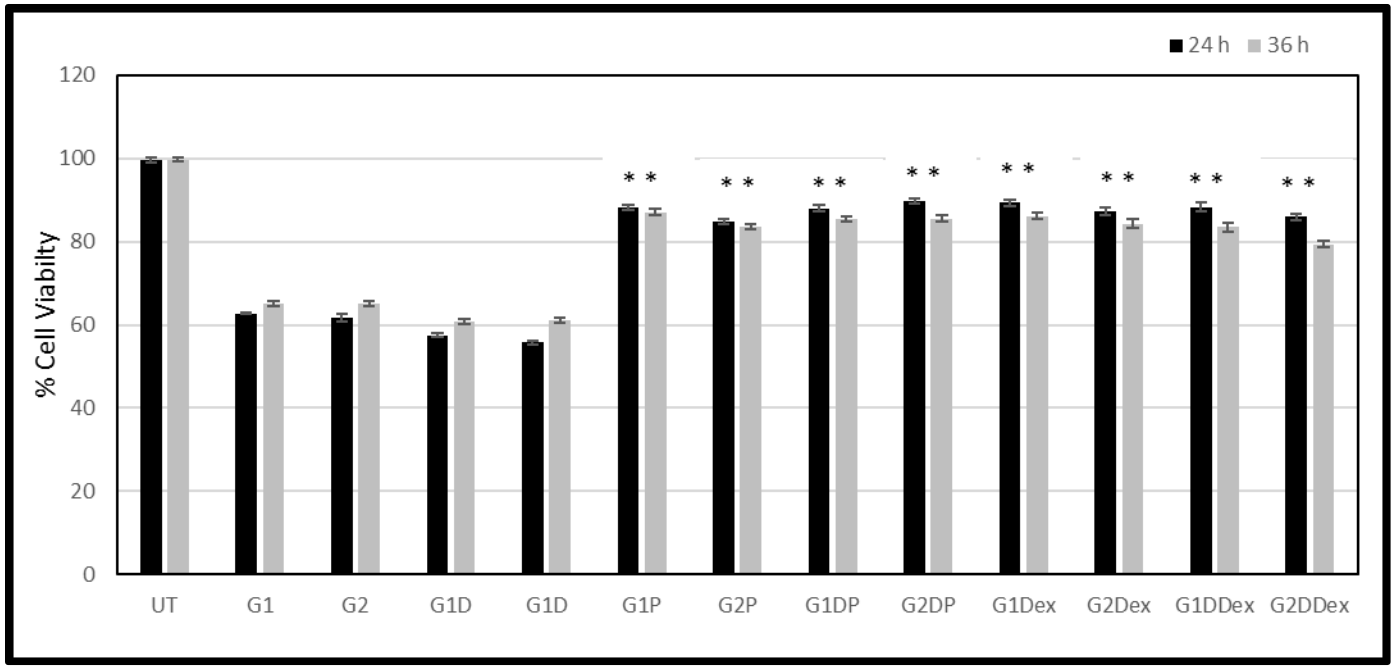

Figure 3: Comparison between the blank gelatin (G1, G2) and drug loaded gelatin nanoparticles (G1D, G2D) before and after treatment with Prednisolone and Dexamethasone and its effect on A-549 cell viability at 24 and 36 h. Data shown were the mean ± S.D. (n=3) *denotes that the treatment results were significantly different (* $p < 0.05$)

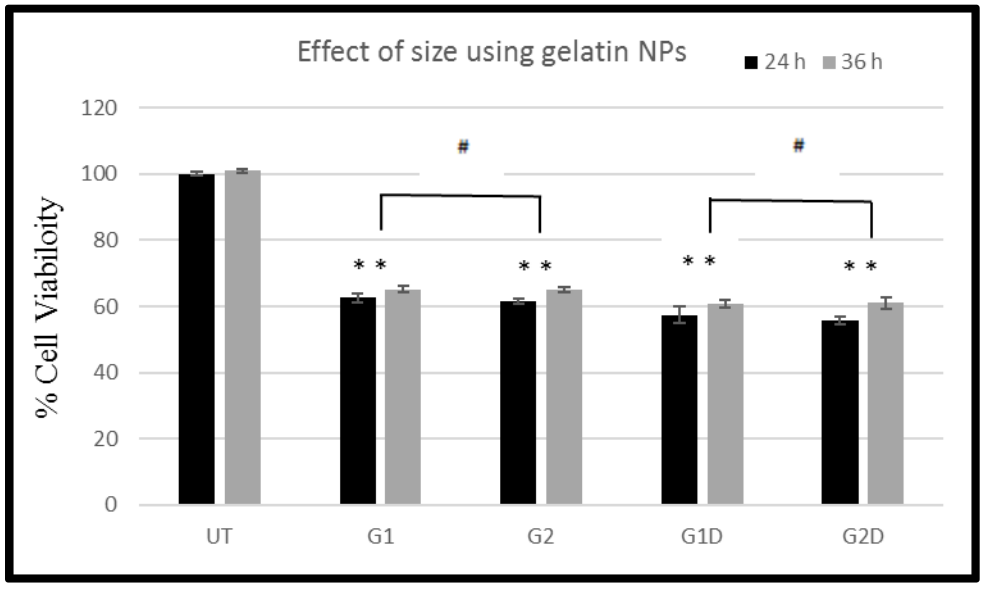

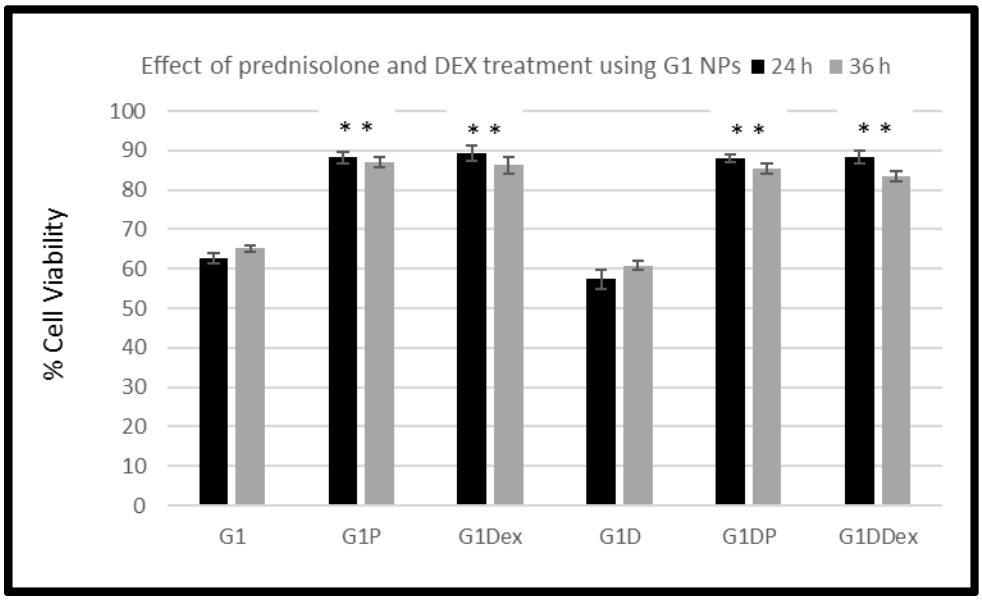
Effect of prednisolone and DEX treatment using G1 NPs
24 h
36 h
% Cell Viability
100
90
80
70
60
50
40
30
20
10
0
* *
* *
* *
* *
G1
G1P
G1Dex
G1D
G1DP
G1DDex

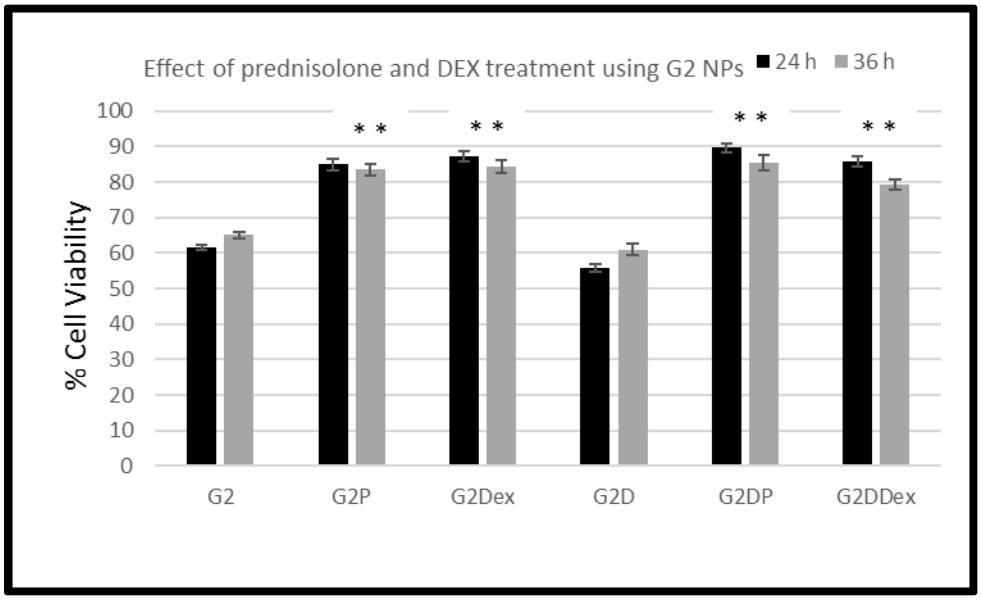
Effect of prednisolone and DEX treatment using G2 NPs
24 h
36 h
% Cell Viability
100
90
80
70
60
50
40
30
20
10
0
* *
* *
* *
* *
G2
G2P
G2Dex
G2D
G2DP
G2DDex

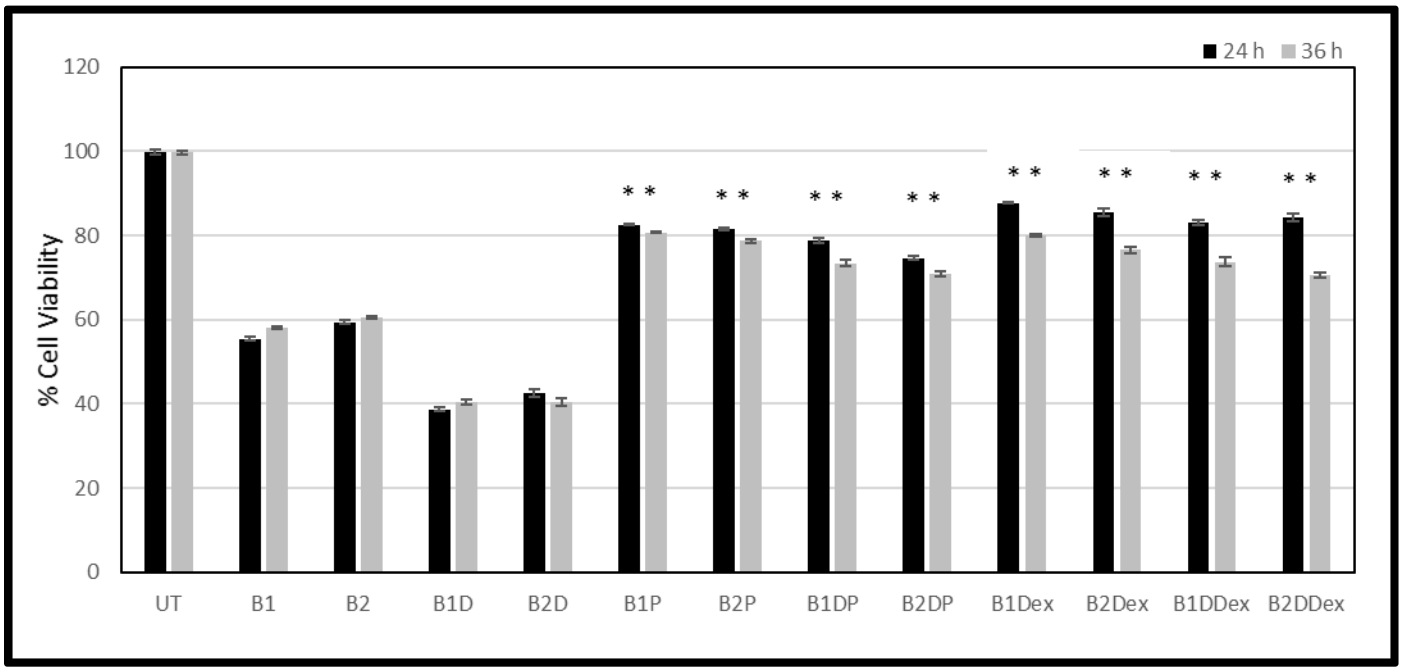

Figure 4: Comparison between the blank PIBCA (B1, B2) and drug loaded PIBCA nanoparticles (B1D, B2D) before and after treatment with Prednisolone and Dexamethasone and its effect on A-549 cell viability at 24 and 36 h. Data shown were the mean ± S.D. (n=3) *denotes that the treatment results were significantly different (* $p < 0.05$)

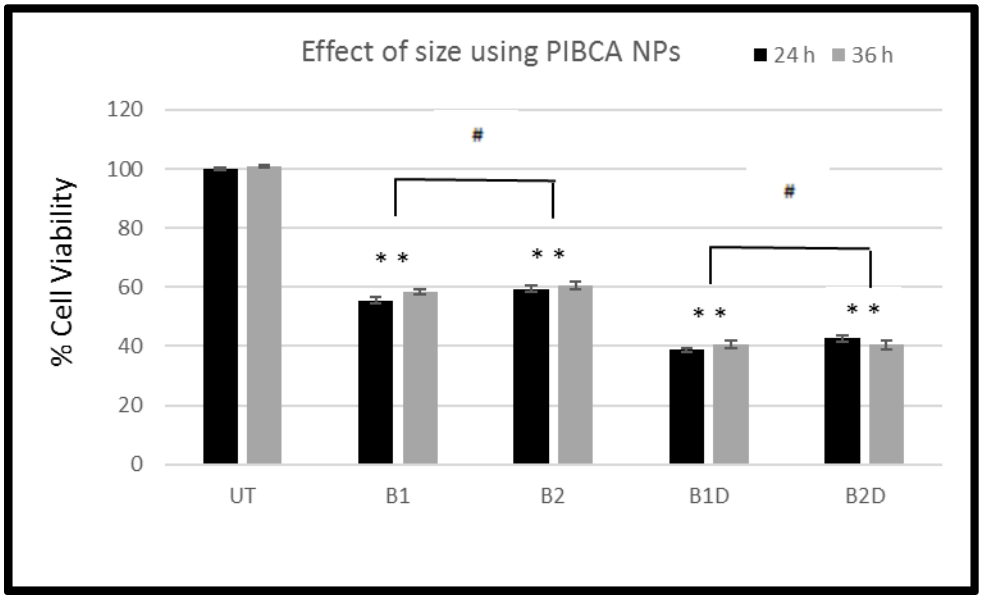

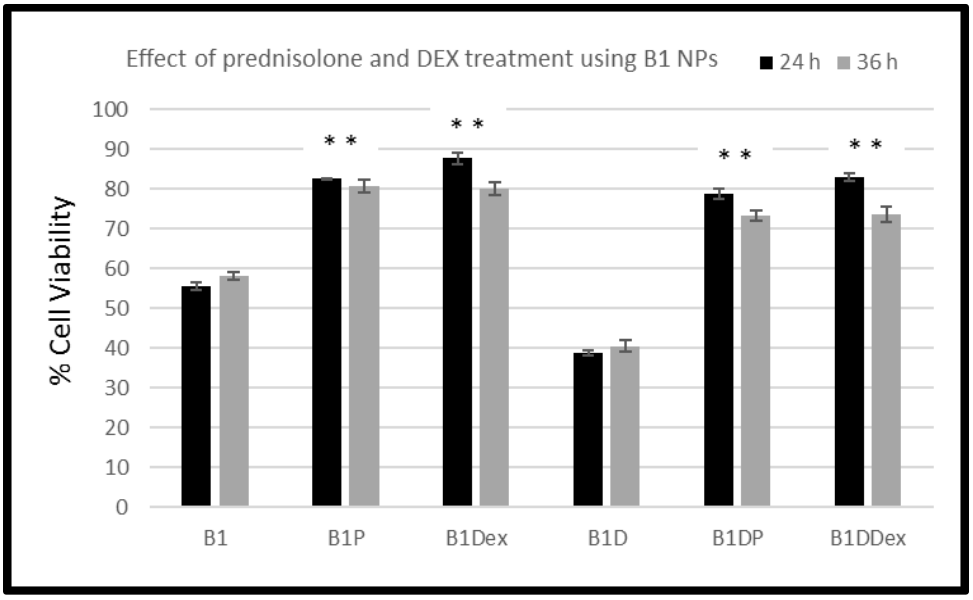
Effect of prednisolone and DEX treatment using B1 NPs
24 h
36 h
% Cell Viability
100
90
80
70
60
50
40
30
20
10
0
* *
* *
* *
* *
B1
B1P
B1Dex
B1D
B1DP
B1DDex

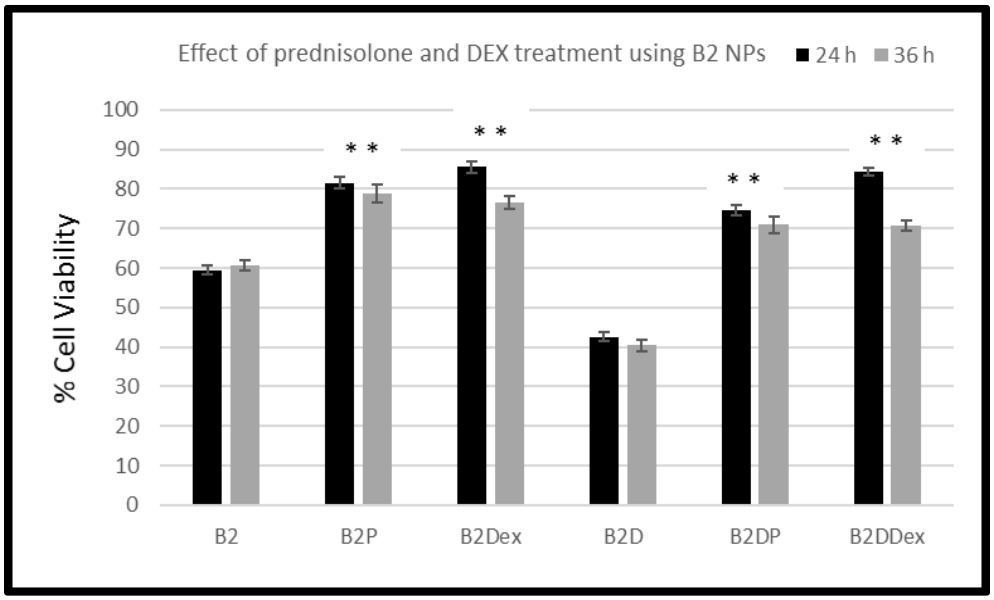
Effect of prednisolone and DEX treatment using B2 NPs
24 h
36 h
% Cell Viability
100
90
80
70
60
50
40
30
20
10
0
* *
* *
* *
* *
B2
B2P
B2Dex
B2D
B2DP
B2DDex

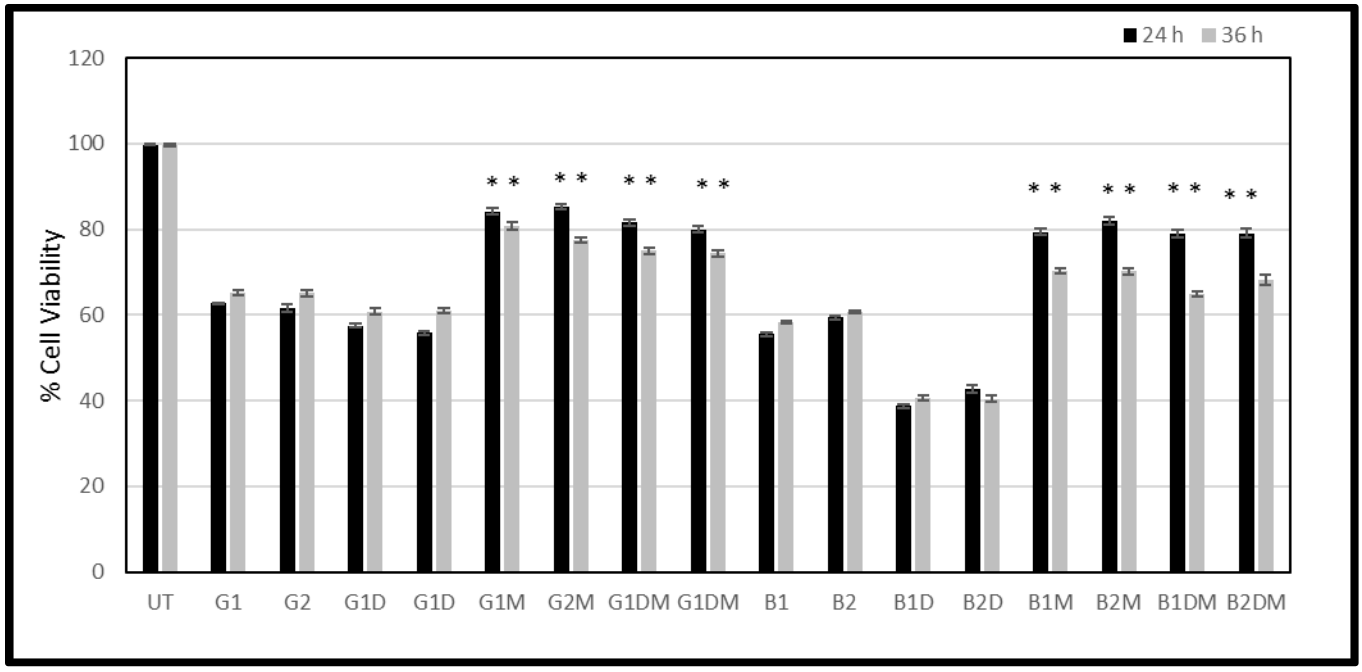

Figure 5: Comparison between blank gelatin (G1, G2) and drug loaded gelatin nanoparticles (G1D, G2D) with it corresponding nanoparticles after methotrexate treatment. Similarly, blank PIBCA (B1, B2) and drug loaded PIBCA nanoparticles (B1D, B2D) with it corresponding nanoparticles after methotrexate treatment and its effect on A-549 cell viability at 24 and 36 h. Data shown were the mean ± S.D. (n=3) *denotes that the treatment results were significantly different (* $p < 0.05$)

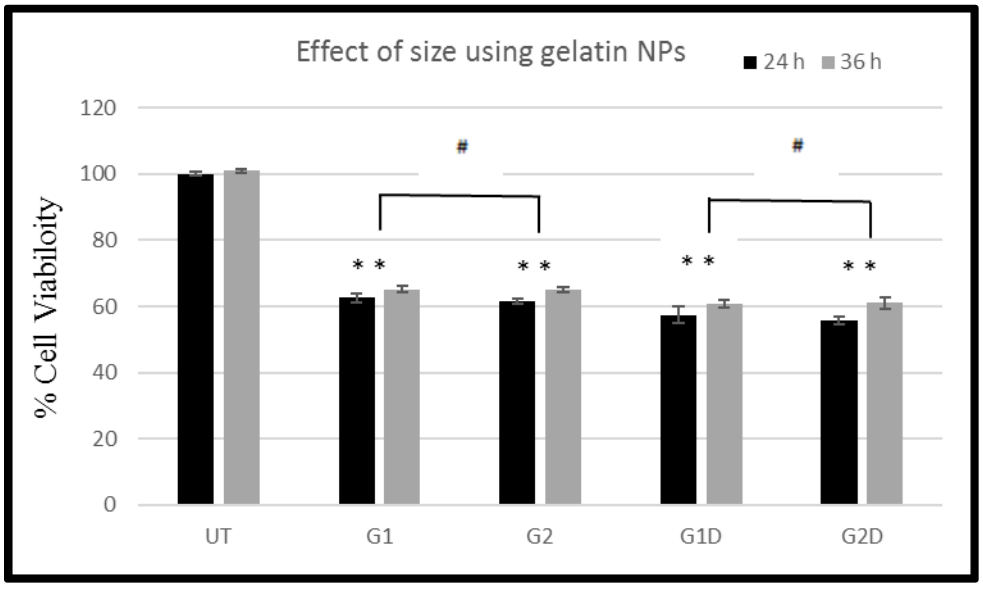

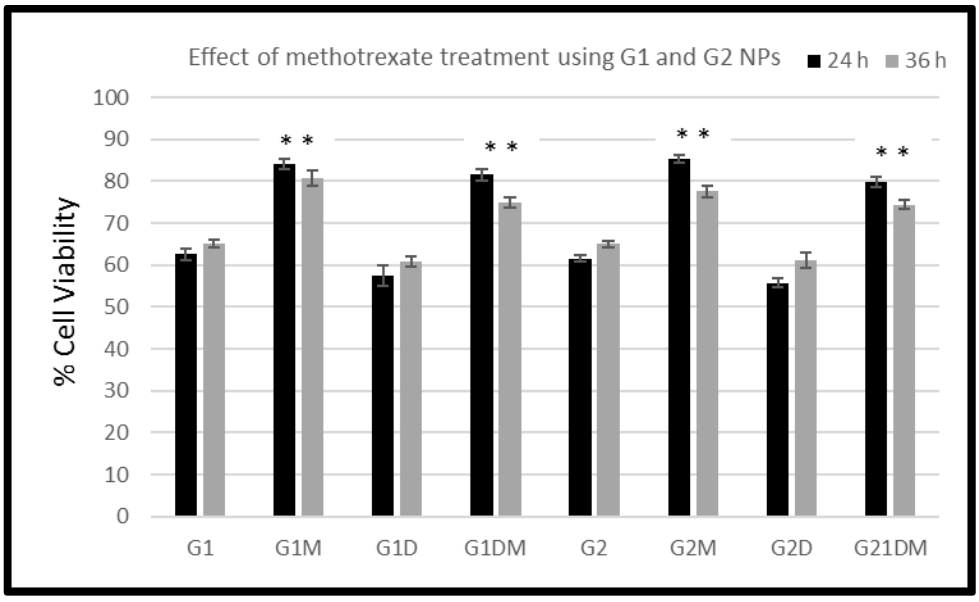
Effect of methotrexate treatment using G1 and G2 NPs
24 h
36 h
% Cell Viability
100
90
80
70
60
50
40
30
20
10
0
* *
* *
* *
* *
G1
G1M
G1D
G1DM
G2
G2M
G2D
G21DM

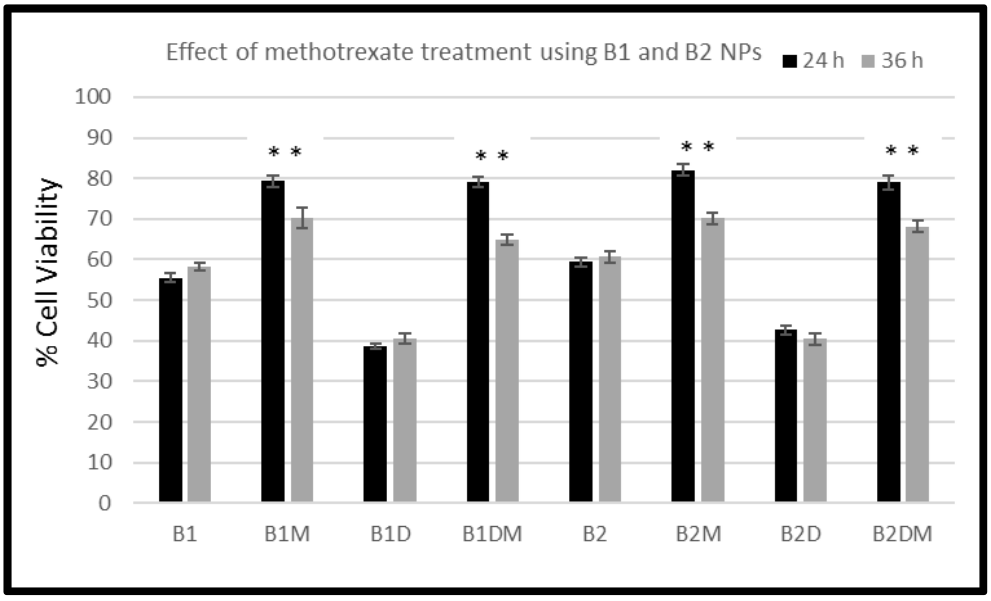
Effect of methotrexate treatment using B1 and B2 NPs
24 h
36 h
% Cell Viability
100
90
80
70
60
50
40
30
20
10
0
* *
* *
* *
* *
B1
B1M
B1D
B1DM
B2
B2M
B2D
B2DM

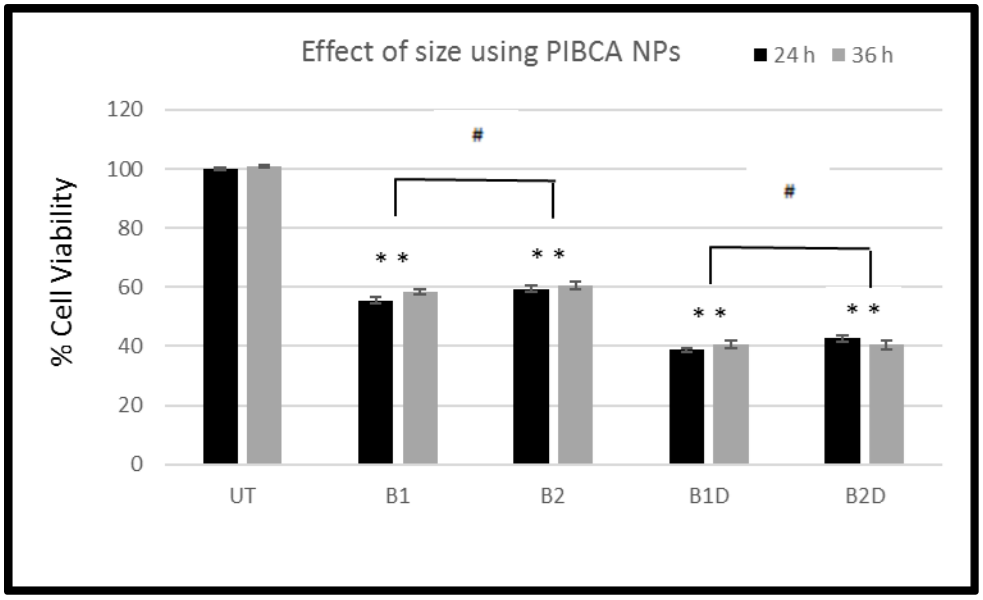
Effect of size using PIBCA NPs
24 h
36 h
% Cell Viability
120
100
80
60
40
20
0
#
#
* *
* *
* *
* *
UT
B1
B2
B1D
B2D